การวิเคราะห์ค่าความสามารถในการซึมผ่านก๊าซของฟิล์มนาโนคอมพอสิต ของพอลิเอธิลีนความหนาแน่นต่ำและดินเหนียว

นาย ภิญโญ โหวิไลลักษ์

วิทยานิพนธ์นี้เป็นส่วนหนึ่งของการศึกษาตามหลักสูตรปริญญาวิศวกรรมศาสตรมหาบัณฑิต
สาขาวิชาวิศวกรรมเคมี ภาควิชาวิศวกรรมเคมี
คณะวิศวกรรมศาสตร์ จุฬาลงกรณ์มหาวิทยาลัย
ปีการศึกษา 2549

ANALYSIS OF PERMEABILITY OF LOW DENSITY POLYETHYLENE/CLAY NANOCOMPOSITE FILMS

Mr. Pinyo Hovilailux

A Thesis Submitted in Partial Fulfillment of the Requirements
for the Degree of Master of Engineering Program in Chemical Engineering
Department of Chemical Engineering
Faculty of Engineering
Chulalongkorn University
Academic Year 2006

Thesis Title	ANALYSIS OF PERMEABILITY OF LOW DENSITY POLYETHYLENE/CLAY NANOCOMPOSITE FILMS
By	Mr. Pinyo Hovilailux
Field of Study	Chemical Engineering
Thesis Advisor	Varun Taepaisitphongse, Ph.D.

Accepted by the Faculty of Engineering, Chulalongkorn University in Partial Fulfillment of the Requirements for the Master's Degree

.....Dean of the Faculty of Engineering
(Professor Direk Lavansiri, Ph.D.)

THESIS COMMITTEE

..... Chairman
(Associate Professor Tawatchai Charinpanitkul, D.Eng.)

..... Thesis Advisor
(Varun Taepaisitphongse, Ph.D.)

..... Member
(Anongnat Somwangthanaroj, Ph.D.)

..... Member
(Associate Professor Somsak Woramongconchai, D.Eng.)

ภิญโญ โหวิไลลักษ์: การวิเคราะห์ค่าความสามารถในการซึมผ่านก๊าซของฟิล์มนาโนคอมพอสิตของพอลิเอธิลีนความหนาแน่นต่ำและดินเหนียว (ANALYSIS OF PERMEABILITY OF LOW DENSITY POLYETHYLENE/CLAY NANOCOMPOSITE FILMS) อาจารย์ที่ปรึกษา: อ. ดร. วรัญ แต้ไพสิฐพงษ์, 112 หน้า.

งานวิจัยนี้มีเป้าหมายสองส่วนคือ (ก) ศึกษาผลของปริมาณอนุภาคดินเหนียวและสารประสารต่อค่าความสามารถในการซึมผ่านก๊าซของฟิล์มนาโนคอมพอสิตของพอลิเอธิลีนความหนาแน่นต่ำและดินเหนียวชนิดมอนต์มอริลโลไนต์ และ (ข) ศึกษาความเหมาะสมของการนำสมการจำลองเนลสันแบบปรับปรุงมาใช้วิเคราะห์หาค่าความสามารถในการซึมผ่านก๊าซของฟิล์มนาโนคอมพอสิตของพอลิเอธิลีนความหนาแน่นต่ำและดินเหนียว

ฟิล์มนาโนคอมพอสิตของพอลิเอธิลีนความหนาแน่นต่ำและดินเหนียวชนิดมอนต์มอริลโลไนต์ถูกผสมแบบหลอมเหลวด้วยเครื่องอัดรีดด้วยวิธีแบบ 3 ขั้นตอนและถูกเป่าเป็นฟิล์ม ระยะห่างระหว่างชั้นของดินเหนียวถูกวัดด้วยเครื่อง XRD เครื่อง TEM ถูกใช้ศึกษาการกระจายตัวของดินเหนียวในฟิล์ม ค่าความสามารถในการซึมผ่านของก๊าซออกซิเจนของฟิล์มถูกวัดด้วยเครื่องวิเคราะห์การซึมผ่านก๊าซ

ผลการทดลองพบว่าฟิล์มนาโนคอมพอสิตของพอลิเอธิลีนความหนาแน่นต่ำและดินเหนียวชนิดมอนต์มอริลโลไนต์ที่มีค่าความสามารถในการซึมผ่านของก๊าซออกซิเจนต่ำกว่าฟิล์มพอลิเอธิลีนความหนาแน่นต่ำสามารถถูกผลิตขึ้นได้ด้วยวิธการผสมหลอมเหลว ฟิล์มนาโนคอมพอสิตของพอลิเอธิลีนความหนาแน่นต่ำและดินเหนียวชนิดมอนต์มอริลโลไนต์ที่ได้ส่วนใหญ่เป็นแบบ intercalated type ค่าความสามารถในการซึมผ่านของก๊าซออกซิเจนสามารถถูกลดลงได้ร้อยละ 50 ที่ปริมาณดินเหนียวที่ร้อยละ 3.14-5.09 โดยน้ำหนัก ความใสของฟิล์มนาโนคอมพอสิตของพอลิเอธิลีนความหนาแน่นต่ำและดินเหนียวชนิดมอนต์มอริลโลไนต์ที่ได้ลดลงเล็กน้อยเมื่อปริมาณดินเหนียวเพิ่มขึ้น สมการจำลองเนลสันแบบปรับปรุงสามารถนำมาวิเคราะห์หาค่าความสามารถในการซึมผ่านก๊าซของฟิล์มนาโนคอมพอสิตของพอลิเอธิลีนความหนาแน่นต่ำและดินเหนียวได้ถ้าค่าสัดส่วนขนาดของดินเหนียว การจัดเรียงตัวของดินเหนียว และปริมาณของดินเหนียวเชิงปริมาตรสามารถถูกหาได้อย่างแม่นยำ

ภาควิชา.....วิศวกรรมเคมี..... ลายมือชื่อนิสิต.....ภิญโญ โหวิไลลักษ์.....

สาขาวิชา.....วิศวกรรมเคมี..... ลายมือชื่ออาจารย์ที่ปรึกษา.....

ปีการศึกษา.....2549..... ลายมือชื่ออาจารย์ที่ปรึกษาร่วม.....

4870419721 : MAJOR CHEMICAL ENGINEERING

KEY WORD: POLYETHYLENE / CLAY / PERMEABILITY / NANOCOMPOSITE FILMS

PINYO HOVILAILUX: ANALYSIS OF PERMEABILITY OF LOW DENSITY POLYETHYLENE/CLAY NANOCOMPOSITE FILMS. THESIS ADVISOR: VARUN TAEPAISITPHONGSE, Ph.D., 112 pp.

The goals of this research were two folds, (i) to study the effects of loading of organoclay and compatibilizer on the permeability of LDPE/PE-g-MA/Org-MMT nanocomposite films, and (ii) to verify the applicability of the modified Nielsen model on prediction of permeability LDPE/PE-g-MA/Org-MMT nanocomposite films.

The LDPE/PE-g-MA/Org-MMT nanocomposites were prepared in the twin screw extruder in three-step mixing procedure and then blown into films. Gallery spacing between clay platelets of the Org-MMT and nanocomposite films were measured by X-ray diffraction. Transmission Electron Microscope (TEM) was used to study the distribution of clays in nanocomposite films. The Oxygen Transmission Rate (OTR) of the nanocomposite films were measured by the Oxygen Permeation Analyzer. The experimental permeability data were fitted by the modified Nielsen model.

The experimental results showed that the nanocomposite films of LDPE with Org-MMT and PE-g-MA as compatibilizer having lower oxygen permeability properties than pure LDPE film can be obtained by melt mixing. The obtained LDPE/PE-g-MA/Org-MMT nanocomposite films were mainly the intercalated type. The oxygen gas permeability was reduced by about 50% at 3.14-5.09 wt% inorganic clay loading. The transparency of nanocomposite films slightly decreased with increasing clay content. The 9 wt% PE-g-MA was the optimum loading found. The modified Nielsen model can be used to predict the relative permeability of nanocomposite films providing that the aspect ratio, orientation angle, and volume fraction of inorganic clay could be found accurately.

Department...Chemical Engineering...	Student's Signature Pinyo Hovilailux
Field of Study Chemical Engineering...	Advisor's Signature
Academic Year.....2006.....	Co-advisor's Signature.....

ACKNOWLEDGMENTS

I wish to express my sincerest gratitude and deep appreciation to my advisor, Dr. Varun Taepaisitphongse, for his kindness, supervision, invaluable guidance, advice, and encouragement throughout the course of this study.

I gratefully thank Associate Professor Dr. Tawatchai Charinpanitkul, Dr. Anongnat Somwangthanaroj, and Associate Professor Dr. Somsak Woramongconchai, for their substantial advice as thesis committee.

Support of Oxygen Permeation Analyzer at the Department of Packaging Technology, Faculty of Industrial Agriculture, Kasetsart University, Bangkok, is appreciated. I wish to thank Mr. Sangpet Nhornchaiyaphumi, at the Suranaree University of Technology, Nakhon Ratchasima, for his assistance and good advice on TEM analysis. Thanks are due to CCC CHEMICAL COMMERCE CO., LTD., Thailand, for providing polyethylene. Partial financial support from the Department of Chemical Engineering, Faculty of Engineering, Chulalongkorn University, Bangkok, is acknowledged.

Many thanks to my friends and colleagues in the Polymer Engineering Laboratory, Chulalongkorn University, especially Ms. Nuchjaree Pairotesak, for their discussion and friendly encouragement. I would like to thank everyone here. I feel so fortunate having a chance to learn here.

Finally, I would like to affectionately give all gratitude to the members of my family for their wholehearted love, understanding, encouragement, patient and support throughout my entire study.

CONTENTS

PAGE

CHAPTER **PAGE**

CHAPTER **PAGE**

LIST OF FIGURES

FIGURE **PAGE**

FIGURE **PAGE**

FIGURE **PAGE**

LIST OF TABLES

TABLE **PAGE**

TABLE **PAGE**

CHAPTER I

INTRODUCTION

1.1Background

Almost all foods, whether fresh or processed, are enclosed in some form of packaging, from processing and manufacturing through handling and storage all the way to the consumer [2,3]. Packaging protects food from the outside environment. Packaging was revolutionized by oil-based polymers. The use of commodity plastics such as polyolefins provides many conveniences including lightweight and desirable physical and mechanical properties with a favorable cost performance for the food industry and the consumer. One important property of packaging is its permeability to gases or liquids.

Polymer/Clay Nanocomposites have been attracting great interest because of their improved properties such as increased moduli and tensile properties, decreased expansion coefficient and permeability to gases or liquids, better resistance to solvents, enhanced thermal stability and flame retardant properties [1,4]. Clay platelets in nanocomposites are known to retard the diffusion of gases or liquids. Compatibilizer are normally used to improve adhesion between hydrophobic polymer and hydrophilic clay.

Although the enhancements in gas barrier properties are well known in polymer-silicate nanocomposites, its dependence on factors such as the relative orientation of the sheets in the matrix and the state of aggregation and dispersion (intercalated, exfoliated, or some intermediate) are not well understood. Several mathematical models that took into account the relative orientation of clays in the matrix were developed to predict the permeability of polymer/clay nanocomposite.

The low density Polyethylene (LDPE), organically modified Montmorillonite clays (Org-MMT) and Polyethylene-graft-Maleic Anhydride (PE-g-MA) were used as model polymer, filler, and compatibilizer in this work to study the effects of clay loading and compatibilizer loading on the permeability of LDPE/PE-g-MA/Org-MMT

nanocomposite films. The data were used to verify the applicability of modified Nielsen model.

1.2 Objectives

1.2.1 To study the effects of loading of organoclay and compatibilizer on the permeability of LDPE/PE-g-MA/Org-MMT nanocomposite films.

1.2.2 To verify the applicability of the modified Nielsen model on prediction of permeability LDPE/PE-g-MA/Org-MMT nanocomposite films.

CHAPTER II

THEORY

2.1 Polyethylene

Polyethylene (PE) was the first olefinic polymer to find use in food packaging. Introduced in the 1950s, it became a common material, used in film, molded containers, and closures by 1960s. Presently, the properties of LDPE such as strength, toughness, thermal and heat sealing properties, optical transparency, and processing conditions have been much improved.

Olefin, which means oil-forming, is an old synonym for alkene, and was, originally, the name given to ethylene. Alkenes are hydrocarbons containing carbon-carbon double bonds, such as ethylene and propylene. In the plastic industry, the term polyolefin strictly applies to polymers made of alkenes, whether homopolymers or copolymers. It includes the family of polyethylene, and the family of polypropylene [5].

Polyethylene is a family of addition polymers based on ethylene. Polyethylene can be linear or branched, homopolymer or copolymer. In the case of a copolymer, the other comonomer can be an alkene such as propene, butene, hexene or octene, or a compound having a polar functional group such as vinyl acetate (VA), ethyl acrylate (EA). If the molar percent of the comonomer is less than 10%, the polymer can be classified as either a copolymer or homopolymer. Figure 2.1 showed molecular structures of polyethylene produced from different processes.

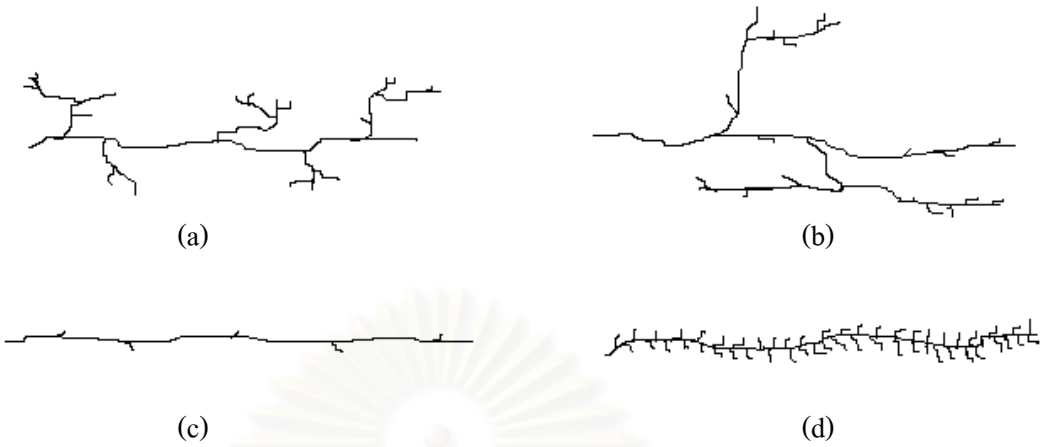

Figure 2.1 Molecular Structures of
(a) Branched LDPE Produced from Tubular Process
(b) Branched LDPE Produced from Autoclave Process
(c) High Density Polyethylene (HDPE)
(d) Linear Low Density Polyethylene (LLDPE) [6]

Low density polyethylene has a branched structure. The family of branched polyethylenes includes homopolymers and copolymers of ethylene, which are non-linear, thermoplastic, and partially crystalline. They are fabricated under high pressure and temperature conditions by a free radical polymeriation process. The random polymeriation of ethylene under these conditions produces a branched polymer that is actually a mixture of large molecules with different backbone lengths, various side chain lengths and with various degrees of side-chain branching.

The chain branching in homopolymer LDPE gives this polymer a number of desirable characteristics such as clarity, flexibility, heat sealability and ease of processing. The actual values of these properties depend on the balance between the molecular weight, molecular weight distribution, and branching.

LDPE is also versatile with respect to processing mode, and is adaptable to blown film, cast film, extrusion coating, injection molding, and blow molding. Film is the single largest form of LDPE produced. Products made of LDPE include containers and bags for food and clothing, industrial liners, vapor barriers, agricultural films, household products, and shrink and stretch wrap films. LDPE can be used

alone or in combination with other members of the PE resin family. A summary of the properties of LDPE is presented in Table 2.1.

Table 2.1 Properties of LDPE [5]

Used plastic in packaging	Most widely
Density	0.91 to 0.94 g/cm^3
Glass Transition Temperature, T_g	-120^{o}C
Melting Temperature, T_m	105-115^{o}C
Material	Flexible
Impact strength	Good
Machinability	Fair
Oil resistance	Good
Chemical resistance	Fair
Heat sealing characteristics	Good
Cost	Low
Use as a film	Largest
Transparency	Better than HDPE because has lower percent crystallinity
Water vapor transmission rate	Good but inferior to HDPE 0.63-1.26 g μm/m^2 day at 95 ^{o}F, 90%RH
Gas permeability	Poor (poorer than HDPE) P_{O_2} = 295 cm^3 μm/m^2 day atm

The range of ethylene polymers and copolymers available for the manufacture of blown films is very extensive. The film producer has the possibility of meeting end product requirements by the appropriate choice of raw material. In practice, polyethylene grades are distinguished by the following criteria such as manufacturing process, MFI value (melt-flow index according to DIN 53735), molecular weight distribution and density (according to DIN 53479) [7].

2.1.1 Low Density Polyethylene (LDPE)

LDPE is produced from high pressure production process. The core applications of LDPE have become solidly established for the following PE melt-flow index (MFI) ranges as shown below:

MFI 0.3 for sack-and heavy-duty film, shrink film

MFI 0.7 to 1 for carrier bags, general packaging film, refuse bag film

MFI ~2 for thin films, laminating film, thin shrink films

MFI ~4 for thin films

(Note: MFI (190 ^{o}C/21.6 N) in (g/10 min))

2.1.1.1 Molecular Weight Distribution

The breadth of the molecular weight distribution has effects upon the melt strength (bubble stability) and on the strength properties. LDPE with broad molecular weight distribution has high melt strength, good bubble stability. But LDPE with narrow molecular weight distribution has low melt strength, poor bubble stability, and general increase of strength characteristics.

2.1.1.2 Density

The density range for LDPE is 0.91 to 0.94 g/cm^3 and for HDPE is 0.94 to 0.97 g/cm^3. The density of the material relates to the mechanical properties to be expected, the drawability, and the gas-barrier properties. As with choice by MFI value, certain density ranges have become established for particular uses as the followings:

Density 0.92 to 0.93 g/cm^3 for sack-and heavy-duty film

Density 0.92 to 0.925 g/cm^3 for carrier bags

Density 0.925 g/cm^3 for thin films

2.1.1.3 Property Trends in the Polyethylene Family

The family of polyethylene has many properties in common. The properties of LDPE and HDPE films are given for comparison in Table 2.2. Table 2.3 shows the relationship of density to the water vapor transmission rate and oxygen permeability.

Table 2.2 Comparison of Properties of LDPE and HDPE Films [6]

Material		**LDPE**	**HDPE along/across**
Density	g/cm^3	0.91 to 0.94	0.94 to 0.97
Tensile Strength (DIN 53455)	N/cm^2	1,500 to 2,000	4,500 to 3,500
Extension At Break (DIN 53455)	%	600	650 to 450
Tear Strength (DIN 53455)	N/100 mm	8	32 to 27
Tensile Impact Toughness (DIN 53448)	N/cm^2	20,000	20,000 to 18,000
Water Vapor Permeability (DIN 53122)	$g/m^2/day$	3	1 to 1.5
Maximum Use Temperature	^oC	≈ 80	110 to 115

Table 2.3 Effect of Density of Polyethylene on the WVTR and Permeability of Oxygen [5]

Density of Polyethylene (g/cm^3)	**Water Vapor Transmission Rate (WVTR) ($g\ \mu m/m^2\ day$)**	**Oxygen Permeability ($cm^3 \mu m/m^2\ day\ atm$)**
0.910	0.866	275
0.915	0.779	256
0.920	0.685	225
0.925	0.579	201
0.930	0.465	165
0.935	0.366	137
0.940	0.276	104
0.945	0.244	91.3
0.950	0.208	76.4
0.955	0.185	70.1
0.960	0.145	61.0

2.2 Clay

Clay implies a natural, earthy, fine grained material which develops plasticity when mixed with a limited amount of water. By plasticity, it means that the property of the moistened material is deformed under the application of pressure, with the deformed shape being retained when the deforming pressure is removed. According to chemical analysis of clays, it composes of silica, alumina, and water, frequently with appreciable quantities of iron, alkali, and alkaline earth metals. The two major types of clay minerals are 1:1 and 2:1 type minerals [8].

1:1 type minerals

The 1:1 clay-mineral type consists of one tetrahedral sheet and one octahedral sheet. These two sheets are approximately 0.7 nm thick as shown in Figure 2.2.

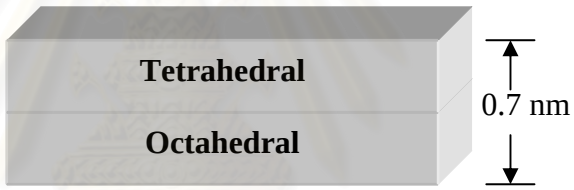

Figure 2.2 1:1 Type Clay Minerals [8]

A kaolinite mineral is one of 1:1 type minerals. The structure is composed of a single silica tetrahedral sheet and a single alumina octahedral sheet combined in a unit so that the tip of the silica tetrahedron and one of the layers of the octahedral sheet form a common layer.

2:1 type minerals

The three sheets or 2:1 layer lattice silicates consist of two silica tetrahedral sheets between which is an octahedral sheet. These three sheets form a layer approximately 1 nm thick as shown in Figure 2.3.

Figure 2.3 2:1 Type Clay Minerals [8]

Clays are extremely fine grained (<2 μm), creating a large surface area (per unit mass) on which reactions can occur. Most clay minerals have a negative charge within the tetrahedral-octahedral layers owing to isomorphic substitutions. The charge is balanced by cation from the surrounding soil solution that attaches to the surface of the crystallites. These cations exchange easily and are a major source of plant nutrients. Soil scientists define cation exchange capacity (CEC) as the amount of negative charge in the tetrahedral-octahedral layers per 100 g soil. Soil minerals with a higher CEC can hold on to more soil ions and are more reactive, benefiting plants. Examples of surface area and cation exchange capacity of some clays are shown in Table 2.4.

Table 2.4 Surface Area and Cation Exchange Capacity of Some Clay Minerals and Humus [9]

Mineral	**Surface Area (10^3 m^2/kg)**	**Cation Exchange Capacity (cmol charge/kg)**
Kaolinite	10-20	1-10
Chlorite	70-150	20-40
Mica	70-120	20-40
Montmorillonite	600-800	80-120
Vermiculite	600-800	120-150
Humus	900	150-300

The 2:1 layer typed aluminosilicate can be classified into the following subgroups: pyrophylite, smectite, vermiculite, illite, mica, brittle mica, and chlorite. Their difference is their layer charge density as shown in Table 2.5. Typical property values of some of these clays are shown in Table 2.6. The chemical formula of commonly used 2:1 type clays are shown in Table 2.7 [10].

Table 2.5 Classification of Clay in Phyllosilicates Types

where x = Charge per Formula Unit [10]

Layer type	**Group**	**Subgroup**	**Species**
1:1	Kaolinite-serpentine (x~0)	Serpentine (Tr) Kaolinite (Di)	Chrysotile, Amesite, Lizardite, Kaolinite, Dickite, Halloysite
2:1	Pyrophyllite-talc (x~0)	Talc (Tr) Pyrophyllite (Di)	Talc Pyrophyllite
	Smectite (x~0.2-0.6)	Tr smectite Di smectite	Saponite, Hectorite, Sauconite Montmorillonite, Bentonite, Beidellite
	Vermiculite (x~0.6-0.9)	Tr vermiculite Di vermiculite	Trioctahedral vermiculite Dioctahedral vermiculite
	Illite (x<0.9-0.6)	Tr illite Di illite	
	Mica (x~1.0)	Tr mica Di mica	Biotite, Phlogopite, Lepidolite Muscovite, Paragonite
	Brittle mica (x~2.0)	Tr brittle mica Di brittle mica	Clintonite, Anandite Margarite
	Chlorite (x variable)	Tr, Tr chlorites Di, Di chlorites Di, Tr chlorites Tr, Di chlorites	Common name based on Fe^{2+}, Mg^{2+} Mn^{2+}, Ni^{2+}, Ponbassite Sudoite, Codecite (Li)

(Tr = Trioctahedral, Di = Dioctahedral)

Table 2.6 Summary of Properties of Different Clays [8]

Type	Size (mm)	Surface area (m^2/g)		Interlayer Spacing (nm)	Cation sorption (meq/100g)
		External	Internal		
Kaolinite	0.1 - 5.0	10 - 50	-	0.7	10 - 50
Smectite	< 0.1	70 - 150	500 - 700	1.0 - 2.0	85 - 110
Vermiculite	0.1 - 5.0	50 - 100	450 - 600	1.0 - 1.4	100 - 120
Illite	0.1 - 2.0	50 - 100	5 - 100	~1.0	15 - 40

Table 2.7 Chemical Formula of Commonly Used 2:1 Layer Type Aluminosilicate [10]

Clay	General formula
Montmorillonite	$M_x(Al_{4-x}Mg_x)Si_8O_{20}(OH)_4$
Hectorite	$M_x(Mg_{6-x}Li_x)Si_8O_{20}(OH)_4$
Saponite	$M_xMg_6(Si_{8-x}Al_x)O_{20}(OH)_4$

M = Mono valent cation, x = degree of isomorphous substitution

2.2.1 Montmorillonite

Montmorillonite clays are relatively common throughout the world. Deposits of commercial clay are referred to as bentonite, which generally contains in excess of 50% montmorillonite. Conventional purification methods are adequate for the clays used in most common applications, such as binders for metal casting, well-drilling legs, and cosmetics.

Montmorillonite is one in smectite group which has a low thermal expansion coefficient and a high gas barrier property. Stacking of a layered structure with aluminum octahedron sandwiched between two layers of silicon tetrahedron leads to a regular weak dipolar or van der Waals interaction between the layer. Isomorphic substitution in each layer generates negative charges that are counterbalanced by hydrated sodium or potassium ions residing in the interlayer spaces. Due to this special characteristic, montmorillonite can be easily dispersed in water resulting in a stable colloid. Typically, the natural montmorillonite is too hydrophilic to disperse in an organic matrix. Its dispersibility can be improved to make it useful by ion exchanges with an organic cation molecule, such as cation surfactant, onto the surface

of filler [8, 11-12]. The arrangement of smectite-clay structure by cation exchanges with cation surfactants shown in Figure 2.4.

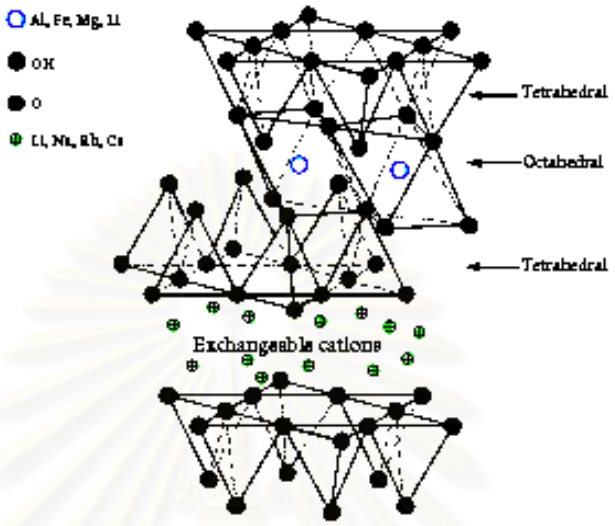

Figure 2.4 Schematic Illustration of Atoms Arrangement in a Typical MMT Layer [13]

Montmorillonite has the widest acceptability for use in polymers. It is a type of smectite clay that can absorb water, and it is a layered structure with aluminum octahedron sandwiched between two layers of silicon tetrahedron. Each layered sheet is slightly less than 1 nm thin, with surface dimensions extending to about 1000 nm. The aspect ratio is about 1000 to 1 and the surface area is in the range of 750 m^2/g.

2.2.1.1 Surface Treatment

Montmorillonite clay is hydrophilic; hence, it is not inherently compatible with most polymers and must be chemically modified to make its surface more hydrophobic. Stacking of the silicate layers leads to a regular van der Waals gap between the layers, which was termed as the interlayer gallery. Isomorphic substitution within the layers generates negative charges that are normally counterbalanced by cations like Na^+, Ca^{2+}, or K^+ residing in the gallery space. Ion exchange reactions with various organic cations, such as alkylammonium cations, expand the interlayer space and make the silicate hydrophobic. The most widely used surface treaments are ammonium cations which can be exchanged for existing cations already on the surface of the clay. The treatments minimize the attractive forces

between the agglomerated platelets [8] as shown in Figure 2.5. The organic cations promote the miscibility of the silicate layers with the polymer matrix.

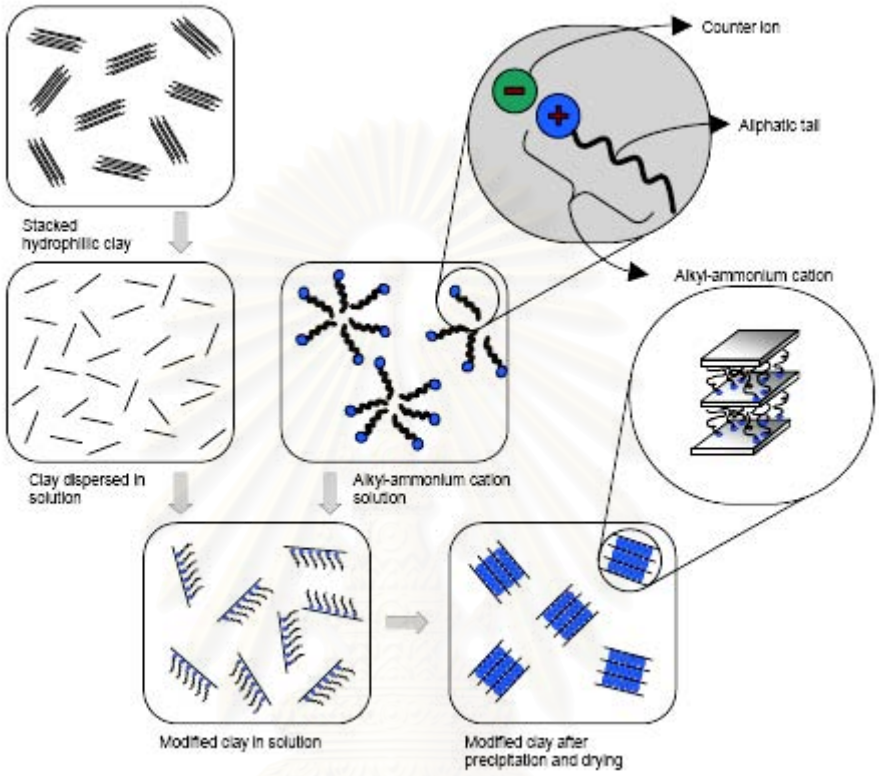

Figure 2.5 Schematic Representation of Clay Surface Treatment [11]

2.3 Compatibilizer

The use of a compatibilizer, namely a chemical able to render compatible two different materials, made it possible for the melt intercalation technique to be accepted as the most promising approach leading to nanocomposites formation. In this way the use of solvents and dedicated processes could be avoided providing a formation procedure which is both "*environmental friendly"* and "*user friendly*". It is noted that the surface treatment and the compatibilizer are two different, independent and complementary ways adopted to solve the problem of poor miscibility between polymer and clay. They act on parallel levels to overcome the same difficulty. The incompatibilities between PE and Organophilic Montmorillonite clay (Org-MMT) are, in fact, both of thermodynamic and of physical nature. The first kind of obstacle for a successful hybrid formation is the fact that the stacks of layers in the pristine Org-

MMT form are very stable and unwilling to reach the state of disorder required to a well formed nanocomposites. The second impediment to the desired exfoliated structure is the chemical unsuitability of the non-polar PE to be bonded in any way to the polar MMT platelets, at least to hold them in a non-thermodynamically favourable arrangement. Through the surface treatment, it is possible to change the interlayer structure of Org-MMT both by increasing the gallery gap and modifying the silicate surface in an organic fashion, but this artifice is not enough to render compatible matrix and filler; thus, the 'polarizing' compatibilizer such as PE-g-MA as shown in Figure 2.6, needs to be introduced in the PE

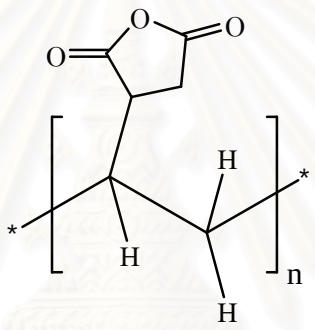

Figure 2.6 Model Structure of Polyethylene-graft-Maleic Anhydride (PE-g-MA)

According to this representation the Maleic Anhydride (MA) groups should be randomly grafted in the PE chain. Nevertheless this kind of product is usually made by reactive extrusion with a peroxide initiator which causes a free radical formation by scission of the PE chain. Such radical is the reactive site to which the MA group attaches. The compatibilizer vendor suggests more than one group can react with PE chain leading to a dimer or even trimer formation. This means a Polyethylene-graft-Maleic Anhydride (PE-g-MA) representation as a 'surfactant', where a polar head is attached to an aliphatic tail, would be more adequate than the one commonly used and depicted in the sketch above. Hence, in simple binary mixtures of PE and Org-MMT, the task of PE-g-MA is to establish the film between two such different materials: the hydrocarbon part of the molecule tends to be kept in the polyethylene matrix, while the oxygen atoms in the maleic anhydride ring can be linked to the hydroxyl groups of the clays by electrostatic attraction generating a strong hydrogen bonding between

them which is expected to help the exfoliation process [14]. Figure 2.7 illustrates a scheme of the clay dispersion process.

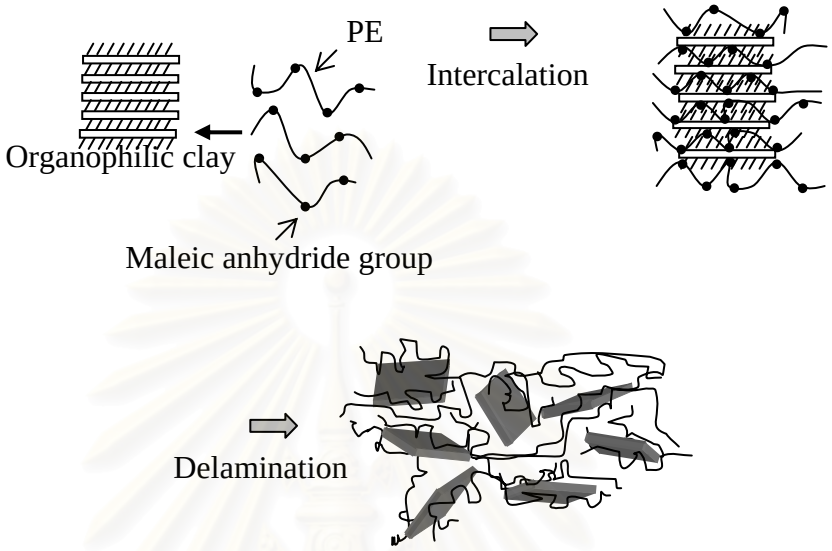

Figure 2.7 Schematic Representation of the Clay Dispersion Process [15]

It has already been anticipated that there exists an optimum in PE-g-MA functionality between a too little functionalized PE, which would be unproductive, and a functionalized PE with an excessive content of MA which, in contrast, would have too large polarity difference with the matrix PE molecules to diffuse in them [16].

The PE-g-MA molecular weight (MW) also seems to affect some mechanical properties of the resulting nanocomposites. Svoboda *et al.* tested different compatibilizer grades and found that tensile strength and impact strength actually depended on the molecular weight of PE-g-MA; in particular, the best overall properties have been showed by the sample with the highest molecular weight (MW=330,000). On the other side, from a dispersion point of view, such a 'heavy' compatibilizer hampered the diffusion of PE molecules from the bulk polymer when is used in high concentration; a higher level of dispersion is, in fact, given by lower MW PE-g-MA [17].

2.4 Nanocomposites

A polymer-clay nanocomposite is a polymer that contains nanometer sized clay particles (in which the filler is < 100 nm in at least one dimension (Figure 2.8)). As a result of their small dimensions, the clay platelets have a large specific surface area of about 700 m^2/g. Their small size also results in small inter platelet distances in a polymer-clay nanocomposite [18]. Although some nanofilled composites (carbon black [19] and fumed silica [20] filled polymers) have been used for more than a century, research and development of nanofilled polymers has greatly increased in recent years for several reasons. First, unprecedented combinations of properties have been observed in some polymer nanocomposites; for example, Yano *et al*. [21] showed a 50% decrease in the permeability of polyimides at a 2 vol% loading of Mica-Type Silicates (MTS). Many of these nanocomposites are optically transparent and/or optically active. A second reason for the large increase in research and development efforts was the 'discovery' of carbon nanotubes in the early 1990s [22]. Third, significant development in the chemical processing of nanoparticles and in the in-situ processing of nanocomposites has led to unprecedented control over the morphology of such composites. It has also created an almost unlimited ability to control the interface between the matrix and the filler.

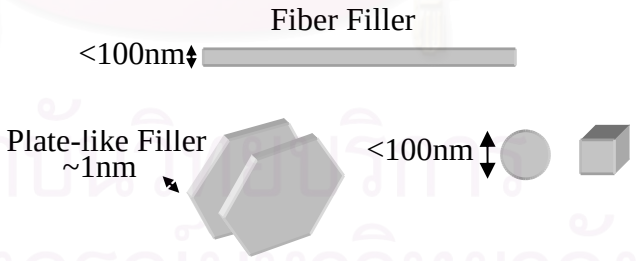

Figure 2.8 Schematic of Nanoscale Fillers [1]

The small size of nanofillers can also lead to unique properties of the particles themselves. For example, single-walled nanotubes are essentially molecules, free from defects, and have a modulus as high as 1 TPa and strengths that may be as high as 500 GPa. Single-crystal particles that are optically active, but are unmanageable on

the macro scale can be combined in a polymer to achieve the optical gain of the material and the ease of processing afforded by the polymer.

There are three general ways of dispersing nanofillers in polymers. The first is direct mixing of the polymer and the nanoparticles either as discrete phases or in solution. The second is solution mixing, and the third is in-situ polymerization in the presence of the nanoparticles [1].

1. Direct Mixing (Melt mixing)

Direct mixing takes advantage of well established polymer processing techniques. Nanocomposites can be sufficiently rapid processed in a twin-screw extruder. The strategy is to blend a molten thermoplastic with an organosilicate in order to optimize the polymer/layered silicate interaction.

2.Solution Mixing

Some of the limitations of melt-mixing can be overcome if both the polymer and the nanoparticles are dissolved or dispersed in solution. This allows modification of the particle surface without drying, which reduces particle agglomeration. The nanoparticle/polymer solution can then be cast into a solid, or the nanoparticle/polymer can be isolated from solution by solvent evaporation or precipitation.

3. In-Situ Polymerization

Another method is in-situ polymerization. Here, nanoscale particles are dispersed in the monomer or monomer solution, and the resulting mixture is polymerized by standard polymerization methods.

In addition to the effect of size on particle properties, the small size of the fillers leads to an exceptionally large interfacial area in the composites. The interface controls the degree of interaction between the filler and the polymer and thus controls the properties. Therefore, the greatest challenge in developing polymer nanocomposites may be learning to control the interface.

2.4.1 Nanocomposite Types

Generally, polymer/layered silicate composites are ideally divided into three types as shown in Figure 2.9 [8,23].

2.4.1.1 Conventional Composites (Immiscible Composites)

This type composes of silicate tactoids with the silicate layers aggregated in the unintercalated form. Consequently, discrete phases usually take place because of no penetration of polymer molecules into layer silicate phase.

2.4.1.2 Intercalated Nanocomposites

This type occurs when insertion of polymer chains into the layered silicate structure occurs in a crystallographically regular fashion, regardless of the Organically Modified Layered Silicate (OMLS) to polymer ratio, and a repeat distance of few nanometers.

2.4.1.3 Exfoliated Nanocomposites

In an exfoliated nanocomposite, the individual silicate layers are separated in a continuous polymer matrix by an average distance that totally depends on Organically Modified Layered Silicate (OMLS) loading. Usually, the OMLS content of an exfoliated nanocomposite is much lower than that of intercalated nanocomposite.

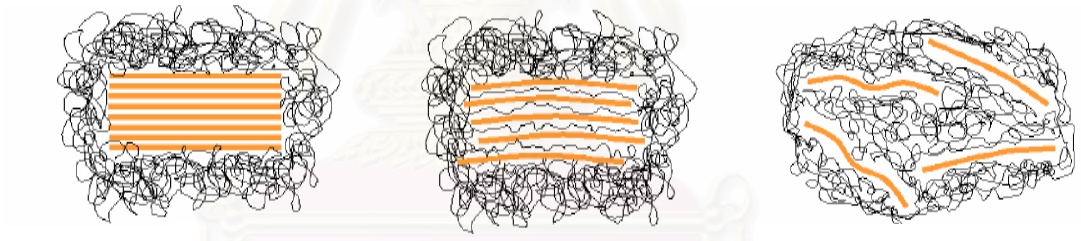

a) b) c)

Figure 2.9 Pattern of Composites a) Conventional Composites b) Intercalated Nanocomposites c) Exfoliated Nanocomposites [24]

Inclusion of clay in a polymer matrix leads to many reported improvements, such as increased tensile strength and modulus (probably because the layers partially immobilize a certain amount of polymer phase), improved flame retardancy, enhanced barrier to gas (oxygen and carbon dioxide), water and hydrocarbons (gasoline, methanol, and organic solvents) permeation, better scratch resistance even for very modest nanocomposites loadings (1-5 wt%). it should be noted though that not all of these properties depend on dispersion level of clay.

2.5 Barrier Properties (Permeability)

A key characteristic of glass and metals as packaging materials is their high barrier properties to gases and vapors. While polymers can provide an attractive balance of properties such as flexibility, toughness, lightweight, formability and printability, they do allow the transport of gases and vapors to some extent. The selection of a barrier polymer for a particular application typically involves tradeoffs between permeation, mechanical and aesthetic properties as well as economic and recycling considerations.

Quality and shelf life are reduced when food, through interaction with the outside environment, gains or loses moisture or aroma, takes up oxygen (leading to oxidative rancidity), or becomes contaminated with micro-organisms. There is an ongoing interest in optimising property sets of barrier polymers to provide an efficient and economical method for packaging and for extending the shelf life of packaged foods and beverages.

Barrier properties are determined by the steady-state rate of mass transport through the films [25, 26]. The permeability coefficient, P, can be defined by

$$P = \frac{(volume\ of\ \ permeant)\cdot(film\ thickness)}{(area)\cdot(time)\cdot(pressure\ drop\ in\ \ film)} \qquad (1)$$

The permeability coefficient is not only a function of the chemical structure of the polymer, but it also depends on many physical factors such as density, crystallinity, orientation, cross-linking, plasticizers, moisture sensitivity and temperature. Thus, film properties should be compared at as near identical testing conditions as possible as the conditions at which the test or analysis is carried out affect the results. Oxygen Transmission Rate (OTR) and Water Vapor Transmission Rate (WVTR) are two of the most important parameters that affect food.

2.5.1 Oxygen Permeability

The transfer of oxygen from the environment to food has an important effect on food quality and shelf life. Oxygen causes food deterioration such as lipid and vitamin oxidation, leading to sensory and nutrient changes. Due to the large amount of hydrogen bonds biopolymer films are hydrophilic, which makes them excellent barriers to non-polar substances, such as oxygen and some aroma compounds [27].

This hydrophilicity makes their gas barrier properties very much dependent on the humidity conditions for the measurements. That is why the gas permeability of these materials may increase manifold when humidity increases. Olabarrieta [18] found that the modification of polymer structure combined with optimized selection of plasticizer may produce, at low to intermediate RH, biodegradable films with oxygen barrier properties that are as good as those of poly(vinylidene chloride) (PVDC) and ethylene vinyl alcohol copolymer (EVOH) films. (see Figure 2.10).

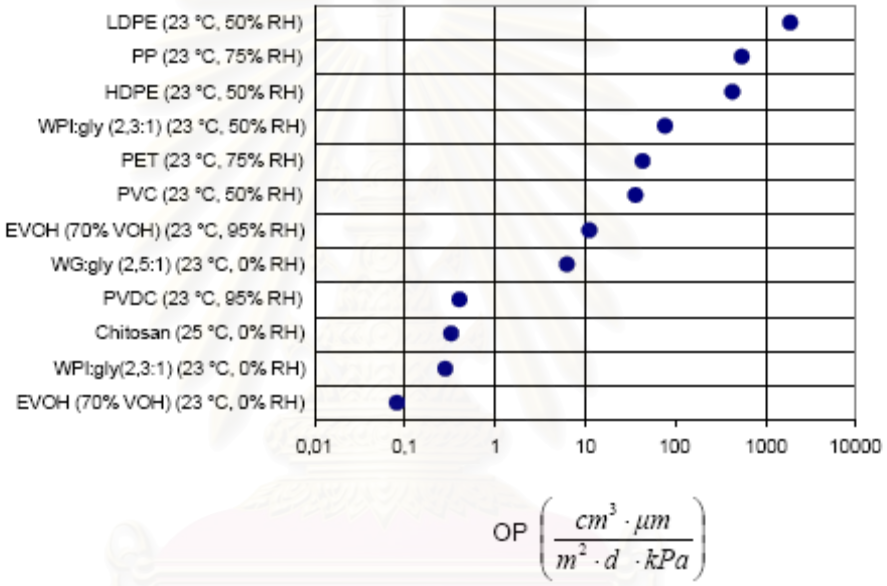

Figure 2.10 Comparison of Oxygen Permeability of Biobased Materials Compared to Conventional Synthetic Polymers [18]

(LDPE=Low-Density Polyethylene; PP=Polypropylene; HDPE=High-Density Polyethylene; WPI=Whey Protein Isolate; gly=glycerol; PET=Polyethylene Terephthalate; PVC=Polyvinyl Chloride; EVOH=Ethylene Vinyl Alcohol; WG=Wheat Gluten; PVDC=Polyvinylidene Chloride)

2.5.2 Variables Affecting Permeability

2.5.2.1 Chemical Structure of the Polymer

The chemical structure of the constitutional unit of polymer is the fundamental determinant of the barrier behavior of polymer. In addition to chemical composition, polarity, stiffness of the polymer chain, bulkiness of side and backbone-chain groups, and degree of crystallinity significantly impact the sorption and diffusion of penetrants, and hence permeability. Of particular significance are influences on the free volume and molecular mobility of the polymer, and influences on the affinity between the permeant and the polymer [5].

Table 2.8 shows some examples of the effect on oxygen permeability of functional groups attached to a vinyl polymer backbone, with structure shown in Figure 2.11.

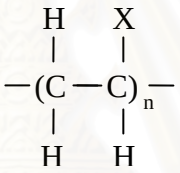

Figure 2.11 Structure Model of Polymer

Table 2.8 Effect of Functional Group X on Oxygen Permeability of Vinyl Polymers [5]

Functional Group, X	**Polymer**	**P (cc mil/m^2 day atm)**	**Comments**
H	HDPE	1,550-3,100	Nonpolar, very low cohesion between chains, tiny side group, high flexibility, high crystallinity
H	LDPE	3,900-5,400	Nonpolar, branched, less crystalline
CH_3	PP	2,300-3,900	Nonpolar, larger side group, stiffer than PE, lower crystallinity
C_6H_5	PS	3,900-6,200	Bulky side group, atactic, hinders packing, Noncrystalline
$COOCH_3$	PMA	265	Polarity produced by ester linkage, but bulky atactic side group hinders packing, noncrystalline
OH	PVOH	0.15	Strong polarity, hydrogen bonding between chains, crystalline
CN	PAN	0.60	Strong polarity, bulkier side group than OH, Noncrystalline
Cl	PVC	75-310	Strong polarity, less than PAN
F	PVF	45	More polar than PVC, smaller side group
$CH_2CH(CH_3)_2$	Poly-4-methyl pentene-1	62,000	Nonpolar, very bulky side group, amorphous

(Note: HDPE = High density Polyethylene, LDPE = Low density Polyethylene, PP = Prolypropylene, PS = Polystyrene, PMA = Polymethacrylate, PVOH = Poly(vinyl alcohol), PAN = Polyacrylonitrile, PVC = Poly(vinyl chloride), PVF = Poly(vinyl fluoride), Poly-4-methyl pentene-1 = Polymethyl-pentene)

2.5.2.2 Chemical Structure of the Permeant Molecule

The size of the permeant molecule, as well as the chemical affinity between the permeant and the polymer, is an important determinant of permeablity. Polymers can act as molecular sieves, allowing some molecules pass through rapidly while retarding the passage of others. This is the principle used industrially in polymer membrane separation of gas blends [5].

The effect of size on permeability is complex, because permeability is the product of diffusion and solubility. Larger permeant molecules generally have lower diffusivity than smaller ones, but higher solubility.

The effect of size on solubility is related to the dependence of solubility on vapor pressure. As size increases, the energy required to vaporize the molecule increases, so its vapor pressure decreases. For gases, the lower the vapor pressure, the greater is the tendency for the gas to remain dissolved in the liquid rather than converting to the gas form, so the greater the solubility. Of course, solubility is also strongly influenced by the chemical similarity between the solvent (the plastic) and the permeant.

The effect of size on diffusivity is more straightforward. The larger the molecule, the greater the amount of energy required to move it, and the greater the amount of energy required to create the large free volume necessary for it to have a place to move. Therefore, diffusivity decreases with increasing size.

The size of a permeant molecule is related to its molecular weight, but this is an inaccurate measure. The van der Waals diameter is a good measure for isotropic molecules, but many permeants of interest, such as n-alkanes, are strongly anisotropic.

Table 2.9 illustrates the effect of molecular size, as indicated by molecular weight, and of polarity, on the permeability of amorphous Poly(ethylene terephthalate) (PET).

Table 2.9 Effect of Molecular Size and Polarity on Permeability of Amorphous Poly(ethylene terephthalate) (PET) (P in cc cm/cm^2 s cmHg) [5]

Permeant	**MW**	**Polarity**	**Px10^{10}**
He	2	nonpolar	3.280
CH_4	16	nonpolar	0.090
N_2	28	nonpolar	0.013
O_2	32	nonpolar	0.040
CO_2	44	nonpolar	0.300
H_2O	18	polar	130.0

2.5.2.3 Effect of Temperature

Both diffusion and solubility are functions of temperature, and have been found to follow an Arrhenius type of equation [5]

$$\Gamma = \Gamma_0 e^{\frac{-E_\Gamma}{RT}} \tag{2}$$

where Γ represents either Diffusivity coefficient (D) or Solubility coefficient (S), Γ_0 is a proportionality constant (known as the pre-exponential term), E_Γ is the activation energy, R the gas constant, and T is absolute temperature. This equation also generally holds for P, which is the product of D and S. Equation 2 is valid over a relatively small range of temperatures. When a polymer passes through a transition, such as the glass transition temperature, there is a discontinuity, and a new relationship is needed.

Equation 2 can be rewritten specifically for change in permeability with temperature as follows:

$$P = P_0 e^{\frac{-Ep}{RT}} \tag{3}$$

where E_p is the activation energy, R the gas constant, P_0 is a pre-exponential term and T is absolute temperature. Activation energy is given in units of energy/mole, such as calories/mole or Joules/mole. The gas constant, R, has a variety of values depending

on the units chosen. A typical plot of equation 3 is shown in Figure 2.12. From this plot, the slope and intercept can be determined. The equation can then be used to predict the permeability at any temperature within the range of applicability.

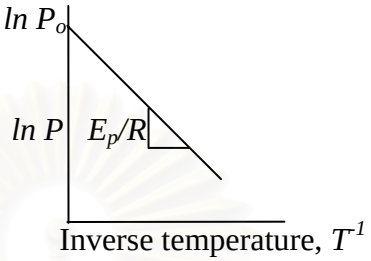

Figure 2.12 Permeability as a Function of Temperature [5]

The relationship between a P determined at one temperature and that at another temperature is as follows:

$$P_2 = P_1 e^{-\frac{E_p}{R}\left(\frac{1}{T_2}-\frac{1}{T_1}\right)} = P_1 e^{\frac{E_p}{R}\left(\frac{1}{T_1}-\frac{1}{T_2}\right)} \tag{4}$$

Equation (4) can be written as

$$P_2 = P_1 \text{ f} \qquad \text{where } f = e^{\frac{E_p}{R}\left(\frac{1}{T_1}-\frac{1}{T_2}\right)} \tag{5}$$

The factor f gives the ratio of P_2/P_1, i.e. by what factor the permeability coefficient changes when temperature varies from T_1 to T_2.

2.5.2.4 Effect of Humidity

Hydrophilic polymers such as polyamides and ethylene vinyl alcohol copolymer (EVOH), which contain polar groups and hydrogen bonding capability, strongly absorb water from humid air. Therefore, one can determine a water sorption isotherm for the polymer; that is, the equilibrium moisture content at any temperature and humidity condition. The presence of the water vapor in the polymer changes the permeation of other gases and vapors through the polymer. In most cases, the permeation rate increases with higher water sorption because the water acts as a plasticizer and increases the free volume of the polymer [5].

2.5.2.5 Effect of Permeant Concentration

The concentration of permanent gases below one atmosphere of pressure generally does not affect the permeability coefficient. However, strong effects have been observed on the permeability of organic compounds. The permeability of organic vapor such as aromas, flavors, and solvents is usually strongly dependent on concentration [5].

2.6 Processing Techniques

2.6.1 Extrusion

In nearly all applications of plastics in packaging, the first step is to convert the solid plastic, usually in pellet form, into a melt. This melt can then be shaped using heat and pressure into a useful form. The equipment used to do this is an extruder. It is used for film and sheet, and it is part of a blow molder for bottles, and of an injection molding machine for injection molded or injection blow molded packaging. The extruders used in all of these applications work in a similar manner, but they deliver the melt to the shaping operation differently.

The purpose of an extruder is to use heat, pressure, and shear to transform the solid plastic into a uniform melt, for delivery to the next stage of processing. It frequently involves mixing in additives such as color concentrates, blending resins together, and incorporating regrind (Regrind is the granulated scrap from the conversion process). The final melt must be uniform in temperature and in composition. Because single screw extruders are often not very good mixers, an additional mixing device may be needed. The pressure of the melted viscous polymer as it exits the extruder must be high enough to force it through a die to produce a desired shape, or to force it into a mold chamber.

The extruder accomplishes all this by using a *barrel*, a hollow tube, containing a *screw* with helical channels. A simplified extruder diagram is shown in Figure 2.13. The screw is generally divided into three sections: (1) the solids conveying section, (2) the compression or melting section, and (3) the metering or pumping section. The standard single screw extruder has a right-hand helix on the screw, and the screw rotates in the counterclockwise direction. The basic screw design has only a single flight, but other designs have double flights along part or all of the screw length.

Other important components are the hopper, which feeds the plastic or other components into the extruder through the feed port, and the die or nozzle, through which the melted plastic exits the extruder.

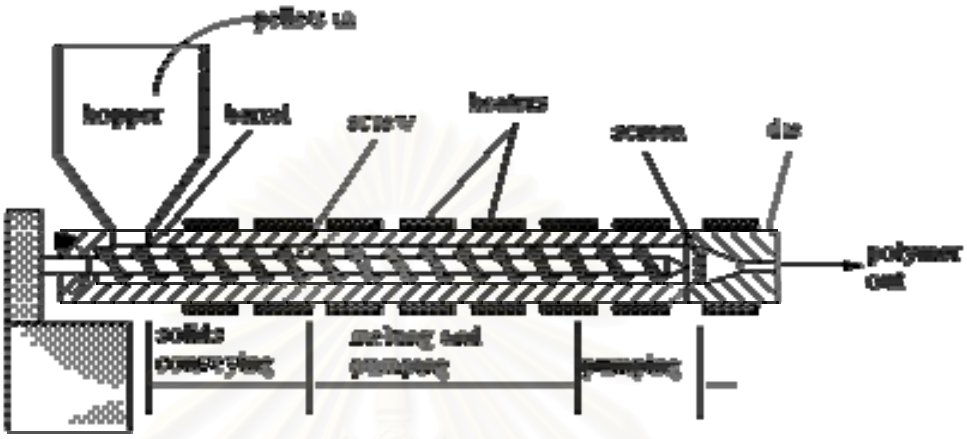

Figure 2.13 Extruder (Change in Screw Diameter Exaggerated) [5]

2.6.1.1 Blown Film

Blown film extrusion is a continuous process in which the polymer is melted, the melt is forced through an annular die, and the resulting tube is inflated with air into a “bubble” and cooled (Figure 2.14). Air is always blown on the outside of the bubble to cool the film; to increase production rates, internal bubble cooling can also be used. The film is stretched in the longitudinal and circumferential directions during production, resulting in biaxial orientation of the film. The amount and relative degree of stretching determine the degree of orientation. The circumferential stretching is inherent in the blowing process. Longitudinal stretching is imparted by drawing of the film between the extruder and the nip rolls.

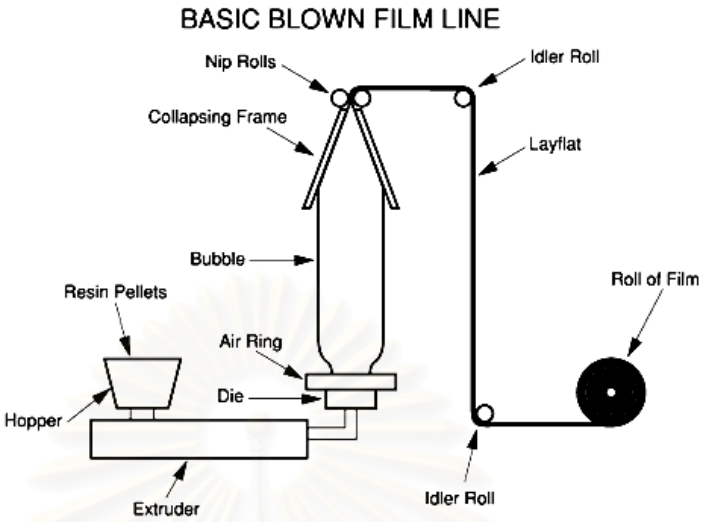

Figure 2.14 Production of Blown Film [28]

The principal polymers used in blown film production are polyolefins, although other polymers can also be used. The major applications are those that require biaxial strength, and include bags of all kinds, as well as agricultural and construction film. In food packaging, coextruded structures with three to five layers, or even more, are common, with major markets including packaging for cereal, meat, snacks, and frozen foods.

The properties of the film are determined by the *blow-up ratio* and the linear line speed. The blow-up ratio is the ratio between the diameter of the final tube of film and that of the die. The internal air pressure that expands the tube into the bubble is typically supplied through a port into the mandrel, the interior part of the die. Once the process is running steadily, little air is usually lost, so make-up requirements are small. When internal bubble cooling is used, air is constantly being exchanged inside the bubble.

The travel of the film through the blown film tower is aided by various guiding and sizing devices. The film turns from molten to semi-solid at the "frostline" but is still easily deformed as it moves up the tower. However, the orientation of the film is generally complete at this point. When the film is cool enough, the bubble is collapsed by plates and rollers (pinch rollers), and wound up, with or without slitting, gusseting, or other treatment. Thus, the blown film process can produce tubular as well as flat film.

2.7 Characterization of Nanocomposites

2.7.1 X-Ray Diffraction (XRD)

This very important experimental technique has long been used to address all issues related to the crystal structure of bulk solids including lattice constants and crystallography, identification of unknown materials, orientation of single crystals and preferred orientation of polycrystals, defects, stresses, etc. X-ray methods are nondestructive and do not require elaborate sample preparation or film removal from the substrate [29].

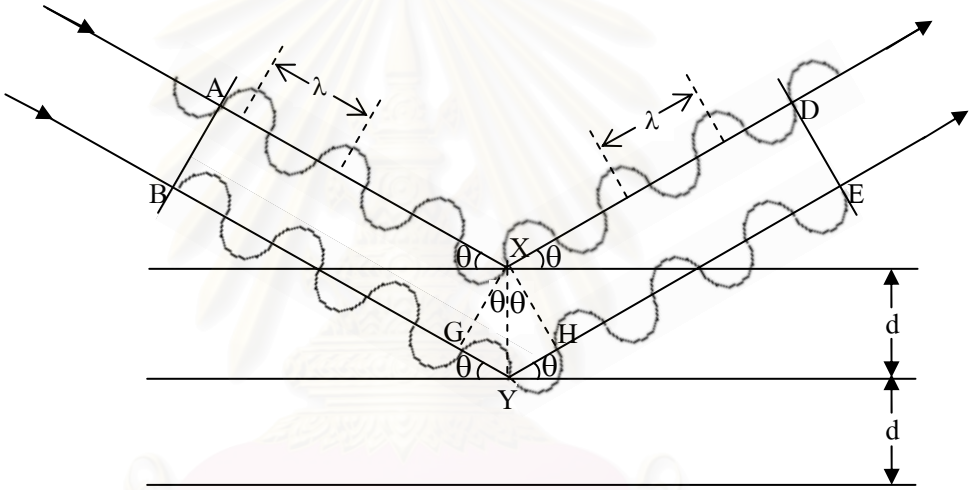

Figure 2.15 The Bragg Condition

From above image (Figure 2.15), the two reflected rays, XD and YE, will constructively interfere when the path difference is equal to the wavelength (λ) or a multiple of it. Thus the condition for X-ray diffraction is

$$2d \sin \theta = n \lambda \qquad (6)$$

where n is an integer (1, 2, 3, etc.) called the order of reflection and d = distance of plate. Equation 6 is known as the *Bragg Equation*. Figure 15 shows the Bragg condition when n = 1, so the path difference equals one wavelength, shown in Equation 7,

$$GY + YH = \frac{\lambda}{2} + \frac{\lambda}{2} \qquad (7)$$

2.7.2 Transmission Electron Microscopy (TEM)

The transmission electron microscopy (TEM) is indispensable for the structural imaging of nanometer-sized features. In comparison, the resolution of the Scanning Electron Microscope (SEM) is about an order of magnitude poorer. As its name implies, the TEM is used to obtain structural information from specimens thin enough to transmit electrons. Thin film are, therefore, ideal for study but the must be removed from electron-impenetrable substrates prior to insertion into the TEM [29].

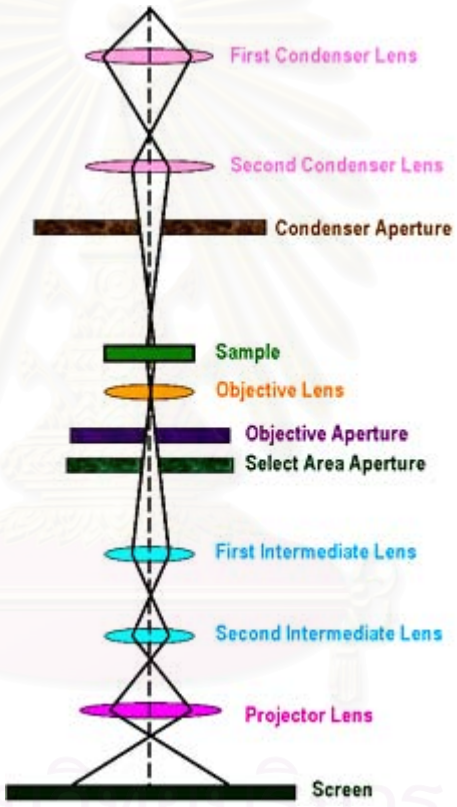

Figure 2.16 Structure and Equipment of TEM [30]

As a gross simplification, the TEM may be compared to a slide projector with the slide (specimen) illuminated by light (electron beam) that first passes through the condenser lens (electromagnetic condenser lens). The transmitted light forms an image that is magnified by the projector lens (electromagnetic objective and projector lenses) and viewed on a screen (or photographed) as shown in Figure 2.16. In operation, electrons are emitted from the gun and typically accelerated to anywhere from 125 to 300 keV or higher (e.g. 1 MeV) in some microscopes. High

magnification in TEM method is a result of the small effective wavelengths (λ) employed according to the deBroglie relationship

$$\lambda = h/(2mqV)^{1/2} \quad (8)$$

where m and q are the electron mass and charge, h is Planck's constant value of 6.62618×10^{-34} J·s, and V is the potential difference.

2.7.3 Oxygen Permeation Analyzer: Oxygen Transmission Rate (OTR)

The OTR is a rate at which the volume of oxygen that pass through a unit thickness of material per unit area per unit time per unit barometric pressure, following ASTM D-3985, ISO 15105-2, DIN 53380, or JIS K-7126.

In the OTR machine, the test specimen is held such that it separates two sides of a test chamber. One side (lower half of chamber) is exposed to a nitrogen (oxygen-free carrier gas) atmosphere while the other (upper half of chamber) is exposed to an pure oxygen (99.9%) atmosphere. A coulometric sensor monitoring the exit port of the nitrogen side measures the amount of oxygen present. Testing is complete when the concentration of oxygen in the nitrogen side atmosphere is constant [31], as shown in Figure 2.17.

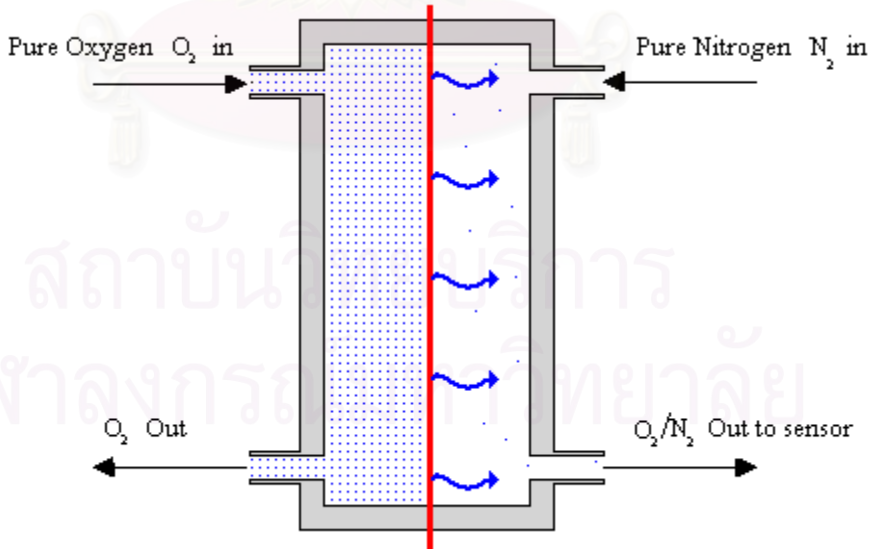

Figure 2.17 Oxygen Permeability Test [32]

2.8 Modeling of Barrier

Polymer nanocomposites have been intensely researched in the last few decades since the addition of a small quantity of reinforcement fillers (up to 10 wt%) such as clays in the polymer matrix have led to improvements of mechanical and barrier properties. Barrier property improvements, in particular, have made polymer/clay nanocomposites a promising technology for a multitude of packaging applications. The presence of silicate layers in nanocomposites improves the gas barrier properties of the nanocomposites by reducing the polymer volume accessible for gas transport and also by creating a tortuous path for the diffusing species.

Several factors such as silicate dispersion and orientation must be taken into account to achieve reasonable predictions for the behavior of nanocomposites. Gas barrier in polymer clay nanocomposites was traditionally explained in terms of Nielsen model, originally adopted to describe the tortuosity effect of plate-like particulates on gas permeability of polymer filled composite structures. Nielsen model [33] predicted the effect of filler composition on gas permeability in the model system consisting of uniform platelets homogeneously dispersed in the polymer matrix and oriented parallel to the polymer film surface. When this structural assumption is met, the model typically shows a good agreement with experimental data as in the case of polymer films or thin sheets with plate-like particulates (talc, mica, metal flakes) added to increase gas barrier. Parallel platelet orientation presumably gives a better gas barrier performance as compared to random platelet orientation, as shown schematically in Figure 2.18. Recently, Bharadwaj [34] modified the Nielsen model to predict gas barrier in the case of randomly dispersed silicates. However, the model was reported to over estimate the actual aspect ratio of the fillers.

Figure 2.18 Model of Gas Barrier Enhancement [11]

2.8.1 Nielsen Model

Nielsen model [33] predicts the effect of filler composition on gas permeability in the model system consisting of uniform platelets homogeneously dispersed in the polymer matrix and oriented parallel to the polymer film surface. The model is given in equation (9). In the equation, P_c is the permeability of the nanocomposite, P_m is the permeability of the pure polymer, and ϕ_f is the volume fraction of the clay. L and W are length and width of the clay sheets, respectively; its ratio, L/W, defines the aspect ratio, of the fillers. The model assumes that the fillers are impermeable to the diffusing gas or liquid molecule, and are oriented perpendicular to the diffusion direction. Thus, the presence of the filler particles creates a tortuous path for the permeant to travel through the composites. The denominator on the right hand-side of equation (9) is also referred to the tortuousity factor, τ, defined as the distance a molecule must travel to get through the film (d') divided by the thickness of the film (d). Figure 2.19 illustrates Nielsen's approach.

$$\frac{P_c}{P_m} = \frac{1-\phi_f}{1+\frac{L}{2W}\phi_f} \tag{9}$$

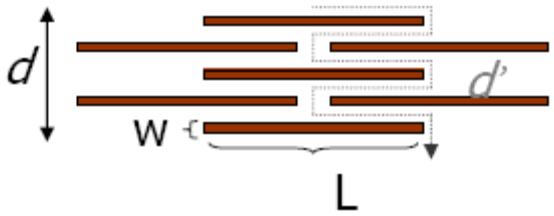

Figure 2.19 Path of the Diffusing Gas Molecule through Polymer Containing Clay Platelets in Nielsen Model [33]

Polymer clay nanocomposites exhibit improved barrier properties compared to their polymer matrix. In Figure 2.19, the random pathway of a gas molecule through a composite filled with high aspect ratio particle is shown, the pathway becomes much larger due to the presence of filler.

The Nielsen model does not take into account Brownian motion and assumes impermeability of the filler for the gas as well as perfect alignment of the mineral conclusions. The ratio of permeability coefficient of the composite P_c to the one of the polymer matrix P_m, is given by

$$\frac{P_c}{P_m} = \frac{\phi_m}{\tau} \tag{10}$$

where ϕ_m is the polymer volume fraction and τ is the increase of the pathway length of the diffusing particle which is given by

$$\tau = \frac{d'}{d} \tag{11}$$

d' describes the path length of the diffusing particle and *d* the thickness of the membrane. With perfect alignment and a rectangular shape of the filler, *d'* can be described with

$$d' = d + d \cdot \frac{L}{2 \cdot W} \cdot \phi_f \tag{12}$$

where *L* is the length of the inclusion and *W*, its width. ϕ_f describes the filler volume fraction. Combining Equation 11 and 12, τ can be written as

$$\tau = 1 + \frac{L}{2 \cdot W} \cdot \phi_f \tag{13}$$

where *L/W* equals the aspect ratio of the filler. Using this and Equation 13 in Equation 10 we obtain an expression for the decrease of the permeability, depending on the filler volume fraction and the aspect ratio.

$$\frac{P_c}{P_m} = \frac{\phi_m}{1 + \frac{L \cdot \phi_f}{2W}} \tag{14}$$

2.8.2 Bharadwaj Model or Modified Nielsen Model

Bharadwaj [34] modified Nielsen model to incorporate an orientation parameter S, in which a range of relative orientations of the clay sheets with respect to each other represented by θ (the angle between the direction of preferred orientation and the sheet normal) could be applied. Bharadwaj's expression is shown in equation (15) accompanied by orientation parameter in equation (16):

$$\frac{P_c}{P_m} = \frac{1 - \phi_f}{1 + \frac{L}{2W}\phi_f\left(\frac{2}{3}\right)\left(S + \frac{1}{2}\right)} \tag{15}$$

$$S = \frac{1}{2}\left(3\cos^2\theta - 1\right) \tag{16}$$

In the case of random platelet orientation (S = 0), the tortuousity decreases with orientation and diffusion is facilitated as opposed to parallel orientation (S = 1 or Nielsen model).

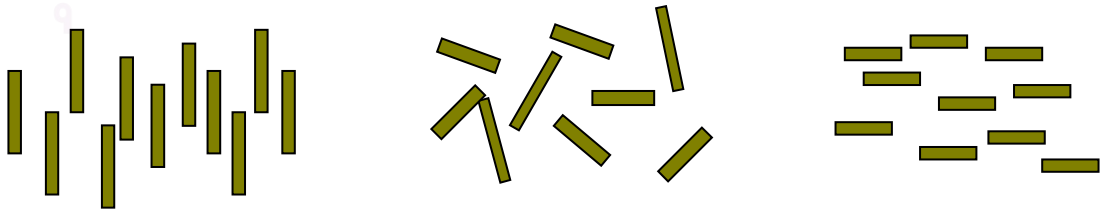

S = -0.5 S = 0 S = 1

Figure 2.20 Example of Degree of Orientation of Filler in Composites

2.9 Least Square Fitting of Discrete Point

2.9.1. Curve Fitting

The nature of most experimental data are such that the data typically include noises due to many different effects [35]. The values of dependent variables obtained from experiments can vary even though all the independent variables are constant. Therefore, the estimation of the relationship of the dependent variables with respect to the independent variables is needed. This process is called regression or curve fitting. Different estimated equations can satisfy the same raw data. However, the equation or curve with a minimal deviation from all data points is desirable. This desirable best-fitted equation can be obtained by the least square method which requires that the sum of the square of deviations of the values predicted by the estimated equation from the given set of experimental data should be minimal.

2.9.2. Least Square Method

For the following experimental data points, y_i for $i = 1,..., n$ in which n is the total number of data points, the following properties of the data can be calculated as follows:

Average $\left(\bar{y}\right)$ $\quad \bar{y} = \dfrac{\sum y_i}{n} \qquad i = 1,..., n$

Standard deviation $\left(S_y\right)$ $\quad S_y = \sqrt{\dfrac{S_t}{n-1}}$

or Variance $\left(S_y{}^2\right)$ $\quad S_y{}^2 = \dfrac{S_t}{n-1}$

where S_t is summation of the squares of difference between any data point with the average and is given by

$$S_t = \sum \left(y_i - \bar{y}\right)^2$$

For any calculated data generated by the desired equation, $y_{cal,i}$ for $i = 1,..., n$ in which n is the total number of data points, the summation of the squares of the residuals between the calculated values and the experimental values, S_r, can be obtained as

$$S_r = \sum \left(y_{cal,i} - y_i\right)^2$$

And the standard deviation between experimental data and calculated values generated from the regression line can be determined as

$$S_{y/x} = \sqrt{\frac{S_r}{n-2}}$$

where $S_{y/x}$ = standard error of the estimation

y/x = error value of y at x

Figure 2.21 below shows example of residuals between the experimental data points (represented as dots) and the calculated values generated from the desired equation (represented as dashed line) for the case of linear equation.

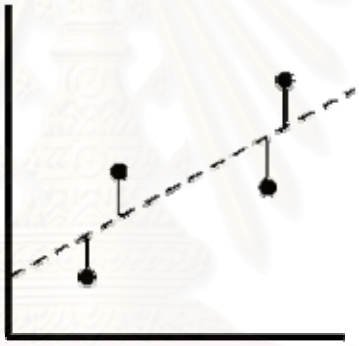

Figure 2.21 The Vertical Distance between Data Point and the Straight Line represents The Residual in Least Square Regression

The best-fitted equation is the equation where the sum of square of residuals is minimal. The quality of best-fitted can be determined from the coefficient of determination as the following

$$r^2 = \frac{S_t - S_r}{S_t}$$

where r^2 = coefficient of determination

$r = \sqrt{r^2}$ = correlation coefficient

If r^2 = 1, it means that the estimated equation perfectly fit all experimental data points. If r^2 = 0, it means that there is no relationship between the estimated equation and the experimental data.

CHAPTER III

LITERATURE REVIEWS

3.1 Influence of Compatibilizer on Exfoliation of Nanocomposites

Balazs et al. [37,38] had considered the surfactant chains (SFC) in order to investigate the factors promoting the penetration of polymers into layered silicates. They varied properties related to the nature of tethered surfactant chains. They found out that an increase in the surfactant length (approaching the length of the polymer chains) improved the layers separation by allowing the polymer to adopt more conformational degrees of freedom. On the contrary, increase in the length of polymer chains tended to render the interlayer mixture immiscible.

Wang et al. [39] investigated the effects of alkylammonium modifier to clay (montmorillonite) and the maleic anhydride (MA) grafted level of polyethylene on morphology of maleated polyethylene/clay nanocomposite prepared by simple melt compounding. The treatment surfactants for organoclays were dimethyl dihydrogenated tallow ammonium ions types of C12M, C16M and C18M with different alkylammonium chain lengths. Also, an organophilic clay, 20A, had two long alkyl chains. Several types of nanocomposites with different compositions of the organically modified clays and maleated polyethylene were prepared by melt compounding at 140 ^{o}C , using Brabender mixer with the chamber size of 50 cm^3. Screw speed was 60 rpm and the mixing time was 20 min for all the cases. The X-ray diffraction patterns of organophilic clays were analyzed, which the interlayer distance was determined by the diffraction peak in the X-ray method, using the Bragg equation. The X-ray pattern showed clearly that the interlayer spacing increases with the increase in size of alkylamine chain length. The interlayer spacings of C12M, C16M, C18M and 20A were 1.36, 1.79, 1.85 and 2.47 nm, respectively. They concluded that these spacings were related to the successful modification of MMT. The longer the chain length of the modifier, the larger the interlayer spacing becomes.

Hongbo et al. [40] studied effect of polymer matrix on exfoliation in polymer nanocomposites. Polyethylene was chemically modified by grafting maleic anhydride

(MA) monomer on its backbone. Then the melt-direct intercalation method was employed to prepare two kinds of nanocomposites, polyethylene (PE)/organic montmorillonite (Org-MMT) and maleic anhydride grafted polyethylene (PE-g-MA)/ Org-MMT nanocomposites, which organic montmorillonite (Org-MMT) was modified by C18 alkyl trimethyl ammonium chloride (C-18). In the first experiment, polyethylene and org-MMT were melt mixed on the two rollers for 10 min at a temperature of 175 ^{o}C. The mixture was press molded to get a plate of 4 mm thick. The content of Org-MMT was set as 0, 1, 3, 5 wt% and the acquired materials were defined as PE, PE1, PE3 and PE5, respectively. The graft copolymer (PE-g-MA) and organic montmorillonite were melt mixed on the same procedure as above and the materials were named as PEM, PEM1, PEM3 and PEM5, correspondingly. X-ray diffractometry (XRD) was used to investigate the intercalation effect and transmission electron microscopy (TEM) to observe the dispersion of Org-MMT interlayers in matrices. The results showed that, for the PE/Org-MMT nanocomposites, the intercalate effect was limited and the dispersion of clay in the system was unsatisfactory. However, for the PE-g-MA/Org-MMT nanocomposites, MMT was exfoliated in the matrix, which was testified by XRD and TEM.

Morawiec et al. [41] studied preparation of nanocomposites based on low density polyethylene, containing 3 or 6 wt% of organo montmorillonite nanoclay which was octadecyl amine modified (MMT-ODA) and low density polyethylene grafted maleic anhydride (PE-g-MA) as a compatibilizer. The nanocomposites were prepared by melt mixing and characterized. The compositions of LDPE/PE-g-MA/MMT-ODA were prepared in the Brabender internal mixer in two steps mixing procedure. First, PE-g-MA/MMT-ODA masterbatch was prepared by mixing PE-g-MA with the clay in weight proportion of 2:1, at 160 ^{o}C, for 20 min, at the speed of 60 rpm. In the second step, the masterbatch was blended with LDPE at 190 ^{o}C for 20 min, at 60 rpm. Two compositions of LDPE/PE-g-MA/MMT-ODA were prepared, having the weight proportion of 91:6:3 and 82:12:6. A composite of 94 wt% LDPE with 6wt% of MMT-ODA and also a blend of LDPE with 13 wt% of PE-g-MA were also obtained for comparison in one step blending at 190 ^{o}C, for 20 min, at 60 rpm. Pure LDPE was also processed in the same way. Exfoliation of silicate layers was achieved. In both compatibilized compositions the peak significantly decreased,

indicating good exfoliation of MMT-ODA clay in the polyethylene matrix, although the exfoliation was less complete in LDPE/PE-g-MA/MMT-ODA 82:12:6 wt% than in LDPE/PE-g-MA/MMT-ODA 81:6:3 wt%. The LDPE/MMT-ODA 94:6 wt% sample resulted in partly exfoliation.

Sung et al. [42] investigated the gas permeability and dispersion behavior of nanoparticle in linear low density polyethylene/montmorillonite nanocomposite as a function of compatibilizer and processing conditions. LLDPE/PE-g-MA/MMT nanocomposites were mixed simultaneously and compounded using internal mixer or co-rotating twin screw extruder. Concentration of MMT was varied from 1 to 5 wt%. For internal mixer, rotor speed was 80 rpm and mixing time was 20 min. Processing temperature was 170 °C. For twin screw extruder (D= 25 mm and L/D=30), barrel temperatures were 150 – 170 °C under various throughput rate. The amount of PE-g-MA was based on LLDPE, while MMT concentration was based on PE-g-MA/LLDPE mixture. XRD and TEM were used to evaluate the degree of intercalation/exfoliation of montmorillonite. Significant changes of dispersion behavior of montmorillonite were observed depending on the processing conditions and concentration of compatibilizer. The interlayer distance of LLDPE/PE-g-MA/MMT nanocomposites were measured using X-ray diffraction. Little increase of interlayer distance was observed for uncompatibilized LLDPE/MMT nanocomposite which indicated that the intercalation of MMT was not significant. Maleic anhydride grafted polyolefin's have been known as an excellent compatibilizer to improve the dispersion of MMT in polyolefin/MMT systems. Increasing interlayer distance of MMT is observed with the concentration of PE-g-MA's. It is observed that degree of exfoliation of MMT was strongly dependent on the concentration of PE-g-MA and the concentration of grafted maleic anhydride in PE-g-MA. Improved intercalation is obtained with increasing concentration of PE-g-MA's, while exfoliation begins at different concentration of PE-g-MA depending on the concentration of grafted maleic anhydride. For PE-g-MA, intercalation behavior was observed at 5 wt% and exfoliation behavior was observed at 10 wt%.

Nitrogen, oxygen and carbon dioxide barrier characteristics of nanocomposite with various concentration of MMT were determined. Gas barrier property was improved with increasing concentration of PE-g-MA for all gases and was attributed

to the improved dispersion of MMT. In conclusions, LLDPE/montmorillonite nanocomposites with/without maleic anhydride grafted polyethylene were prepared using melt blending. Melt blending was done by internal mixer or co-rotating twin screw extruder. Interlayer distance of MMT increased with concentration of PE-g-MA and also concentration of grafted maleic anhydride of PE-g-MA. Gas barrier property was enhanced with increasing concentration of PE-g-MA and was attributed to the improved intercalation/exfoliation. Twin screw extruder induced better intercalation/exfoliation behavior than internal mixer

3.2 Gas Permeability on Polymer/Clay Nanocomposites

Choi et al. [43] studied the effect of the sonication to the suspension of organoclay in N,N'-Dimethyl formamide (DMF) in polyurethane/clay nanocomposites. The polyurethane and polyurethane/clay nanocomposites were synthesized by one-shot process. To control the dispersibility of organoclay in polyurethane matrix, the sonication was applied to the suspension of organoclay in 1, 3 and 5 wt% based on polyurethane/clay nanocomposites in DMF either for 0 min or for 60 min by sonicator. The aggregate clay particles ranging from 10 to 100 μm were broken into fine clay particles below 10 μm by the sonication. Therefore, they found sample which was sonicated for 60 min to better disperse than the sample which was not sonicated. The d-spacing of organoclay was found to be 2.29 nm compared to 1.18 nm of Cloisite$^{®}Na^{+}$. The polyurethane/clay nanocomposites formed the intercalated structure with some disorder and their d-spacing was about 2.6-2.7 nm. The barrier properties significantly increased with increasing dispersibility of organoclay. They suggested that gas permeability can depend on length, orientation and degree of delamination of layered silicate. Degree of delamination could be increased and the tortuous path for a diffusing penetrant could also be increased by the sonication.

Hotta and Paul [44] studied the effect of number of alkyl groups in surfactant treatment on degree of dispersion in LLDPE/LLDPE-g-MA/organoclay nanocomosites. Nanocomposites were formed by melt compounding each organoclay with LLDPE and/or LLDPE-g-MA using a corotating twin-screw extruder with the barrel temperature set at 200 ^{o}C. The screw speed and feed rate were at 280 rpm and

1.0 kg/h, respectively. LLDPE and LLDPE-g-MA were dried in a vacuum oven at 80 ^{o}C for a minimum of 16 h prior to extrusion. The exact amount of montmorillonite (MMT) in each nanocomposite was determined by burning the extruded pellets in a furnace at 900 ^{o}C for 45 min and weighing the residual MMT ash. The resulting value was corrected for loss of structural water that occurred during the incineration. They found that two alkyl tails, Dimethylbis(hydrogenated-tallow) ammonium montmorillonite [$M_2(HT)_2$], exhibited better dispersion than nanocomposites based on the organoclay having one alkyl tail, Trimethyl(hydrogenated-tallow) ammonium montmorillonite [$M_3(HT)_1$]. The gas permeability of the nanocomposites derived from the organoclay having two alkyl tails, $M_2(HT)_2$, were investigated. Permeability properties were measured for O_2, N_2 and CO_2. When experimental data were fitted with Nielsen model, they found that the experimental data closely matched this model for an aspect ratio of 5, but image analysis results from TEM were in the range of 9-10.

Wang et al. [45] studied the influence of fillers on free volume and gas barrier properties in styrene-butadiene rubber of layered silicate clay of rectorite and conventional composite materials N326 (carbon black)/SBR. Natural rectorite was dispersed in water with strong stirring for 5 hr and an aqueous suspension of silicate was achieved. To purify natural rectorite, the aqueous suspension was kept for 24 hr at room temperature. They obtained rectorite/SBR nanocomposites by blending SBR and N326 (a type of carbon black) named N326/SBR at different amount of the filler content. The gas permeabilities of rectorite/SBR and N326/SBR were analyzed. At the highest filler concentration examined, the gas permeabilities of rectorite/SBR and N326/SBR permeability were 68.8% and 39.0% lower than that of pure SBR, respectively. The reduction in gas permeability of rectorite/SBR was greater than that of N326/SBR, which was attributed to their plate-like morphology and high aspect ratio. The predictions of the Neilson equation for a particle aspect ratio were 1 and 30, respectively. In conclusion, incorporation of nanolayers of rectorite effectively improved gas barrier property which were attributed to the tortuous diffusional path and lower fractional free volume. The large difference in permeability reduction between rectorite/SBR and N326/SBR was mainly attributed to tortuous diffusional path effects.

CHAPTER IV

EXPERIMENTAL WORK

4.1 Materials

4.1.1 Low Density Polyethylene (LDPE)

LDPE (film grade) was provided by CCC Chemical Commerce Co., Ltd., Thailand. The melt flow rate, density and melting point are 5.0 g/10min, 0.919 g/cm^3 and 110 ^{o}C, respectively. The physical properties of polymer are shown in Table 4.1.

Table 4.1 Physical Properties of Low Density Polyethylene [CCC Product Data Sheet]

Physical Properties	**Unit**	**Testing Method**	**LDPE grade : LD1905F**
Melt Flow Rate	g/10min	ASTM D 1238	5.0
Density	g/cm^3	ASTM D 1505	0.919
Tensile Strength At Break	kg/cm^2	ASTM D 638	MD:210, TD:170*
Elongation At Break	%	ASTM D 638	MD:200, TD:720*
Elmendorf Tear Strength	g/25 micron	ASTM D 1922	MD:370, TD:210*
Dart Impact Strength	g	ASTM D 1790	105*
Haze	%	ASTM D 1003	6*
Gloss	%	ASTM D 2457	85*
Flexural Modulus	kg/cm^2	ASTM D 790	2,100
Hardness, Shore D	-	ASTM D 2240	46
Vicat Softening Point	^{o}C	ASTM D 1525	90
Melting Point	^{o}C	ASTM D 2117	110
Brittleness Temperature	^{o}C	ASTM D 746	<-70

Note: *Properties of film at 38 micron (B.U.R. 2:1), MD = machine direction, and TD = transverse direction.

4.1.2 Organoclay (Org-MMT)

Organoclay used was Bentone SD-1 as obtained from Connell Bros. Co., Ltd., Thailand. It is Montmorillonite clay treated with surfactant. The inorganic content is at 49.55 wt%. (Note: The inorganic content of clay was determined in this work by burning the organoclay in the oven at 1000 ^{o}C for 120 min and measured the residual MMT ashes). The average aspect ratio is 159. The platelet density is 2.83 g/cm^3 [9].

4.1.3 Compatibilizer

Compatibilizer used was DuPont^{TM}Fusabond$^{®}$ E MB226D polyethylene-graft-maleic anhydride (PE-g-MA), obtained from DuPont Packaging & Industrial Polymers, Bangkok, Thailand (local supplier). The maleic anhydride modified polyolefin content is more than 99% and maleic anhydride residual is less than 0.1%. The melt flow rate and density are 1.5 g/10min and 0.93 g/cm^3, respectively. The characteristics of the compatibilizer are shown in Table 4.2.

Table 4.2 Characteristics and Properties of Polyethylene-graft-Maleic Anhydride [Dupont Data Sheet]

Description		
DuPont™Fusabond® E MB226D is a chemically modified polyethylene.		
Product Characteristics		
Processing Method	* not yet determined	
Material Status	* Commercial: Active	
Availability	* Globally	
Uses	* not yet determined	
Manufacturer / Supplier	* DuPont Packaging & Industrial Polymers	
Properties		
Physical	**Nominal Values**	**Test Method**
Density	0.93 g/cm^3	ASTM D1505
Melt Flow Rate	1.5 g/10 min (at 190 ^{o}C/2.16 kg)	ASTM D1238 – ISO 1133
Thermal	**Nominal Values**	**Test Method**
Brittle Temperature	-70 ^{o}C (-94 ^{o}F)	ASTM D746
Melting Point	120 ^{o}C (248 ^{o}F)	ASTM D3418 – ISO 3146
Vicat Softening Point	103 ^{o}C (217 ^{o}F)	ASTM D1525 – ISO 306
Heat Deflection Temperature	41 ^{o}C (106 ^{o}F)	ASTM D648
Hardness	**Nominal Values**	**Test Method**
Durometer Hardness (D)	60	ASTM D2240 – ISO 868

4.2 Equipments

4.2.1 Twin screw extruder (Thermo Haake PTW 16/15 and 16/25)

4.2.2 Oven

4.2.3 Desiccator

4.2.4 Furnace (Barnstead Thermolyne, model 48000)

4.2.5 Analytical balance (Mettler Toledo, model AG204)

4.2.6 Digital Micrometer (Mitutoyo)

4.2.7 Oxygen Permeation Analyzer (Illinois, model 8500)

4.2.8 X-ray Diffraction (XRD) (Bruker AXS, model D8)

4.2.9 Transmission Electron Microscopy (TEM) (JEOL, model JEM 2010)

4.3 Experimental Procedures

4.3.1 Preparation of Nanocomposite Films

All materials were dried at 100 ^{o}C for 24 hr at least in oven before processed. The LDPE/PE-g-MA/Org-MMT nanocomposites were prepared in the twin screw extruder (ThermoHaake PTW 16/15 and 16/25) in three-step mixing procedure.

First, PE-g-MA/Org-MMT masterbatch was prepared by mixing PE-g-MA with the organoclay in weight proportion of 4:1 in the twin screw extruder. The temperature profile of the screw from hopper to die zone was set at TE1=130 ^{o}C, TE2=140 ^{o}C, TE3=155 ^{o}C, TE4=170 ^{o}C, TD1=180 ^{o}C, TD2=190 ^{o}C. The metering feed rate was at 50; the screw speed was at 90 rpm. The extrudates were pelletized (Figure 4.1a) with multistrand die as shown in Figure 4.1c at 140 rpm. Due to different particle sizes between PE-g-MA and Org-MMT and hence, to ensure uniform concentration throughout the melt mixing process, PE-g-MA and Org-MMT at 4:1 weight ratio at a total weight of 40 g were mixed in the small can first and then was added sequentially into the hopper.

Secondly, the master batch was blended with appropriate amount of LDPE at the same extruder conditions. Different compositions of LDPE/PE-g-MA/Org-MMT were prepared as shown in Table 4.3. Total weight of each composition was 400 g. The extrudates were pelletized at 140 rpm.

Lastly, the resins obtained from the second step were melted again in the extruder at the same condition and blown into films using the blown film setup (Figures 4.1b and 4.1d). The films of each composition were drawn at the same draw down ratio (DDR) to produce thin films with thickness between 30-60 μm.

(a) Melt Mixing Setup

(b) Blown Film Setup

(c) Multistrand Die for Pellet

(d) Blown Film Die for Film

Figure 4.1 Twin Screw Extruder and Die

The fraction of each component were shown in Table 4.3.

Table 4.3 Compositions of Materials in each Batch

Sample Code*	**Polymer (LDPE) (wt%)**	**Compatibilizer (PE-g-MA)(wt%)**	**Filler Organo MMT (wt%)**
100/0/0	100	0	0
91/9/0	91	9	0
90/9/1	90	9	1
89/9/2	89	9	2
88/9/3	88	9	3
87/9/4	87	9	4
85/9/6	85	9	6
81/9/10	81	9	10

* x/y/z denoted the wt% of LDPE, PE-g-MA and Org-MMT, respectively.

The exact amount of montmorillonite (MMT) in each nanocomposite was determined by burning the extruded pellets obtained in the second step in a furnace at 1000 ^{o}C for 120 min and weighing the residual MMT ashes.

4.3.2 Characterization

4.3.2.1 X-ray Diffraction (XRD) Spectrometer

Gallery spacing between clay platelets of the Org-MMT and nanocomposite films were measured by X-ray diffraction. The machine was Bruker AXS Model D8, and located at the Scientific and Technological Research Equipment Centre, Chulalongkorn University (Figures 4.2-4.4). The CuKα radiation of wavelength 1.542 Å was used. The voltage and the current of X-ray tubes were 40 kV and 40 mA, respectively. The scanning was done with a step size of 0.025^{o} in 2θ. An scanning time of 1 second/step in the range of 0.4^{o} to 8^{o} in 2θ were used. Each sample film was cut to about 1x1 cm, and then put into glass base (sample block of XRD measurement) for analysis with X-ray.

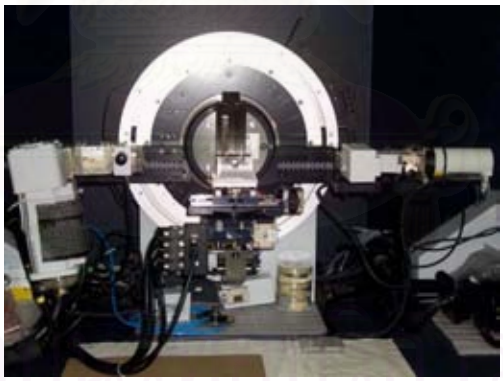

Figure 4.2 X-ray Diffraction Spectrometer (inside)

Figure 4.3 X-ray Diffraction Spectrometer (outside)

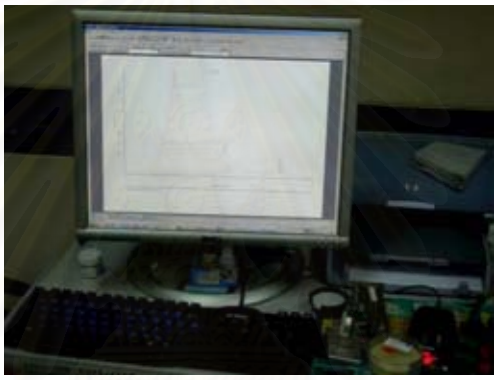

Figure 4.4 Computer supported X-ray Diffraction

4.3.2.2 Transmission Electron Microscope (TEM)

Transmission Electron Microscope (TEM) was used to study the distribution of clays in nanocomposite films. The machine by JEOL, JEM 2010 TEM, located at the Suranaree University of Technology, Nakhon Ratchasima, Thailand, as shown in Figure 4.5, was used. For examination of the nanocomposites morphology, stripes of approximate 1 mm width were cut out of the film samples used for permeation measurements, oxygen plasma-etched and subsequently embedded in an epoxy matrix. The 50-100 nm thick sections were then cut with a diamond knife of cryo-ultramicrotome under liquid nitrogen condition.

Figure 4.5 Transmission Electron Microscope (TEM)

4.3.2.3 Permeability Properties

The Oxygen Transmission Rate (OTR) ($cm^3/m^2/day$) of the nanocomposite films were measured by the Oxygen Permeation Analyzer, Illinois model 8500 as shown in Figure 4.6 according to ASTM D-3985, ISO 15105-2, DIN 53380, or JIS K-7126. All films were kept in desiccator as shown in Figure 4.7 before measurement. Extreme pressure lube (as shown in Figure 4.8) had to be applied on the rim of the film sample before insertion of the film into the analyser. The film thickness was measured by the digital micrometer (shown in Figure 4.9-4.10) at 18 different points on the film according to the paper template (where each point had an area of $1/18$ of the total surface area of film sample as shown in Figure 4.11) and the average film thickness was calculated. The obtained average film thickness was then used to convert OTR into permeability.

Figure 4.6 Oxygen Permeation Analyzer

Figure 4.7 Desiccator

Figure 4.8 Extreme Pressure Lube

Figure 4.9 Digital Micrometer

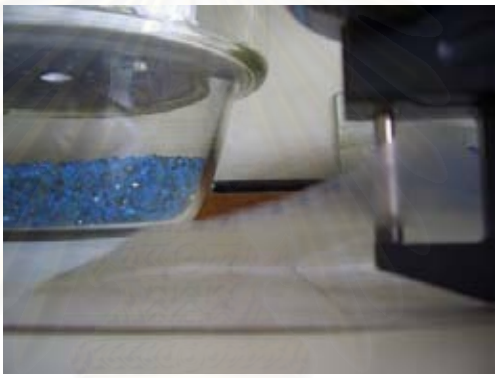

Figure 4.10 Determination of Film Thickness

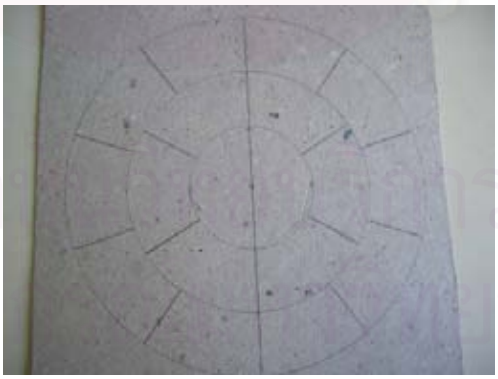

Figure 4.11 Paper Template for Determination of Film Thickness

4.3.2.4 Determination Inorganic Clay

The exact amount of inorganic clay in the Org-MMT and nanocomposites were determined by burning the samples in furnace at 1000° C (because all of organic in clay burned off at 900 ^{o}C) for 2 hours and measuring the residual weight. Samples with the initial weight of about 3 grams/crucible were used. Figure 4.12 showed the digital analytical balance and furnace used (experimental data shown in Appendix D).

(a) Digital Analytical Balance (b) Furnace

Figure 4.12 Analytical Balance and Furnace

4.3.3 Determination of Clay Orientation and Aspect Ratio

The determination of filler aspect ratio for layered aluminosilicate nanocomposites is not straightforward. Good evaluates require a thorough analysis of TEM photomicrographs at different magnifications. Clay platelets intrinsically have a distribution of lateral dimensions. The refinement, recovery, and chemical treatment of these clays may contribute to the variation in clay platelets geometry. Moreover, extrusion of these clays with polymer and compatibilizer in melt processing steps more than one time will amplify the range of particle shapes and sizes, particularly when the layered aluminosilicates is not completely exfoliated. Lastly, microtoming of the nanocomposite sample into thin sections for TEM analysis will also results in

an apparent distribution of observed particle sizes and platelets orientation even if all disk-like platelets were the same average size and orientation. Accurate and reliable image analysis requires an original image having exceptional resolution and contrast; an ideal image would display sharp transitions from black to white. In reality, a large majority of bright field TEM images of polymers consist of different shades of gray, which is primarily an indication of mass-thickness contrast throughout the sample.

In this work, two TEM images for each film sample were taken. The first TEM image was at 10,000X magnification and was taken around the edge of the sample in order to get the reference plane for clay orientation measurement. The second TEM image was taken at 50,000X magnification and was used to measure clay orientation and aspect ratio. The orientation angle of each clay was then manually measured with respect to the picture frame and then corrected with the reference plane taken from the first TEM image. The aspect ratio was determined by manually measuring the length and width of each clay in the second TEM image.

CHAPTER V

RESULTS AND DISCUSSION

5.1 Determination of Actual Weight Percent of Clay

As only the inorganic part of clay has effect on the mechanical properties and permeability of composites [46], the actual amount of inorganic MMT in the nanocomposite films prepared in this work must be determined. The Org-MMT clay sample or the LDPE/PE-g-MA/Org-MMT pellet samples were burned in the furnace at 1000 ^{o}C for 120 min and the residual MMT ashes were measured as described in Chapter IV. The raw experimental data were reported in Appendix D. The results were shown in Table 5.1. The data showed that the organically modified MMT (Org-MMT) contains only 49.55 wt% inorganic MMT. And the actual wt% of Org-MMT in the prepared LDPE/PE-g-MA/Org-MMT nanocomposite films were quite close to the designated value used in the sample code.

Table 5.1 Actual Amount of Inorganic MMT in the prepared LDPE/PE-g-MA/ Org-MMT Nanocomposite Films

Sample Code *	Actual wt% Org-MMT	Actual wt% Inorganic MMT
0/0/100	100	49.55
88/6/6	5.99	2.97
85/9/6	6.33	3.14
82/12/6	6.09	3.02
90/9/1	1.53	0.76
89/9/2	2.40	1.19
88/9/3	3.35	1.66
87/9/4	4.26	2.11
81/9/10	10.27	5.09

* x/y/z are the designated wt% LDPE / wt% PE-g-MA / wt% Org-MMT, respectively

5.2 Effects of PE-g-MA Compatibilizer on Permeability

To study the effect of compatibilizer loading on the oxygen permeability of the LDPE/PE-g-MA/Org-MMT nanocomposite films, the following LDPE/PE-g-MA/Org-MMT nanocomposite films were prepared: 88/6/6, 85/9/6, 82/12/6, 94/6/0, 91/9/0 and 88/12/0. The oxygen permeabilities of these films were measured as described in Chapter IV and reported in Appendix B. The thickness of these films were measured as described in Chapter IV and reported in Appendix A. The results were summarized in Table 5.2.

Table 5.2 Effect of PE-g-MA on Permeability of LDPE/PE-g-MA/Org-MMT Nanocomposite Films

Sample Code *	Permeability # (P_c)	Sample Code *	Permeability # (P_m)	Relative Permeability (P_c/P_m)
88/6/6	248,107	94/6/0	302,793	0.82
85/9/6	158,215	91/9/0	310,801	0.51
82/12/6	172,244	88/12/0	296,581	0.58

* x/y/z are the designated wt% LDPE / wt% PE-g-MA / wt% Org-MMT, respectively

Permeability is in $cm^3.\mu m/m_2.atm.day$

It can be seen from column no. 2 of Table 5.2 that the permeabilities of LDPE/PE-g-MA/Org-MMT nanocomposite films at 6 wt% Org-MMT went to the minimum at 9 wt% PE-g-MA. The relative permeabilities of LDPE/PE-g-MA/Org-MMT nanocomposite films at 6 wt% Org-MMT with respect to LDPE/PE-g-MA blends also showed the similar behavior as shown in column no. 5 of Table 5.2. These indicated that there was an optimum loading of PE-g-MA compatibilizer in the composites to maximize the reduction of permeability of films. This effect was supported by the XRD measurements of nanocompsite films (the procedure was described in Chapter IV) with the results shown in Table 5.3. (The d-spacing calculation was described in Appendix C.) Data in Table 5.3 showed that the PE-g-MA compatibilizer increased the d-spacing of Org-MMT in the composites with respect to neat Org-MMT, i.e. the d-spacing increased from 3.705 nm (for neat

Org-MMT) to 3.879 nm (for 85/9/6 LDPE/PE-g-MA/Org-MMT nanocomposite). The MA group compatibilizer interacts with the cations agent in clay and helps polymer molecules to penetrate the clay interlayer easier. However, the increase of d-spacing went to the maximum at 9 wt% PE-g-MA. This implied that 9 wt% PE-g-MA was optimal for expanding the clay interlayers. Therefore, the loading of 9 wt% PE-g-MA were used in the subsequent studies below.

Table 5.3 Effect of wt% PE-g-MA on D-spacing of MMT Clay in LDPE/PE-g-MA/ Org-MMT nanocomposite films at 6 wt% Org-MMT

Sample Code *	0/0/100	88/6/6	85/9/6	82/12/6
Wt% PE-g-MA	0	6	9	12
Average X-ray Diffraction Angle ($2\theta^{\circ}$)	2.382	2.326	2.275	2.311
Average d-spacing between clay platelet (nm)	3.705	3.796	3.879	3.820

* x/y/z are the designated wt% LDPE / wt% PE-g-MA / wt% Org-MMT, respectively

5.3 Effect of Clay Loading on Morphology of Nanocomposite Films

To study the effect of clay loading on the morphology of the LDPE/PE-g-MA/Org-MMT nanocomposite films, the following LDPE/PE-g-MA/Org-MMT nanocomposite films were prepared: 90/9/1, 89/9/2, 88/9/3, 87/9/4, 89/9/6 and 81/9/10. The XRD patterns of these films were measured as described in Chapter IV and shown in Figure 5.1. The d-spacing calculation was described in Appendix C. The results were summarized in Table 5.4.

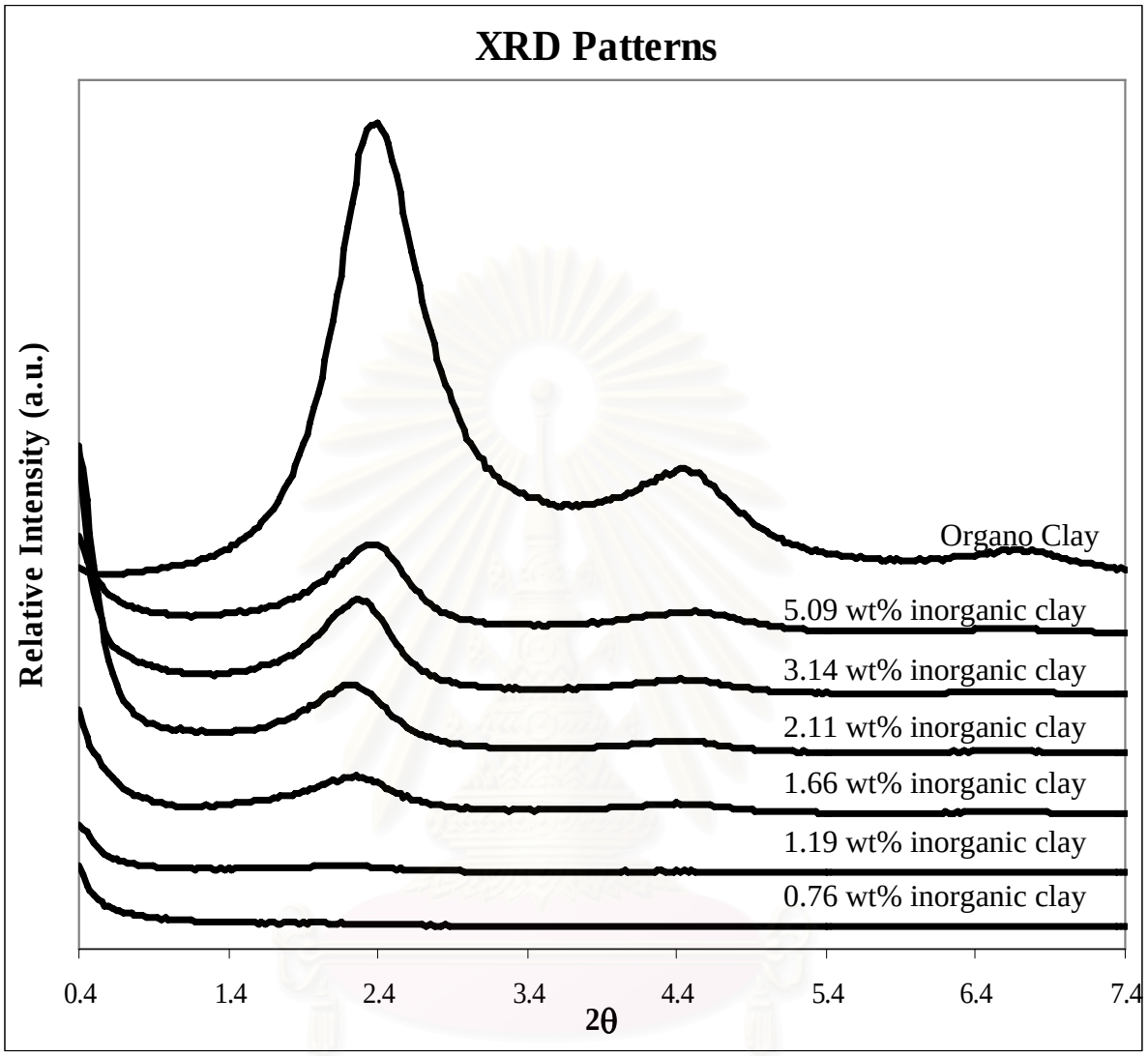

Figure 5.1 XRD Patterns of LDPE/PE-g-MA/Org-MMT Nanocomposite Films at Different Clay Loading

Table 5.4 Effect of Clay Loading on D-spacing of MMT Clay in LDPE/PE-g-MA/ Org-MMT nanocomposite films with 9 wt% PE-g-MA

Sample Code *	0/0/100	90/9/1	89/9/2	88/9/3	87/9/4	85/9/6	81/9/10
Actual Wt% Org-MMT	100	1.53	2.40	3.35	4.26	6.33	10.27
Actual Wt% Inorganic MMT	49.55	0.76	1.19	1.66	2.11	3.14	5.09
Average X-ray Diffraction Angle ($2\theta^{\circ}$)	2.382	-	-	2.250	2.254	2.275	2.371
Average d-spacing between clay platelet (nm)	3.705	-	-	3.923	3.917	3.879	3.723

* x/y/z are the designated wt% LDPE / wt% PE-g-MA / wt% Org-MMT, respectively

Figure 5.1 above showed that the characteristic diffraction peaks of clay in the nanocomposite films were shifted to the lower angles than the neat clay. These suggested the increase of interlayer spacings between clay platelets. The disappearance of the diffraction peaks for the LDPE/PE-g-MA/Org-MMT nanocomposite films with 0.76 and 1.19 wt% inorganic clay indicated possible exfoliation of the clay platelets. For the LDPE/PE-g-MA/Org-MMT nanocomposite films with 1.66 to 5.09 wt% inorganic clay, the d-spacing between the clay platelets were larger than the d-spacing for neat Org-MMT but were decreased with increased clay loading. These may be that the clay-polymer nanocomposites consist of a hierarchical structure. Polymer chains have to move through the gaps in the agglomerates to reach the clay interlayers, prior to penetrating into the interlayers. Melt compounding in an twin screw extruder helps to penetrate the clay agglomerates. However, in mixing, the breakdown of clay agglomerate is difficult in higher clay concentration, and thus, polymer molecules experience more difficulty diffusing into the agglomerates and the clay interlayers. Nevertheless, the data in Table 5.4 implied the prepared nanocomposite films were the intercalated nanocomposites.

In this study, the thickness of the obtained LDPE/PE-g-MA/Org-MMT nanocomposite films at various contents of clay was controlled to be in the range of 30-80 μm. The blown up ratio (BUR) were about the same at 1.17-1.29 and the drawn down ratio were in the same range of about 0.07-0.12 as reported in Table 5.5.

Table 5.5 Blown Up Ratio (BUR) and Draw Down Ratio (DDR) of LDPE/PE-g-MA/ Org-MMT Nanocomposite Films

Sample Code *	Average Film Outer Diameter ($*10^4$) (μm)	Die Outer Diameter ($*10^4$) (μm)	Blown Up Ratio (BUR) #	Average Film Thickness (μm)	Die Opening ($*10^4$) (μm)	Draw Down Ratio (DDR) ##
90/9/1	4.52	3.50	1.29	52.542	0.045	0.117
89/9/2	4.40	3.50	1.26	41.236	0.045	0.092
88/9/3	4.35	3.50	1.24	54.139	0.045	0.120
87/9/4	4.27	3.50	1.22	43.042	0.045	0.096
85/9/6	4.11	3.50	1.17	29.667	0.045	0.066
81/9/10	4.14	3.50	1.18	55.708	0.045	0.124

* x/y/z are the designated wt% LDPE / wt% PE-g-MA / wt% Org-MMT, respectively

Blown Up Ratio (BUR) $= \frac{Average\ Film\ Outer\ Diameter}{Die\ Outer\ Diameter}$

Draw Down Ratio (DDR) $= \frac{Average\ Film\ Thickness}{Die\ Opening}$

The clay loading had been found to have some effect on the transparency of the prepared films as shown in Figure 5.2 below. Normally for high transparency, the dispersed phase should have an average size smaller than the wavelength of visible light, i.e. 400-800 nm (Chang et al., 2003). Qualitatively, the transparency slightly decreased with increasing clay content possibly because of agglomeration of clay platelets. It can be observed that the film with 5.09 wt% of inorganic clay platelets was the least transparent with respect to the neat LPDE film. This suggested that some agglomeration of the clay nanoparticles existed in the composite films thus resulting in the decreased transparency of the films.

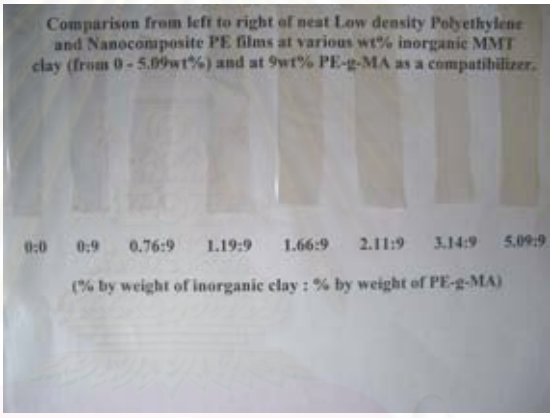

Figure 5.2 Transparency of LDPE/PE-g-MA/Org-MMT Nanocomposite Films at Various Contents of Org-Clay

5.4 Effects of Loading, Aspect Ratio and Orientation of Org-MMT on Permeabiltiy of LDPE/PE-g-MA/Org-MMT Nanocomposite Films

To study the effects of loading, aspect ratio, and orientation of Org-MMT on the oxygen permeability of the LDPE/PE-g-MA/Org-MMT nanocomposite films, the following LDPE/PE-g-MA/Org-MMT nanocomposite films were prepared: 91/9/0, 90/9/1, 89/9/2, 88/9/3, 87/9/4, 85/9/6 and 81/9/10. The thickness of these films were measured as described in Chapter IV and reported in Appendix A. The oxygen permeabilities of these films were measured as described in Chapter IV and reported in Appendix B. The results were summarized in Table 5.6 and shown in Figure 5.3.

Table 5.6 Permeability of LDPE/PE-g-MA/Org-MMT Nanocomposite Films

Sample Code *	Actual wt% inorganic MMT	Actual vol% inorganic MMT	Permeability [#] (P_c)	Relative Permeability (P_c/P_m)
91/9/0	0	0	310,801	-
90/9/1	0.76	0.25	250,570	0.8062
89/9/2	1.19	0.39	228,262	0.7344
88/9/3	1.66	0.55	197,777	0.6364
879/4	2.11	0.70	186,024	0.5985
85/9/6	3.14	1.04	158,215	0.5091
81/9/10	5.09	1.72	160,841	0.5175

* x/y/z are the designated wt% LDPE / wt% PE-g-MA / wt% Org-MMT, respectively

[#] Permeability is in $cm^3.\mu m/m_2.atm.day$

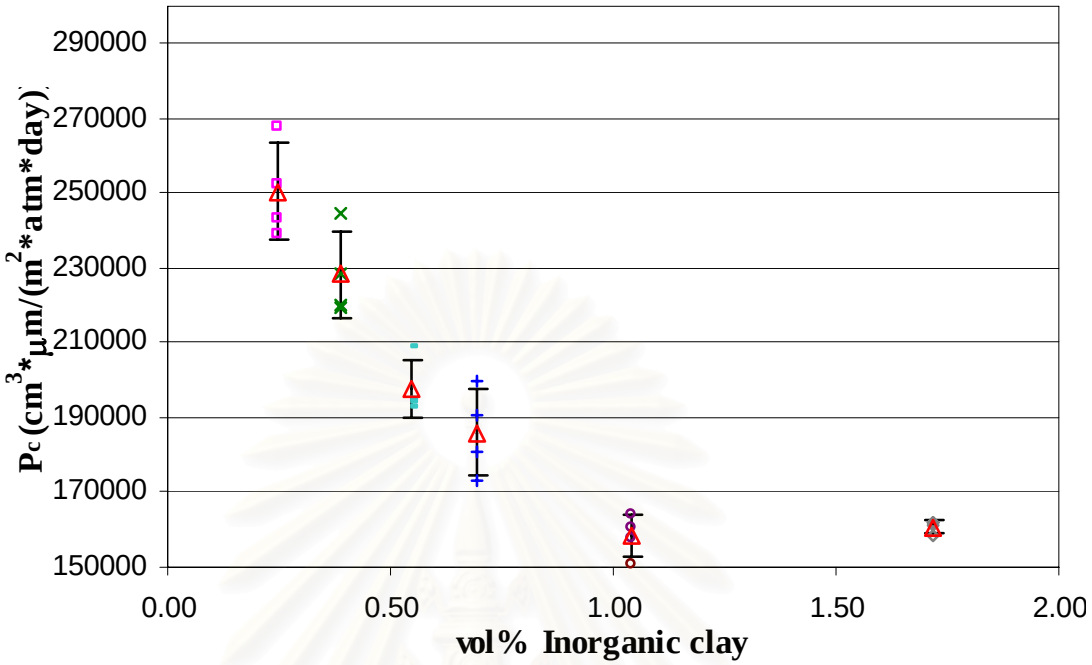

(a)

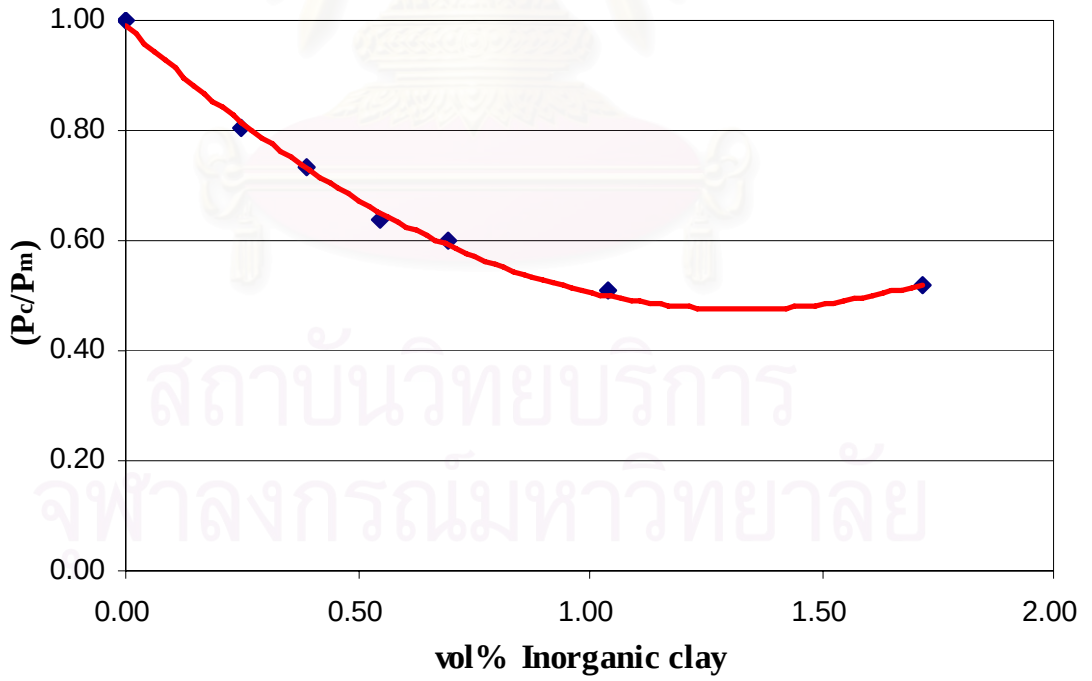

(b)

Figure 5.3 Effect of Volume Fraction of Inorganic MMT on Permeability of LDPE/PE-g-MA/Org-MMT Nanocomposite Films at 9 wt% PE-g-MA

From Table 5.6 and Figure 5.3 it could be clearly seen that the oxygen permeability of LDPE/PE-g-MA/Org-MMT nanocomposite films at 9 wt% PE-g-MA decreased with increasing volume fraction of Inorganic MMT or basically with increasing loading of Org-MMT. The reduction was quite significant at low volume fraction and then tended to level off at higher volume fraction of inorganic MMT. This was typical effect of nanofiller on property of nanocomposite. Only small amount of nanofiller can have big effect on property of nanocomposite. From Figure 5.3, only 0.70 vol% of inorganic MMT caused about 40% reduction in oxygen permeability. It was noted that in calculating the relative permeability of the nanocomposite films, the permeability of LDPE/PE-g-MA blend at 9 wt% PE-g-MA (i.e. 91/9/0 LDPE/PE-g-MA/Org-MMT nanocomposite film) was used as reference.

The above observation should mainly be due to the amount, aspect ratio and orientation of inorganic MMT in LPDE/PE-g-MA phase. The Transmission Electron Microscopy (TEM) of the above LDPE/PE-g-MA/Org-MMT films were taken as described in Chapter IV and shown in Figures 5.4-5.9. The aspect ratio and orientation of clay in each sample were measured as described in Chapter IV and reported in Appendix F.

In Figures 5.4-5.9, small dark lines corresponded to the cross section of a clay platelet 1 nm thickness and the gap between two adjacent lines was the interlayer spacing or stack of the clay used. For each LDPE/PE-g-MA/Org-MMT film sample, two TEM images were taken. The first TEM image was at 10,000X magnification and was taken around the edge of the sample in order to get the reference plane for clay orientation measurement. The solid line labeled “1” represented the film surface plane and the solid line labeled “2” are orthogonal to line “1” and represented the film thickness plane. The second TEM image was taken at 50,000X magnification and was used to measure clay orientation and aspect ratio. The orientation angle of each clay was then manually measured with respect to the solid line “1” (or the film surface plane). The aspect ratio was determined by manually measuring the length and width of each clay in the second TEM image.

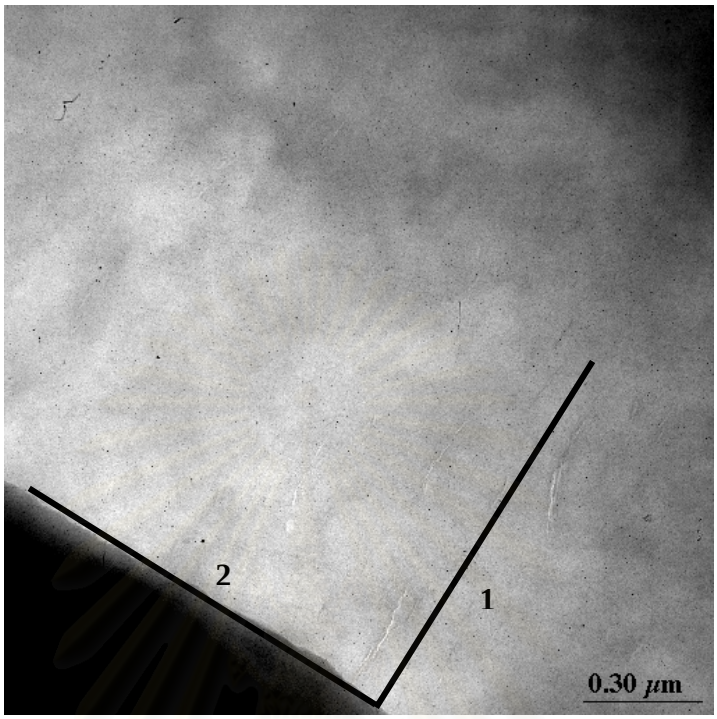

(a) 10,000X

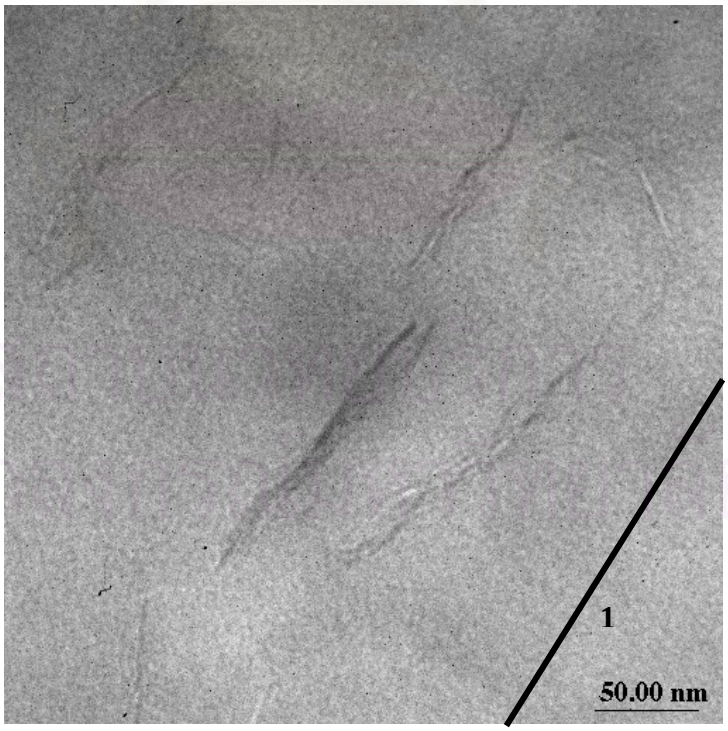

(b) 50,000X

Figures 5.4 TEM Images of 90/9/1 LDPE/PE-g-MA/Org-MMT Nanocomposite Film

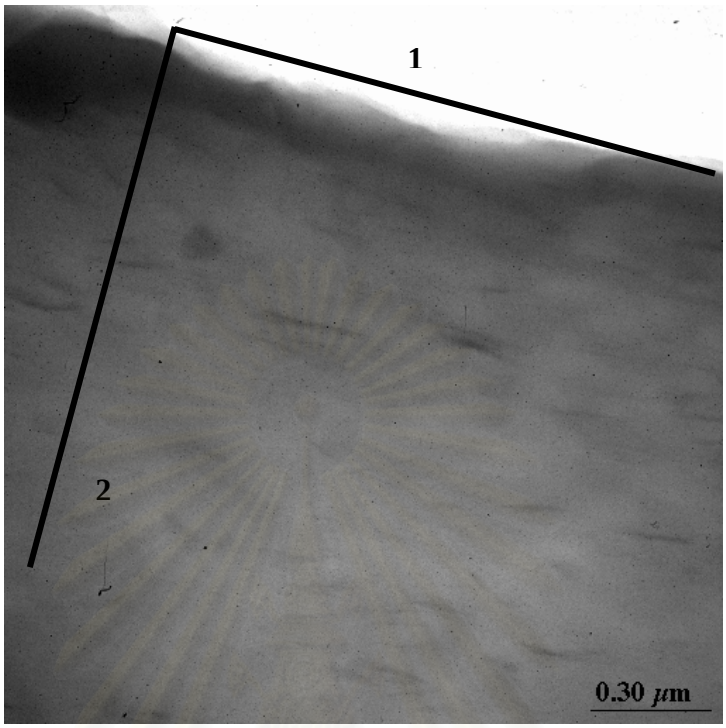

(a) 10,000X

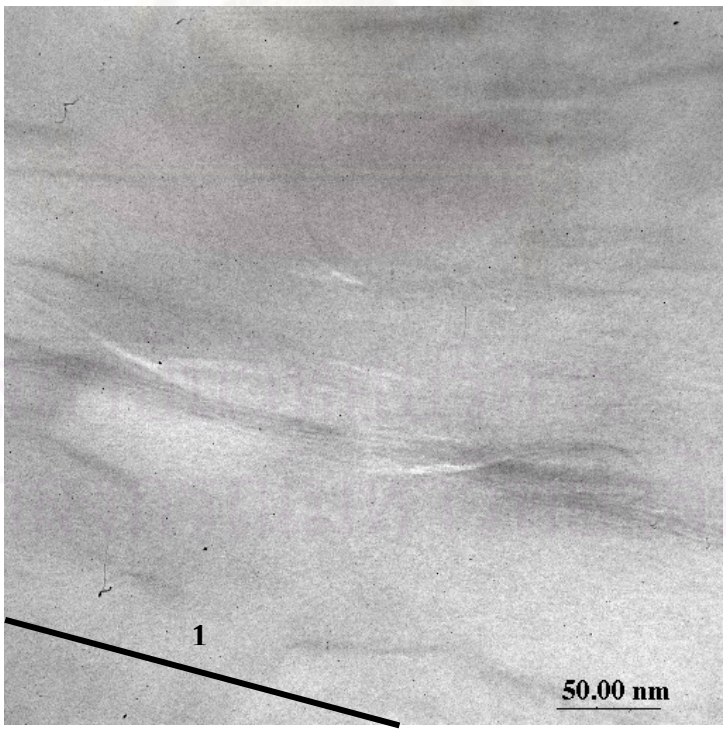

(b) 50,000X

Figures 5.5 TEM Images of 89/9/2 LDPE/PE-g-MA/Org-MMT Nanocomposite Film

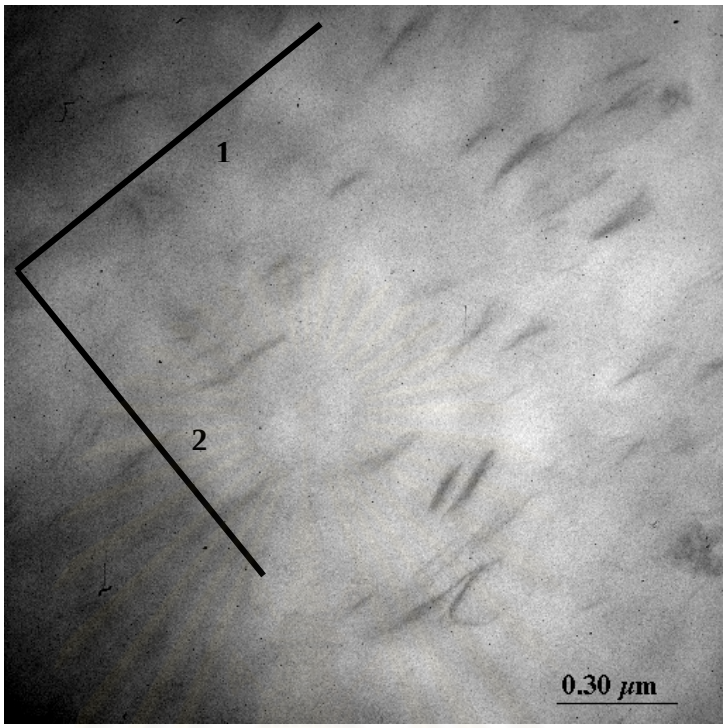

(a) 10,000X

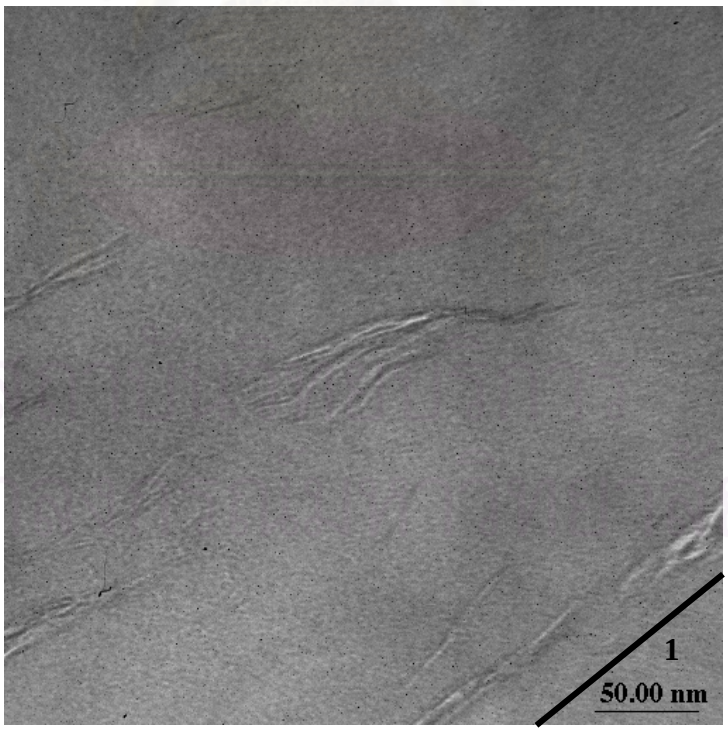

(b) 50,000X

Figures 5.6 TEM Images of 88/9/3 LDPE/PE-g-MA/Org-MMT Nanocomposite Film

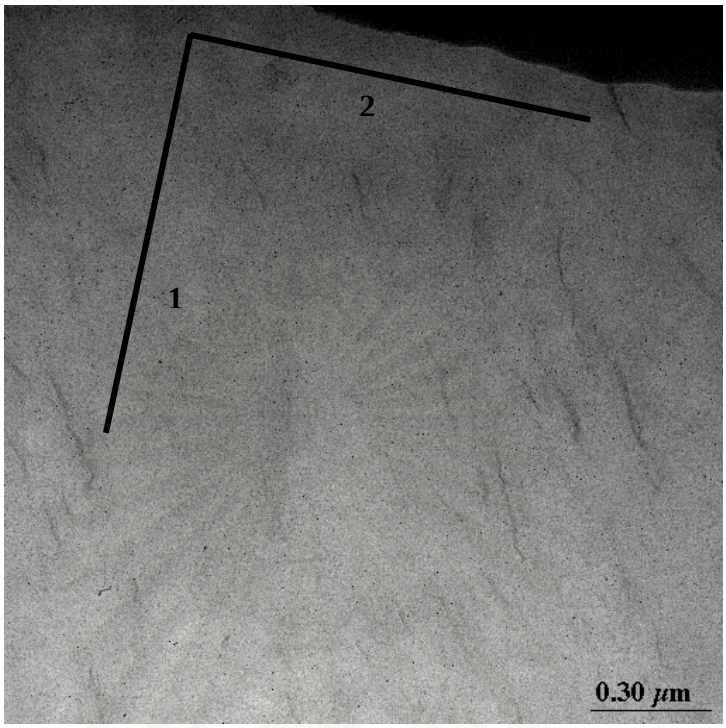

(a) 10,000X

(b) 50,000X

Figures 5.7 TEM Images of 87/9/4 LDPE/PE-g-MA/Org-MMT Nanocomposite Film

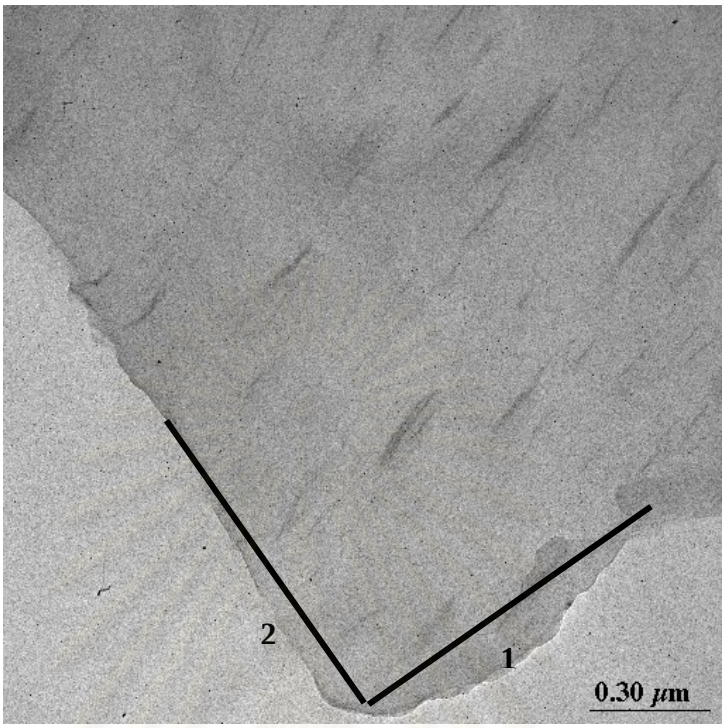

(a) 10,000X

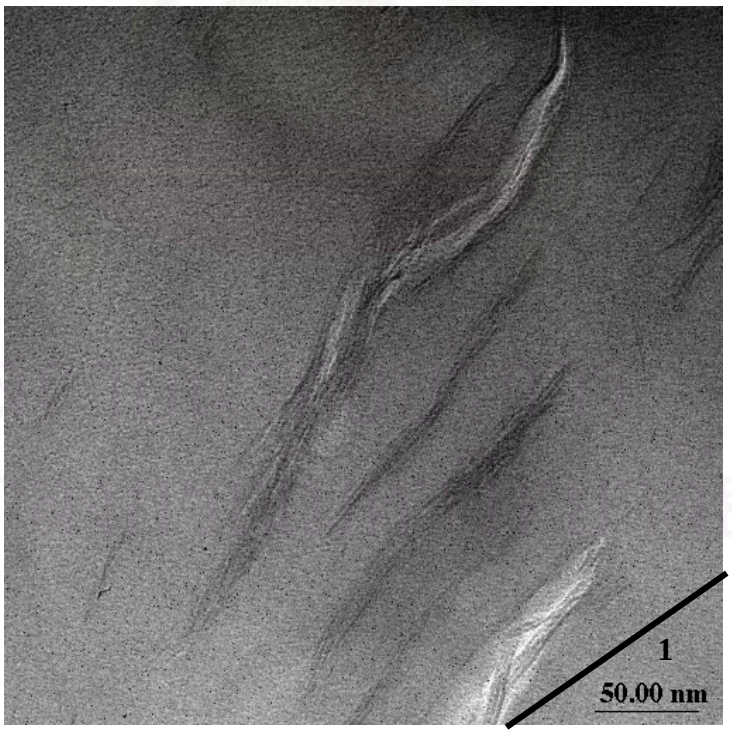

(b) 50,000X

Figures 5.8 TEM Images of 85/9/6 LDPE/PE-g-MA/Org-MMT Nanocomposite Film

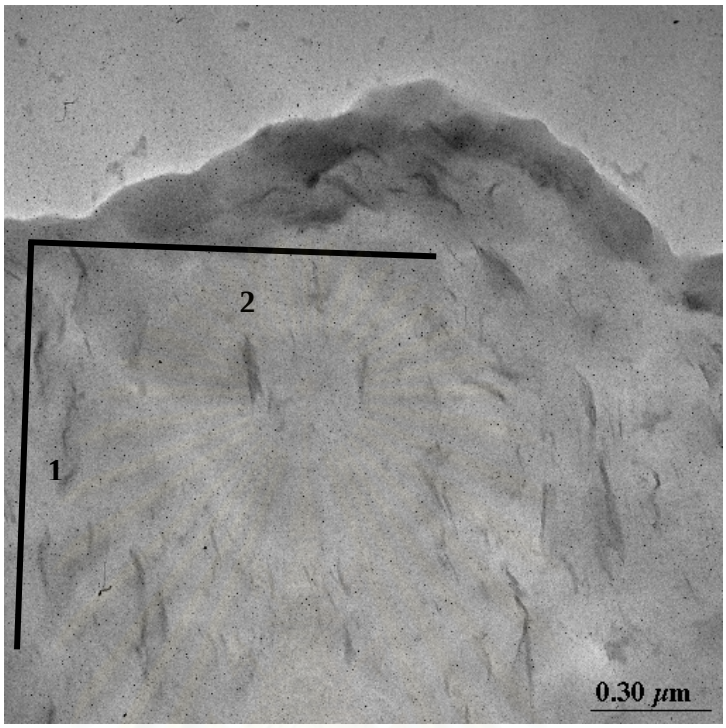

(a) 10,000X

(b) 50,000X

Figures 5.9 TEM Images of 81/9/10 LDPE/PE-g-MA/Org-MMT Nanocomposite Film

From Figures 5.4-5.9 above, the aspect ratio and orientation of clay in each sample were measured as described in Chapter IV, reported in Appendix F, and summarized here in Table 5.7. It should be noted that the determination of filler aspect ratio for layer aluminosilicate nanocomposites is not straightforward. Good evaluation require a thorough analysis of TEM photomicrographs at different magnifications. Clay platelets intrinsically have a distribution of lateral dimensions. They can have variations in length, thickness or diameter of clay platelets.

Table 5.7 Aspect Ratio and Orientation of Org-MMT of LDPE/PE-g-MA/Org-MMT Nanocomposite Films

Sample Code *	Actual wt% inorganic MMT	Actual vol% inorganic MMT	Aspect Ratio (L/W)	Orientation Angle (degree)
91/9/0	0	0	-	-
90/9/1	0.76	0.25	103.37	12.39
89/9/2	1.19	0.39	167.38	15.06
88/9/3	1.66	0.55	122.54	9.90
879/4	2.11	0.70	127.73	32.19
85/9/6	3.14	1.04	258.32	18.64
81/9/10	5.09	1.72	175.29	21.22

* x/y/z are the designated wt% LDPE / wt% PE-g-MA / wt% Org-MMT, respectively

Data in Table 5.7 showed that the aspect ratio of clays were in the range of 100-260 which was in the same order of magnitude of 500 as reported to be aspect ratio of typical MMT clay. The orientation angles of clays were in the range of 10-20 degree with respect to the film thickness plane. This suggested that most of the clays in each sample were not in parallel with the film thickness plane but at an acute angle with it. Hence, the effectiveness of clays in reducing the permeability was not at maximum. The tortuous path needed to be traveled by permeant through film thickness was not the maximum distance. These data in Table 5.7 supported the effect of clay loading on permeability reduction as seen in Table 5.6 above.

5.5 Modeling by Modified Nielsen Model

A number of theories have been proposed to correlate the gas permeability of nanocomposite films to the filler content and geometry. In this study, the experimental gas permeation data were compared to that predicted by the tortuous path model proposed by Modified Nielsen model which approximates the filler particles as platelets with finite length L and thickness W but infinite width. The mathematical form of this model is

$$\frac{P_c}{P_m} = \frac{1-\phi_f}{1+\frac{L}{2W}\phi_f\left(\frac{2}{3}\right)\left(S+\frac{1}{2}\right)} \tag{1}$$

$$S = \frac{1}{2}\left(3\cos^2\theta - 1\right) \tag{2}$$

where P_c is the permeability of the nanocomposite, P_m is the permeability of the pure polymer, and ϕ_f is the volume fraction of the clay. The L and W are length and thickness of the clay sheets, respectively; its ratio, L/W, defines the aspect ratio of the fillers. The S is the orientation parameter which depends on the orientation angle θ.

The modified Nielsen model were fitted to the relative permeability data in Table 5.6 by guessing the values of L/W and S until the best-fitted was obtained. The detailed calculation was shown in Appendix E. The obtained best-fitted parameters were L/W = 175, θ = 9^o or S = 0.963. The best-fitted line was plotted with the experimental data in Figure 5.10. And just for comparison, the predicted values of relative permeability by modified Nielsen model for the case when L/W = 500 and S = -0.5 (i.e. clay oriented in perpendicular to film thickness plane) and for the case when L/W = 500 and S = 1 (i.e. clay oriented in parallel with film thickness plane) were also plotted in Figure 5.10.

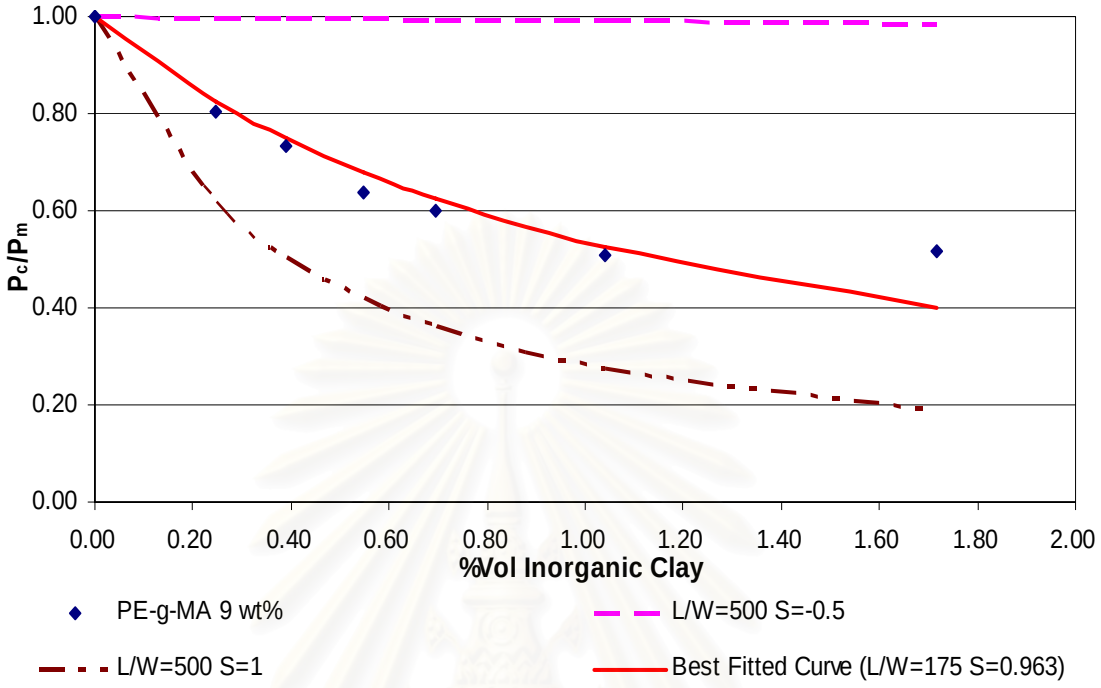

Figure 5.10 Comparison of Experimental Permeability Data of LDPE/PE-g-MA/ Org-MMT Nanocomposite Films with Best-fitted Curve by Modified Nielsen Model

It could be seen from Figure 5.10 that the best-fitted parameters obtained from the modified Nielsen model (L/W = 175, θ = 9^{o}) were in the same range with the experimental values reported in Table 5.7 (L/W between 100-260 and θ between 10-20^{o}). Hence, it could be said that the modified Nielsen model can be used to predicted the relative permeability of the LDPE/PE-g-MA/Org-MMT nanocomposite films providing that the accurate aspect ratio and orientation angle could be obtained.

5.6 Application of Modified Nielsen Model to Other Work

To further verify the applicability of the modified Nielsen model in predicting the gas permeability of composite films, the experimental data from one literature were used. The data were taken from the work of Hotta and Paul [44]. Their system were LLDPE/PE-g-MA/MMT modified with $[M_2(HT)_2]$ (Montmorillonite clay modified with dimethylbis(hydrogenated tallow)). The TEM images were shown in Figure 5.11. The aspect ratio and orientation of clay in each sample were measured as described in Chapter IV, reported in Appendix F. The L/W of inorganic clays were found to be 135.08, 122.22, 102.26, and 77.35 for composite with 0.8, 2.5, 4.6, and 6.9 wt% inorganic MMT, respectively. The orientation angles were 56, 58, 40, and 26 degree for composite with 0.8, 2.5, 4.6, and 6.9 wt% inorganic MMT, respectively.

The best-fitted curves of relative predicted by modified Nielsen model for oxygen, nitrogen, and carbon dioxide were plotted against the experimental data in Figures 5.12. It could be seen from Figure 5.12 and data in Appendix F that the best-fitted parameters obtained from the modified Nielsen model (L/W = 114, $\theta = 44^o$ for oxygen, L/W = 119, $\theta = 43^o$ for nitrogen, and L/W = 114, $\theta = 44^o$ for carbondioxide) were in the same range with the experimental values reported above (L/W between 77-135 and θ between 26-58^o). Hence, it could be said that the modified Nielsen model can be used to predicted the relative permeability of the LLDPE/PE-g-MA/MMT modified with $[M_2(HT)_2]$ nanocomposite films providing that the accurate aspect ratio and orientation angle could be obtained

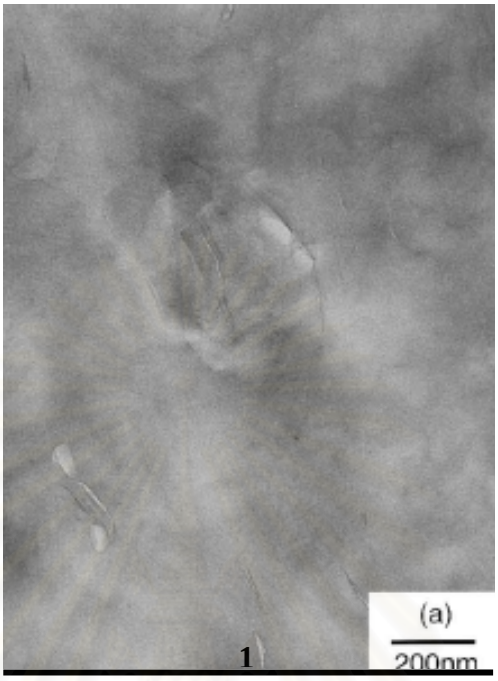

(a) 0.8 wt% inorganic MMT

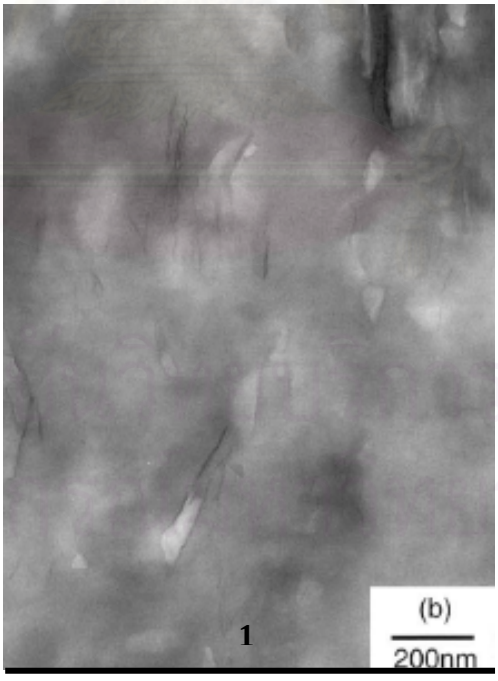

(b) 2.5 wt% inorganic MMT

Figure 5.11 TEM Images of LLDPE/PE-g-MA/MMT modified with $[M_2(HT)_2]$ [44]

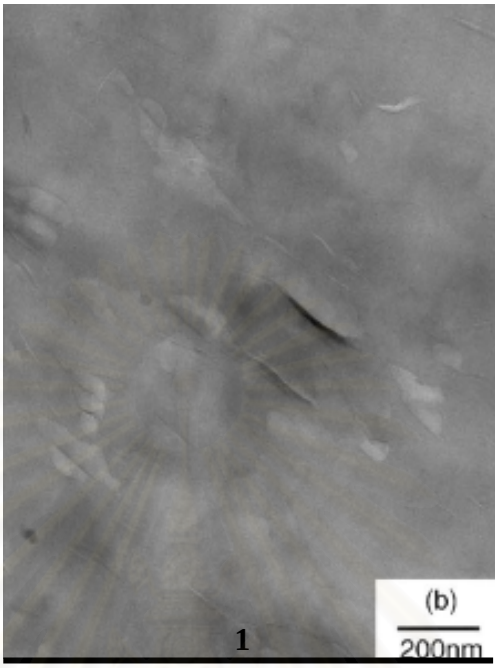

(c) 4.6 wt% inorganic MMT

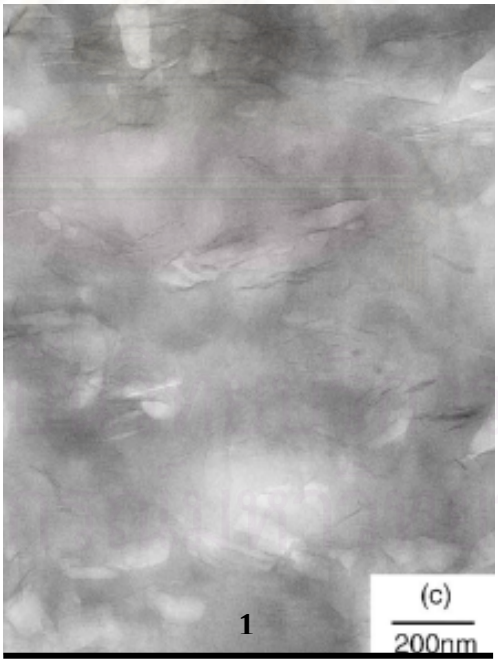

(d) 6.9 wt% inorganic MMT

Figure 5.11 (continued) TEM Images of LLDPE/PE-g-MA/MMT modified with $[M_2(HT)_2]$ [44]

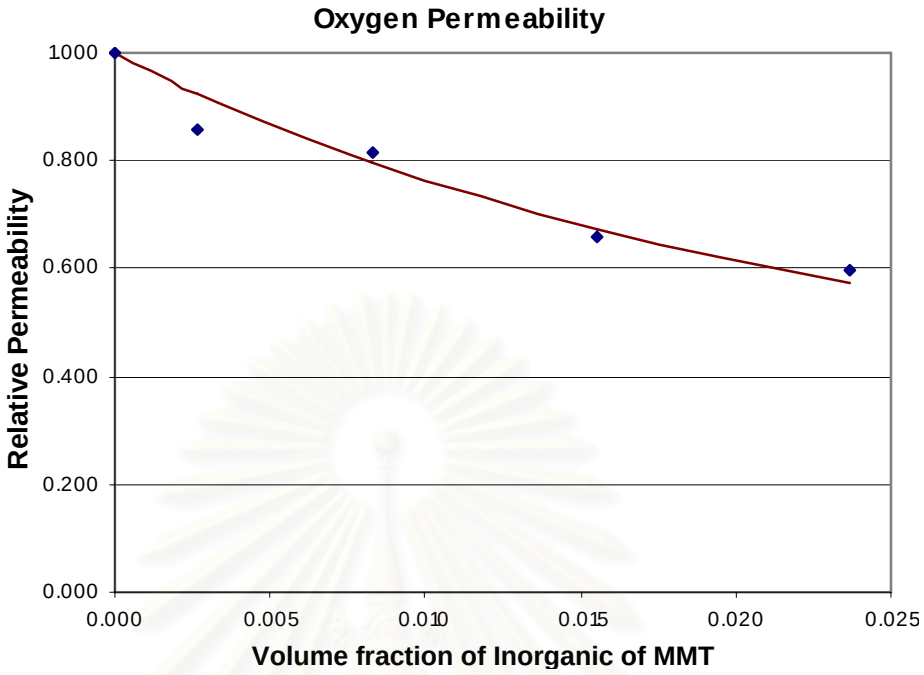

(a) Oxygen

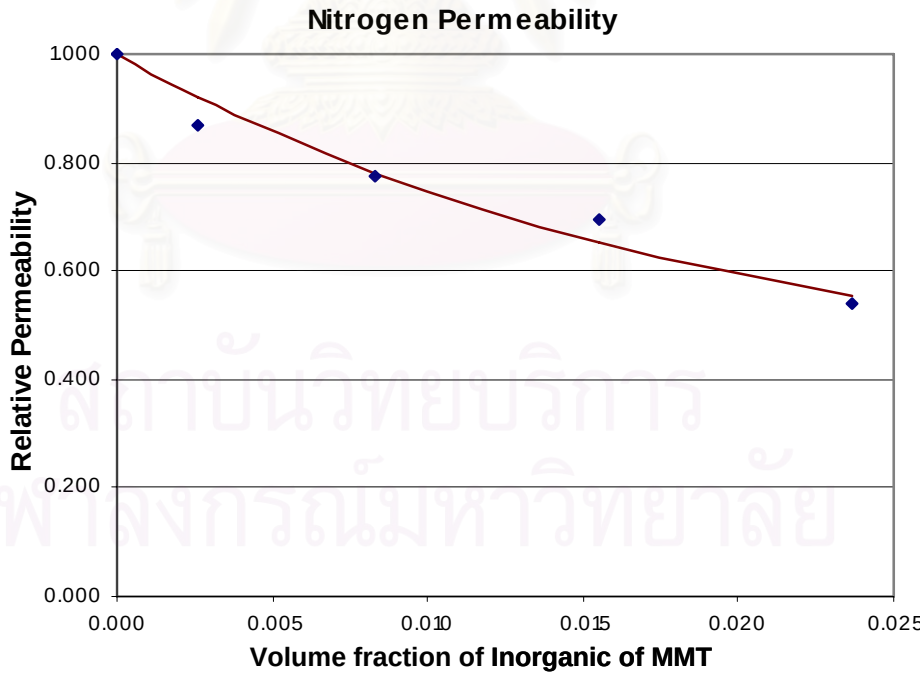

(b) Nitrogen

Figure 5.12 Comparison of Experimental Permeability Data of LLDPE/PE-g-MA/MMT modified with $[M_2(HT)_2]$ Nanocomposite Films with Best-fitted Curve by Modified Nielsen Model

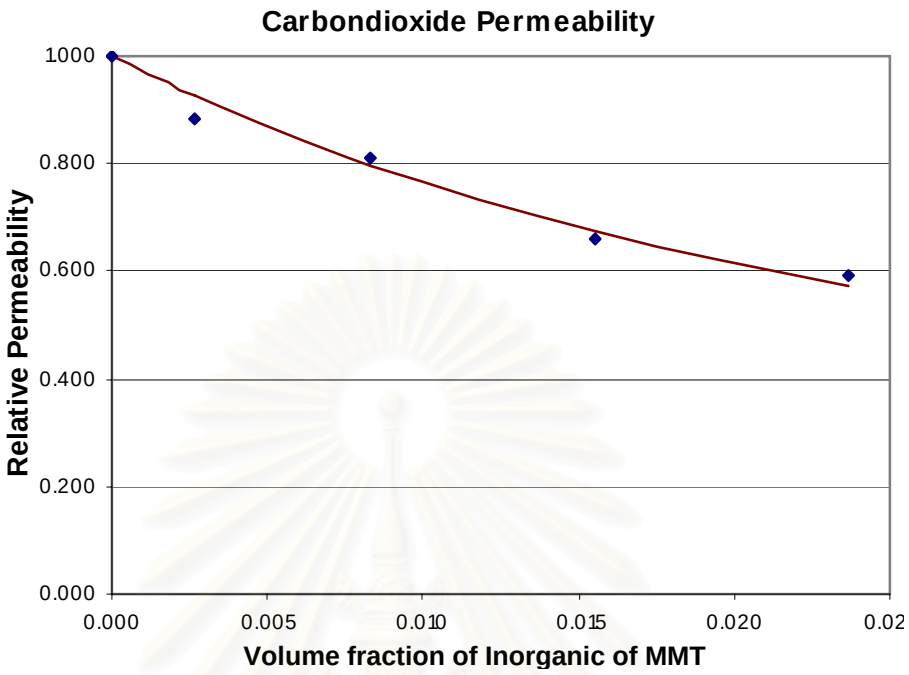

(c) Carbondioxide

Figure 5.12 (continued) Comparison of Experimental Permeability Data of LLDPE/PE-g-MA/MMT modified with $[M_2(HT)_2]$ Nanocomposite Films with Best-fitted Curve by Modified Nielsen Model

CHAPTER VI

CONCLUSIONS & RECOMMENDATIONS

6.1 Conclusions

From the results obtained in this work, the following conclusion can be made:

1. Nanocomposite films of LDPE with Org-MMT and PE-g-MA as compatibilizer having lower oxygen permeability properties than pure LDPE film can be obtained by melt mixing along the route consisting of a masterbatch preparation of a compatibilizer with filler then melt mixing again with LDPE using twin screw extruder.

2. The transparency of nanocomposite films slightly decreased with increasing clay content possibly because some agglomeration of the clay nanoparticles existed in the composite films.

3. The XRD patterns showed a wide peak for each nanocomposites sample resulted from layered Org-MMT structure. For samples with 0.76-1.19 wt% inorganic clay loadings, the peak and 2θ significantly decreased, indicating good exfoliation of Org-MMT clay in the LDPE matrix. But the exfoliation was less complete for samples with 1.66-5.09 wt% inorganic clay loading.

4. PE-g-MA compatibilizer can increase the interlayer spacing of clay platelets. The 9 wt% PE-g-MA was the optimum loading found.

5. The obtained LDPE/PE-g-MA/Org-MMT nanocomposite films were mainly the intercalated type. The oxygen gas permeability was reduced by about 50% at 3.14-5.09 wt% inorganic clay loading.

6. Aspect ratio and orientation angle of clay platelets obtained from TEM images could be used to support the XRD results.

7. The modified Nielsen model can be used to predict the relative permeability of nanocomposite films providing that the aspect ratio, orientation angle, and volume fraction of inorganic clay could be found accurately.

6.2 Recommendations

1. To obtain complete exfoliation in composites, twin screw extruder with larger length to diameter (L/D) should be used.

2. A better way to obtain aspect ratio and orientation angle of clay platelets in the composite samples should be investigated.

REFERENCES

[1] Ajayan, P.M., Schadler, L.S., Braun, P.V. **Nanocomposite Science and Technology.** Wiley-VCH Verlag GmbH & Co. KGaA, Weinheim, 2004.

[2] Goddard R. **Packaging Materials**. 1990: Pira.

[3] Anker M. **Edible and Biodegradable Whey Protein Films as Barriers in Foods and Food Packaging, in Department of Food Science**. Chalmers University of Technology: Göteborg, 2000.

[4] Wang S., Song C., Chen G., Guo T., Liu J., Zhang B., Takeuchi S. **Characteristics and Biodegradation Properties of Poly(3-hydroxybutyrate-co-3-hydroxyvalerate) / Organophilic Montmorillonite (PHBV/OMMT) Nanocomposite.** 2004.

[5] Hernandez, R.J., Selke, S.E.M., Culter, J.D. **Plastics Packaging.** Hanser Gardner Publications, 2000.

[6] Chauyjuljit, S. **Plastic Films.** Department of Materials Science, Faculty of Science, Chulalongkorn University, 2003.

[7] Hensen, F., Knappe, W., Potente, H. **Plastics Extrusion Technology.** Hanser Gardner Publications, 1988.

[8] Kampeerapappun, P. **Preparation of cassava starch/montmorillonite nanocomposite film**. Master's thesis, Department of Materials Science, Faculty of Science, Chulalongkorn University, 2003.

[9] Wenk, H-R., and Bulakh, A. **Minerals Their Constitution and origin**. Cambridge University, 2004.

[10] Aphiwantrakul, S. **Synthesis and Characterization of Polymer-Clay Nanocomposites.** M.Sc. (Physics), Mahidol University.

[11] **http://etd.adm.unipi.it/theses/available/etd-02052004-113442/unrestricted/05_Literature_Review.pdf**

[12] Gorrasia, G., Tortoraa, M., Vittoriaa, V., Kaempferb, D., Mulhauptb, R. **Transport Properties of Organic Vapors in Nanocomposites of Organophilic Layered Silicate and Syndiotactic Polypropylene.** 2003**.**

[13] Giannelis, E.P., Krishnamoorti, R., Manias, E. **Polymer-Silicate Nanocomposites: Model Systems for Confined Polymers and Polymer Brushes,** 1998.

[14] Hasegawa, N., Kawasumi, M., Kato, M., Usuki, A., Okada, A. **Journal of Applied Polymer Scienc.** 67 (1998) : 87.

[15] Hasegawa, N., Okamoto, H., Kato, M., Usuki, A. **Journal of Applied Polymer Scienc.** 78 (2000) 1918.

[16] Kim, KN., Kim, H., Lee, J.W. **Polymer Engineering And Science.** 41 (2001) : 1963.

[17] Svoboda, P., Zeng, C., Wang, H., James, Lee L., Tomasko DL. **Journal of Applied Polymer Science**. 85 (2002) : 1562.

[18] Olabarrieta, I. **Strategies to Improve the Aging, Barrier and Mechanical Properties of Chitosan, Whey and Wheat Gluten Protein Films.** KTH Fibre and Polymer Technology.

[19] Bueche, A.M. **Journal of Polymer Science.** 25, 139 (1957).

[20] Kuriakose, B., De, S.K., Bhagawan, S.S., Sivaramkrishnan, R., Athithan, S.K. **Journal of Applied Polymer Science.** 32, 5509 (1986).

[21] Yano, K., Usuki, A., Okada, A., Kuraychi, T., Kamigaito, O.. **Journal of Polymer Science. Part A: Polym Chem.** 31, 2493 (1993).

[22] Iijima, S. **Nature**. 354, 56 (1991).

[23] Suprakas, S.R., Kazunobu, Y., Masami, O., Youhei, F., Akinobu, O., Kazue, U. **New polylactide/layered silicate nanocomposites. 5. Designing of materials with desired properties.** 2003.

[24] **http://eltweb.mit.edu/3.94/lecturenotes/3_94_Lecture_24_20031202.pdf**

[25] Robertson, G.L. **Food Packaging: Principles and Practice**. 1993, Marcel Dekker.

[26] Pauly, S. **Permeability and Diffusion Data, in Polymer Handbook**. Journal of Brandrup, E.H. Immergut, and E.A. Grulke, Editors. 1999, John Wiley & Sons, Inc.

[27] Miller, K.S., and Krochta, J.M. **Oxygen and Aroma Barrier Properties of Edible Films: A Review**. Trends in Food Science & Technology 8 (1997) : p. 228-237.

[28] **http://www.stevensurethane.com/primer.html**

[29] Ohring, M. **Materials Science of Thin Films.** Second Edition, Academic, 2002.

[30] **http://www.nanoscience.gatech.edu/zlwang/research/tem.html**

[31] **http://www.illinoisinstruments.com**

[32] **http://www.ides.com/property_descriptions/ASTMD3985.asp**

[33] Nielsen, L. **Models for the Permeability of Filled Polymer Systems**. Journal of Macromol. Sci., Chem. A1, (1967) : 929-941.

[34] Bharadwaj, R. **Modeling the Barrier Properties of Polymer-Layered Silicate Nanocomposites.** Macromolecules. 34, (2001): 9189-9192.

[35] Robert, W.H. **Numerical Methods.** New York: : Quantum Publishers.

[36] **http://www.bsu.edu/web/jkshim/mathandstat/lsm/leastsquare.htm**

[37] Balazs, A.C., Singh, C., Zhulina, E. **Macromolecules.** 31, (1998): 8370.

[38] Balazs, A.C., Singh, C., Zhulina, E., Lyatskaya, Y. **Acc Chem Res**. 8, (1999): 651.

[39] Wang, K.H., Choi, M.H., Koo, C.M., Choi, Y.S., Chung, I.J. **Synthesis and characterization of maleated polyethylene/clay nanocomposites.** 2001.

[40] Hongbo, Z., Weibing, X., Hanyang, G., Zhengfa, Z., Shijun, S., Qiusheng, S. **Preparation and characterization of PE and PE-g-MAH/ montmorillonite nanocomposites.** Polymer Journal 40 (2004): 2539-2545.

[41] Morawiec, J., Pawlak, A., Slouf, M., Galeski, A., Piorkowska, E., Krasnikowa, N. **Preparation and properties of compatibilized LDPE/organo-modified montmorillonite nanocomposites,** 2005.

[42] Ryu, S.H., Chang, Y-W. **Factors affecting the dispersion of montmorillonite in LLDPE nanocomposite.** Polymer Bulletin 55 (2005): 385–392.

[43] Choi, W.J., Kim, S.H., Kim, Y.J., Kim, S.C. **Synthesis of chain-extended organifier and properties of polyurethane/clay nanocomposites.** Polymer 45 (2004): 6045-6057.

[44] Hotta, S., and Paul, R. **Nanocomposites formed from linear low density polyethylene and organoclays.** Polymer 45 (2004): 7639-7654.

[45] Wang, Z.F., Wang, B., Qia, N., Zhang, H.F., Zhang, L.Q. **Influence of fillers on free volume and gas barrier properties in styrene-butadiene rubber studied by positrons.** Journa of Polymer 46 (2005): 719–724.

[46] Fornes, T.D., and Paul, D.R. **Journal of Polymer.** 44, (2003): 4993.

APPENDICES

Appendix A

Table A-1 Raw Data of Film Thickness at 20 Positions of Template for Various Composite Films

Code*	1	2	3	4	5	6	7	8	9	10	11	12	13	14	15	16	17	18	Mean**	S.D.**
90/9/1-1	30	29	32	29	27	32	34	42	39	31	31	31	32	35	41	39	30	34	33.2	4.4
90/9/1-2	32	38	60	67	68	64	61	51	42	41	37	56	65	59	49	41	49	42	51.2	11.6
90/9/1-3	75	78	93	84	59	67	72	80	93	79	79	90	72	70	85	84	87	85	79.6	9.2
90/9/1-4	59	49	33	32	33	47	51	53	62	54	44	34	35	49	51	54	50	41	46.2	9.4
89/9/2-1	20	22	27	32	29	28	26	25	21	19	23	26	33	26	26	23	25	25	25.3	3.8
89/9/2-2	47	46	47	46	38	44	39	34	38	42	45	44	39	41	34	40	41	42	41.5	4.0
89/9/2-3	38	31	31	31	33	45	51	50	49	50	34	32	29	30	32	39	47	32	38.0	8.2
89/9/2-4	27	26	32	42	45	50	45	36	30	27	27	29	40	42	33	26	30	39	34.8	7.7
88/9/3-1	18	21	25	25	22	20	18	16	13	15	19	21	19	17	15	12	15	20	18.4	3.7
88/9/3-2	20	22	24	23	23	23	23	24	24	23	22	22	22	22	23	24	22	22	22.7	1.0
88/9/3-3	81	61	54	55	61	66	64	68	76	84	83	73	70	66	64	76	74	76	69.6	9.0
88/9/3-4	154	115	86	76	70	74	94	127	139	158	120	90	82	80	110	119	109	104	105.9	26.9
87/9/4-1	37	38	37	34	31	30	32	31	33	36	36	36	31	33	33	32	36	35	33.9	2.5
87/9/4-2	43	39	34	32	33	33	30	31	34	35	42	35	31	32	38	37	39	37	35.3	3.8
87/9/4-3	45	36	33	32	45	56	62	65	58	54	44	58	59	55	46	34	51	60	49.6	10.6
87/9/4-4	53	62	62	63	56	48	49	47	46	43	60	64	59	49	50	46	45	58	53.3	7.1

Code*	1	2	3	4	5	6	7	8	9	10	11	12	13	14	15	16	17	18	Mean**	S.D.**
85/9/6-1	26	25	25	29	31	31	28	25	23	25	26	28	29	23	24	25	26	28	26.5	2.5
85/9/6-2	29	29	30	29	30	32	32	32	30	28	28	27	30	32	30	31	30	29	29.9	1.5
85/9/6-3	24	25	25	32	34	34	37	32	27	25	26	27	33	35	28	28	27	28	29.3	4.1
85/9/6-4	33	39	39	38	36	33	34	31	29	29	33	38	34	29	31	28	29	31	33.0	3.7
81/9/10-1	58	68	71	71	60	61	68	68	69	60	61	68	62	59	68	67	57	57	64.1	5.0
81/9/10-2	40	46	53	57	56	53	55	49	43	41	47	53	57	57	51	48	50	51	50.4	5.4
81/9/10-3	60	70	68	67	59	58	65	68	68	58	60	64	58	57	64	59	55	56	61.9	4.8
81/9/10-4	48	49	50	49	48	45	41	38	42	45	49	51	50	46	47	47	45	47	46.5	3.4
88/6/6-1	30	23	24	29	30	32	23	25	24	29	28	29	28	30	25	29	30	29	27.6	2.8
88/6/6-2	25	29	25	28	31	39	26	27	26	27	27	28	30	28	28	30	28	27	28.3	3.1
88/6/6-3	24	27	36	26	26	26	28	26	28	24	26	61	27	35	28	25	29	27	29.4	8.5
88/6/6-4	24	24	21	24	26	25	24	23	25	31	23	25	25	24	25	25	25	24	24.6	1.9
82/12/6-1	40	45	47	45	38	41	40	39	40	42	42	40	42	38	45	40	39	42	41.4	2.6
82/12/6-2	57	51	50	49	58	53	37	32	37	56	55	47	50	58	53	58	59	54	50.8	8.0
82/12/6-3	56	51	47	46	55	51	40	33	44	52	50	40	51	54	50	57	56	51	49.1	6.4
82/12/6-4	59	50	50	53	61	54	37	39	37	57	56	47	52	60	53	59	61	58	52.4	7.9
100/0/0-1	46	54	55	50	48	51	47	40	54	53	50	52	51	50	53	48	48	48	49.9	3.6
100/0/0-2	25	26	25	25	27	26	24	25	25	26	25	27	26	24	26	28	24	24	25.4	1.1
100/0/0-3	29	30	29	33	29	28	31	34	32	28	27	31	28	31	33	28	29	31	30.1	2.0
100/0/0-4	31	27	27	25	29	29	25	27	29	30	30	31	28	29	29	30	31	30	28.7	1.9

Code*	1	2	3	4	5	6	7	8	9	10	11	12	13	14	15	16	17	18	Mean**	S.D.**
97/3/0-1	58	59	58	62	58	65	62	65	65	68	54	59	55	63	64	65	67	56	61.3	4.3
97/3/0-2	45	41	35	33	32	32	33	37	44	44	40	37	34	33	37	41	36	36	37.2	4.3
97/3/0-3	25	27	31	35	39	41	36	28	26	25	27	30	34	34	30	25	28	31	30.7	4.9
97/3/0-4	29	30	33	39	41	42	39	31	30	27	41	31	31	41	34	31	33	32	34.2	4.9
95/5/0-1	29	24	23	24	24	21	26	31	37	36	32	29	22	25	21	20	24	27	26.4	5.0
95/5/0-2	36	30	25	22	23	23	22	25	32	35	30	24	22	23	26	32	23	23	26.4	4.7
95/5/0-3	27	28	30	39	40	41	38	29	28	26	27	32	38	38	30	28	35	31	32.5	5.2
95/5/0-4	25	25	25	26	28	34	39	38	39	35	25	24	25	33	38	34	28	31	30.7	5.6
93/7/0-1	33	30	20	22	22	22	20	21	29	34	29	21	21	20	21	30	24	22	24.5	4.8
93/7/0-2	19	20	28	34	33	25	19	20	19	20	21	26	28	23	20	19	20	22	23.1	4.8
93/7/0-3	24	25	26	27	26	31	35	43	40	30	25	26	26	31	35	29	26	25	29.4	5.5
93/7/0-4	25	24	25	27	33	33	29	26	4	26	23	24	27	28	23	22	23	23	24.7	6.1
91/9/0-1	30	28	30	39	42	42	42	39	29	28	27	31	38	39	31	28	30	31	33.6	5.6
91/9/0-2	24	22	24	32	33	38	32	23	22	23	21	24	32	31	24	21	24	24	26.3	5.1
91/9/0-3	22	20	20	20	19	26	38	42	40	26	28	33	28	19	19	18	18	20	25.3	8.0
91/9/0-4	20	19	20	3	35	38	35	25	23	23	31	25	23	22	25	30	25	25	24.8	7.7
88/12/0-1	38	28	24	22	22	22	23	26	33	40	29	25	23	24	27	31	27	25	27.2	5.3
88/12/0-2	22	26	29	24	19	18	19	18	18	19	22	24	22	18	18	18	17	21	20.7	3.3
88/12/0-3	26	33	35	33	26	19	21	22	21	21	24	27	25	21	21	22	21	25	24.6	4.7
88/12/0-4	40	39	37	31	27	27	27	27	28	33	36	34	32	28	29	31	30	31	31.5	4.2

Code*	1	2	3	4	5	6	7	8	9	10	11	12	13	14	15	16	17	18	Mean**	S.D.**
50/50/0-1	25	23	22	23	25	25	25	25	25	24	24	24	25	25	25	23	25	24	24.3	1.0
50/50/0-2	27	25	24	24	24	25	24	26	27	27	27	26	26	26	27	27	27	27	25.9	1.2
50/50/0-3	25	25	28	26	26	25	24	23	24	23	27	24	25	25	25	23	25	27	25.0	1.4
50/50/0-4	26	25	25	24	27	26	25	23	24	26	26	24	25	25	21	20	22	26	24.4	1.9
30/70/0-1	31	28	27	28	33	31	30	27	28	32	33	31	32	32	33	35	32	32	30.8	2.3
30/70/0-2	30	28	25	26	29	29	27	27	28	32	28	28	29	31	27	30	28	28	28.3	1.7
30/70/0-3	41	39	38	38	39	41	36	36	39	42	41	39	41	42	39	45	42	44	40.1	2.4
30/70/0-4	30	27	28	27	28	30	25	26	25	32	29	30	31	30	28	31	30	32	28.8	2.2
0/100/0-1	23	23	23	22	22	21	21	23	22	22	24	27	23	24	23	23	22	21	22.7	1.4
0/100/0-2	25	23	23	23	26	27	25	23	24	25	26	24	27	27	26	27	28	27	25.3	1.7
0/100/0-3	37	30	28	27	33	33	33	27	30	34	35	33	32	31	31	33	41	38	32.6	3.7
0/100/0-4	32	28	25	26	26	26	23	24	26	30	26	27	26	24	24	28	25	27	26.3	2.2

Code : x/y/z-n is wt% LDPE / wt% PE-g-MA / wt% clay – number of sample.

** **Mean and S.D.** are in μm.

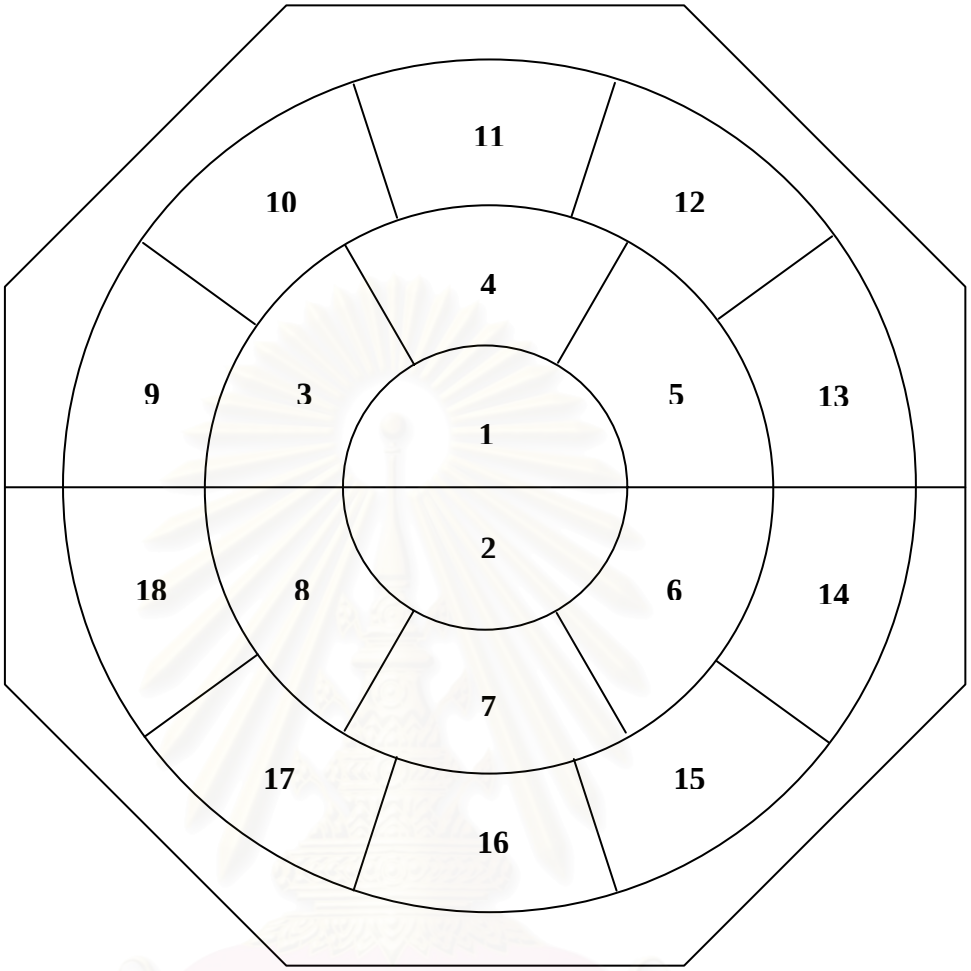

Figure A-1 Paper Template for Film Thickness Measurement

Paper template is divided into 18 equal areas. The largest circle has a diameter of 11.2 cm (or the radius is 5.6 cm).

Appendix B

Table B-1 Oxygen Permeability Data

%wt Inorganic Clay	%wt PE-g-MA	Sample Code	P_c	Average	S.D.	%Error
0.76	9	90/9/1-1	252190	**250,570**	12,767	5.10
		90/9/1-2	267892			
		90/9/1-3	242963			
		90/9/1-4	239236			
1.19	9	89/9/2-1	244847	**228,262**	11,763	5.15
		89/9/2-2	220365			
		89/9/2-3	219450			
		89/9/2-4	228386			
1.66	9	88/9/3-1	194628	**197,777**	7,535	3.81
		88/9/3-2	194435			
		88/9/3-3	193017			
		88/9/3-4	209028			
2.11	9	87/9/4-1	172913	**186,024**	11,613	6.24
		87/9/4-2	180763			
		87/9/4-3	190953			
		87/9/4-4	199467			
3.14	9	85/9/6-1	157781	**158,215**	5,763	3.64
		85/9/6-2	150520			
		85/9/6-3	160384			
		85/9/6-4	164175			
5.09	9	81/9/10-1	161036	**160,841**	1,668	1.04
		81/9/10-2	161748			
		81/9/10-3	158436			
		81/9/10-4	162146			
3.14	6	88/6/6-1	247230	**248,107**	9,597	3.87
		88/6/6-2	243443			
		88/6/6-3	261796			
		88/6/6-4	239958			
3.14	12	82/12/6-1	166797	**172,244**	4,120	2.39
		82/12/6-2	175590			
		82/12/6-3	175278			
		82/12/6-4	171312			

Name	%wt PE-g-MA	Sample Code	P_c	Average	S.D.	%Error
PURE LDPE	0	100/0/0-1	254533	**279,035**	18,846	6.75
		100/0/0-2	291822			
		100/0/0-3	295687			
		100/0/0-4	274096			
LDPE/ PE-g-MA	3	97/3/0-1	265026	**278,226**	11,225	4.03
		97/3/0-2	283447			
		97/3/0-3	290720			
		97/3/0-4	273709			
	5	95/5/0-1	300411	**296,882**	11,485	3.87
		95/5/0-2	307549			
		95/5/0-3	298968			
		95/5/0-4	280600			
	7	93/7/0-1	324625	**302,793**	18,887	6.24
		93/7/0-2	312508			
		93/7/0-3	287878			
		93/7/0-4	286160			
	9	91/9/0-1	312738	**310,801**	11,366	3.66
		91/9/0-2	312972			
		91/9/0-3	295133			
		91/9/0-4	322362			
	12	88/12/0-1	293672	**296,581**	8,728	2.94
		88/12/0-2	302787			
		88/12/0-3	304316			
		88/12/0-4	285548			
	50	50/50/0-1	276160	**278,895**	10,486	3.76
		50/50/0-2	276338			
		50/50/0-3	293825			
		50/50/0-4	269256			
	70	30/70/0-1	337163	**309,502**	22,311	7.21
		30/70/0-2	313877			
		30/70/0-3	283586			
		30/70/0-4	303384			
	100	0/100/0-1	307159	**296,505**	12,931	4.36
		0/100/0-2	297591			
		0/100/0-3	278024			
		0/100/0-4	303246			

Code : x/y/z-n is wt% LDPE / wt% PE-g-MA / wt% clay – number of sample.

P_c, Average and S.D. are in $cm^3.\mu m/m^2.atm.day$.

Appendix C

D-spacing Calculation

The d-spacing of Org-MMT in LDPE /PE-g-MA/Org-MMT nanocomposite films were calculated by Bragg's law equation as shown below.

$$n\lambda = 2d\sin\theta$$

where n = integer

λ = wavelength, 0.154 nm

d = d-spacing of organoclay interlaminar, nm

θ = diffraction angle, degree

MMT powder was measured diffraction angle by XRD. The value of 2θ angle is 2.31 degree which we can calculate d-spacing of powder showing as follow.

$$(1)(0.154) = 2d \sin (1.155)$$

$$d = 3.82 \text{ nm}$$

Appendix D

Table D-1 Raw Data for Determining wt% Inorganic Clay in Composites

Set	wt. cup	wt. lid	Sample wt. before burned	Total wt. after burned	wt. residue	wt% inorganic clay in composites	MEAN wt% inorganic clay in composites
0/0/100-1	26.2503	13.5052	3.0003	41.2421	1.4866	49.55	49.55
100/0/0-1	23.9840	0	3.0185	23.9857	0.0017	0	0
100/0/0-2	17.8040	0	3.0093	17.8202	0.0162	0	
100/0/0-3	21.4258	0	3.0056	21.4270	0.0012	0	
100/0/0-4	24.1386	13.3550	3.0197	37.5023	0.0087	0	
100/0/0-5	22.1029	7.2839	3.0200	29.3942	0.0074	0	
100/0/0-6	21.4222	13.4833	2.9952	34.9123	0.0068	0	
0/100/0-1	26.7770	13.5057	3.0090	40.2743	-0.0084	0	0
0/100/0-2	26.2525	11.7466	2.9998	37.9915	-0.0076	0	
0/100/0-3	25.8476	11.9760	3.0078	37.8167	-0.0069	0	
0/100/0-4	20.1750	11.7488	3.0036	31.9208	-0.0030	0	
0/100/0-5	21.5947	11.4104	3.0072	33.0047	-0.0004	0	
0/100/0-6	17.8025	12.5103	3.0009	30.3117	-0.0011	0	

Set	wt. cup	wt. lid	Sample wt. before burned	Total wt. after burned	wt. residue	wt% inorganic clay in composites	MEAN wt% inorganic clay in composites
90/9/1-1	26.2503	13.5052	3.0046	39.7809	0.0254	0.85	0.76
90/9/1-2	26.9522	11.9755	2.9996	38.9507	0.0230	0.77	
90/9/1-3	25.8466	13.7021	3.0012	39.5697	0.0210	0.70	
90/9/1-4	25.8475	11.9762	2.9979	37.8460	0.0223	0.74	
90/9/1-5	26.7760	13.4833	3.0013	40.2819	0.0226	0.75	
90/9/1-6	23.4589	13.7911	3.0053	37.2717	0.0217	0.72	
89/9/2-1	21.5936	13.8067	3.0028	35.4369	0.0366	1.22	1.19
89/9/2-2	25.3550	11.7460	2.9991	37.1362	0.0352	1.17	
89/9/2-3	24.1389	13.4824	3.0008	37.6564	0.0351	1.17	
89/9/2-4	22.3574	13.7028	3.0011	36.0958	0.0356	1.19	
89/9/2-5	26.9529	13.3551	2.9991	40.3439	0.0359	1.20	
89/9/2-6	26.2525	11.7465	2.9961	38.0341	0.0351	1.17	
88/9/3-1	23.4591	11.4106	3.0018	34.9169	0.0472	1.57	1.66
88/9/3-2	24.6269	13.7910	3.0007	38.4654	0.0475	1.58	
88/9/3-3	22.3610	13.6866	3.0008	36.0943	0.0467	1.56	
88/9/3-4	25.3562	13.8075	3.0057	39.2165	0.0528	1.76	
88/9/3-5	20.1797	13.8808	3.0047	34.1134	0.0529	1.76	
88/9/3-6	22.1032	11.4107	3.0057	33.5664	0.0525	1.75	

Set	wt. cup	wt. lid	Sample wt. before burned	Total wt. after burned	wt. residue	wt% inorganic clay in composites	MEAN wt% inorganic clay in composites
87/9/4-1	26.9525	13.4873	3.0008	40.4951	0.0553	1.84	2.11
87/9/4-2	25.3552	13.8797	3.0004	39.2959	0.0610	2.03	
87/9/4-3	24.1381	13.7023	3.0006	37.9030	0.0626	2.09	
87/9/4-4	23.9830	13.9432	3.0017	37.9904	0.0642	2.14	
87/9/4-5	24.1405	13.6809	3.0032	37.8926	0.0712	2.37	
87/9/4-6	17.8043	13.5055	3.0026	31.3754	0.0656	2.18	
85/9/6-1	20.1816	13.3559	3.0017	33.6291	0.0916	3.05	3.14
85/9/6-2	21.5941	13.8076	2.9999	35.4962	0.0945	3.15	
85/9/6-3	22.1016	13.9424	3.0012	36.1394	0.0954	3.18	
85/9/6-4	24.6255	12.5104	3.0028	37.2306	0.0947	3.15	
85/9/6-5	21.5947	0	3.0034	21.6900	0.0953	3.17	
85/9/6-6	21.4227	7.2843	3.0034	28.8003	0.0933	3.11	
81/9/10-1	22.3560	13.7903	3.0037	36.2980	0.1517	5.05	5.09
81/9/10-2	24.6260	13.9425	3.0018	38.7208	0.1523	5.07	
81/9/10-3	26.7751	13.3544	3.0018	40.2806	0.1511	5.03	
81/9/10-4	26.7767	11.9764	3.0004	38.9071	0.1540	5.13	
81/9/10-5	26.2503	13.6869	3.0013	40.0915	0.1543	5.14	
81/9/10-6	23.9834	13.7031	3.0023	37.8407	0.1542	5.14	

Set	wt. cup	wt. lid	Sample wt. before burned	Total wt. after burned	wt. residue	wt% inorganic clay in composites	MEAN wt% inorganic clay in composites
88/6/6-1	23.4577	11.4100	3.0016	34.9569	0.0892	2.97	2.97
88/6/6-2	17.8035	13.8800	2.9991	31.7721	0.0886	2.95	
88/6/6-3	23.9820	13.6858	3.0010	37.7557	0.0879	2.93	
88/6/6-4	22.3572	13.8809	3.0042	36.3281	0.0900	3.00	
88/6/6-5	25.8480	13.9430	3.0018	39.8801	0.0891	2.97	
88/6/6-6	25.3560	13.7910	2.9998	39.2368	0.0898	2.99	
82/12/6-1	22.1019	12.5100	2.9999	34.7009	0.0890	2.97	3.02
82/12/6-2	21.4213	7.2833	3.0042	28.7958	0.0912	3.04	
82/12/6-3	20.1806	0	3.0004	20.2710	0.0904	3.01	
82/12/6-4	24.6233	13.8080	3.0050	38.5225	0.0912	3.03	
82/12/6-5	23.4592	13.5056	3.0019	37.0560	0.0912	3.04	
82/12/6-6	26.9537	0	3.0020	27.0445	0.0908	3.02	

Set : x/y/z-n are wt% LDPE / wt% PE-g-MA / wt% clay – number of sample.

All weights are in grams.

wt% Inorganic Clay = (wt. Residue / Sample wt. before burned) *100%

Appendix E

Data of L/W and S from TEM Image Analysis

N = Average number of a clay platelets in stack
θ = Angle of clay (degree)
L/W = Aspect ratio of one clay platelet

Table E-1 Data for 90/9/1 LDPE/PE-g-MA/Org-MMT Films

No.	N	θ	L/W	No.	N	θ	L/W	No.	N	θ	L/W	No.	N	θ	L/W
1.	6.0	21	60.0	**6.**	4.5	6	49.5	**11.**	4.5	4	60.0	**16.**	4.5	26	90.0
2.	4.5	21	49.5	**7.**	7.5	11	138.0	**12.**	4.5	25	45.0	**17.**			
3.	4.5	17	55.5	**8.**	4.5	7	124.5	**13.**	6.0	3	55.5	**18.**			
4.	4.5	6	75.0	**9.**	4.5	16	75.0	**14.**	16.5	7	229.5	**19.**			
5.	4.5	3	57.0	**10.**	3.0	25	115.5	**15.**	4.5	20	49.5	**20.**			

Mean: θ = 12.39, L/W = 103.37

Table E-2 Data for 89/9/2 LDPE/PE-g-MA/Org-MMT Films

No.	N	θ	L/W	No.	N	θ	L/W	No.	N	θ	L/W	No.	N	θ	L/W
1.	15.0	19	151.5	**6.**	15.0	7	124.5	**11.**	20.5	1	259.5	**16.**	7.5	12	109.5
2.	14.0	21	175.5	**7.**	11.0	15	120.0	**12.**	16.0	7	199.5	**17.**	11.0	10	120.0
3.	23.5	13	205.5	**8.**	10.5	12	139.5	**13.**	18.5	2	169.5	**18.**			
4.	33.5	43	154.5	**9.**	10.5	3	180.0	**14.**	9.0	22	190.5	**19.**			
5.	6.0	11	109.5	**10.**	4.5	13	139.5	**15.**	10.0	11	79.5	**20.**			

Mean: θ = 15.06, L/W = 167.38

Table E-3 Data for 88/9/3 LDPE/PE-g-MA/Org-MMT Films

No.	N	θ	L/W	No.	N	θ	L/W	No.	N	θ	L/W	No.	N	θ	L/W
1.	4.5	21	87.0	**6.**	10.0	9	93.0	**11.**	7.5	21	180.0	**16.**	25.5	2	142.5
2.	3.0	22	90.0	**7.**	10.5	12	115.5	**12.**	12.0	8	120.0	**17.**	9.0	25	93.0
3.	16.5	14	139.5	**8.**	15.0	6	97.5	**13.**	6.0	20	94.5	**18.**			
4.	6.0	9	60.0	**9.**	10.5	6	70.5	**14.**	7.5	13	139.5	**19.**			
5.	13.5	9	124.5	**10.**	7.5	8	90.0	**15.**	16.5	3	180.0	**20.**			

Mean: θ = 9.90, L/W = 122.54

Table E-4 Data for 87/9/4 LDPE/PE-g-MA/Org-MMT Films

No.	N	θ	L/W	No.	N	θ	L/W	No.	N	θ	L/W	No.	N	θ	L/W
1.	4.5	30	90.0	**6.**	12.0	88	64.5	**11.**	30.0	40	124.5	**16.**	20.0	37	105.0
2.	4.5	27	85.5	**7.**	24.5	7	360.0	**12.**	15.0	22	55.5	**17.**			
3.	16.5	7	85.5	**8.**	15.0	28	91.5	**13.**	6.0	80	97.5	**18.**			
4.	15.0	26	91.5	**9.**	6.0	15	97.5	**14.**	9.0	60	94.5	**19.**			
5.	4.5	23	63.0	**10.**	4.5	23	70.5	**15.**	10.5	37	124.5	**20.**			

Mean: θ = 32.19, L/W = 127.73

Table E-5 Data for 85/9/6 LDPE/PE-g-MA/Org-MMT Films

No.	N	θ	L/W	No.	N	θ	L/W	No.	N	θ	L/W	No.	N	θ	L/W
1.	46.5	22	540.0	**5.**	10.5	17	196.5	**9.**	10.5	10	139.5	**13.**	7.5	35	76.5
2.	13.5	17	169.5	**6.**	12.0	17	150.0	**10.**	12.0	25	91.5	**14.**	7.5	25	64.5
3.	15.0	18	295.5	**7.**	9.0	12	139.5	**11.**	13.5	13	75.0	**15.**			
4.	22.5	13	337.5	**8.**	12.0	40	121.5	**12.**	6.0	20	85.5	**16.**			

Mean: θ = 18.64, L/W = 258.32

Table E-6 Data for 81/9/10 LDPE/PE-g-MA/Org-MMT Films

No.	N	θ	L/W	No.	N	θ	L/W	No.	N	θ	L/W	No.	N	θ	L/W
1.	60.0	12	319.5	**6.**	6.0	14	115.5	**11.**	10.5	57	79.5	**16.**	7.5	29	139.5
2.	4.5	57	82.5	**7.**	10.5	19	124.5	**12.**	31.5	24	220.5	**17.**	9.0	7	112.5
3.	10.5	22	75.0	**8.**	4.5	19	115.5	**13.**	7.5	15	94.5	**18.**	4.5	2	82.5
4.	9.0	15	85.5	**9.**	7.5	32	61.5	**14.**	19.5	12	150.0	**19.**			
5.	6.0	9	124.5	**10.**	13.5	57	79.5	**15.**	15.0	3	120.0	**20.**			

Mean: θ = 21.22, L/W = 175.29

Table E-7 Curve Fitting of Oxygen Permeability of LDPE/PE-g-MA/Org-MMT Nanocomposite Films with Modified Nielsen Equation

ϕ_f	$P/P_{0\ Exp.}$	$L/W_{Exp.}$	$L/W_{avg\ Exp.}$	$\theta_{Exp.}$	$\theta_{avg\ Exp.}$	L/W_{Guess}	θ_{Guess}	$P/P_{0\ Cal.}$	Exp. $(P/P_0Exp - P/P_0avg)^2$	Cal. $(P/P_0Cal - P/P_0Exp)^2$
0	1.000000	0		0				1.000	0.099	0.000000000
0.0025	0.806210	103.37		12.39				0.822	0.014	0.000251615
0.0039	0.734430	167.38		15.06				0.747	0.002	0.000166112
0.0055	0.636350	122.54	159	9.90	18	175	9	0.677	0.002	0.001634039
0.0070	0.598530	127.73		32.19				0.622	0.008	0.000531853
0.0104	0.509060	258.32		18.64				0.524	0.031	0.000230047
0.0172	0.517510	175.29		21.22				0.398	0.028	0.014237323

average	0.686013									
SUM									0.185	0.017
R^2									0.9079	

Oxygen	L/W	θ	R^2
Initial	159	18	0.8787
1	159 →	**0** ↓	0.9053
	167 ←	**0** ↓	0.9086
2	**187** ↓	← 18	0.9084
	187 ↓	→ 19	0.9086
Mean	175	9	0.9079

Table E-8 Calculated Relative Oxygen Permeability from Modified Nielsen Model

L/W , θ	175, 9	159 , 18	159 , 0	167 , 0	187 , 18	187 , 19	ϕ_f
P_c/P_m =	1.0000	1.0000	1.0000	1.0000	1.0000	1.0000	0.0000
P_c/P_m =	0.8221	0.8455	0.8321	0.8252	0.8234	0.8251	0.0025
P_c/P_m =	0.7473	0.7779	0.7604	0.7514	0.7490	0.7512	0.0039
P_c/P_m =	0.6768	0.7126	0.6919	0.6815	0.6788	0.6813	0.0055
P_c/P_m =	0.6216	0.6605	0.6380	0.6267	0.6237	0.6264	0.0070
P_c/P_m =	0.5242	0.5662	0.5417	0.5297	0.5265	0.5294	0.0104
P_c/P_m =	0.3982	0.4394	0.4151	0.4034	0.4004	0.4032	0.0172

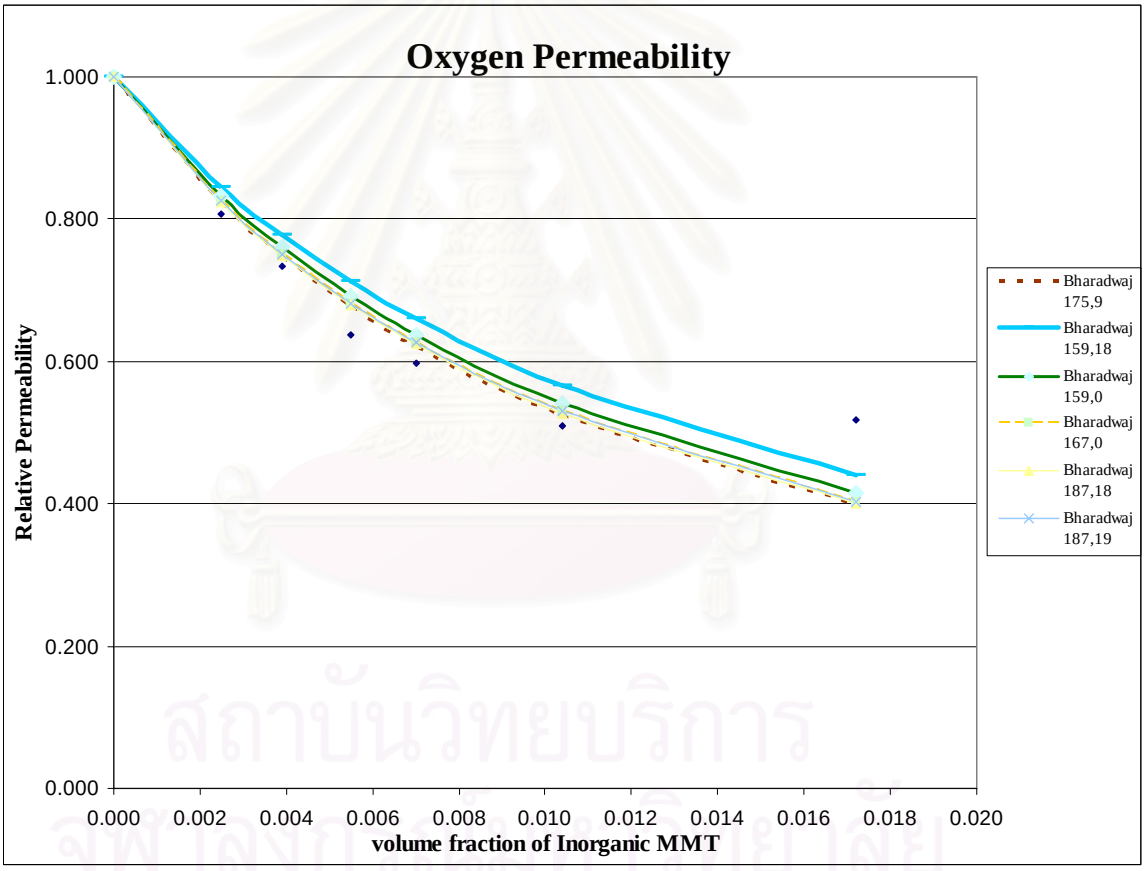

Figure E-1 Calculated Relative Oxygen Permeability from Modified Nielsen Model

Appendix F

Experimental Data from Journal

The following data are taken from the work of S. Hotta and D.R. Paul [44].

Nanocomposites formed from linear low density polyethylene and organoclays

Table F-1 Gas Permeability at 35°C

Sample Name	P_{O_2}	P_{N_2}	P_{CO_2}
LLDPE	5.55	1.79	22.3
LLDPE-g-MA	4.33	1.57	20.7
$M_2(HT)_2$-1	4.75	1.55	19.7
$M_2(HT)_2$-3	4.46	1.38	18.0
$M_2(HT)_2$-5	3.58	1.23	14.6
$M_2(HT)_2$-7	3.22	0.95	13.1

Permeability are in the units of Barrer; 1 Barrer = 10^{-10} cm^3(STP)cm/(cm^2s cmHg).
Sample Name were the same as used in the work of S. Hotta and D.R. Paul [44].

TEM Image Analysis

θ = Angle of clay (degree)
L/W = Aspect ratio of one clay platelet

Table F-2 Data for $M_2(HT)_2$-1 sample

No.	θ	L/W	No.	θ	L/W	No.	θ	L/W	No.	θ	L/W	No.	θ	L/W
1.	70	94	**6.**	34	190	**11.**	85	154	**16.**	67	75	**21.**	52	84
2.	65	96	**7.**	8	177	**12.**	57	271	**17.**	70	151	**22.**	78	141
3.	45	132	**8.**	15	71	**13.**	45	180	**18.**	45	144	**23.**	50	86
4.	32	165	**9.**	35	172	**14.**	64	84	**19.**	70	125	**24.**	87	88
5.	73	181	**10.**	80	177	**15.**	65	142	**20.**	38	95	**25.**	69	102

Mean: θ = 55.96, L/W = 135.08

Table F-3 Data for $M_2(HT)_2$-3 sample

No.	θ	L/W	No.	θ	L/W	No.	θ	L/W	No.	θ	L/W	No.	θ	L/W
1.	71	35	**8.**	57	191	**15.**	66	66	**22.**	81	225	**29.**	44	72
2.	63	285	**9.**	60	75	**16.**	68	207	**23.**	47	194	**30.**	15	81
3.	17	203	**10.**	60	52	**17.**	89	191	**24.**	46	193	**31.**	56	102
4.	67	78	**11.**	63	80	**18.**	72	184	**25.**	61	135	**32.**	46	83
5.	76	65	**12.**	62	76	**19.**	83	171	**26.**	79	111			
6.	64	53	**13.**	43	45	**20.**	89	98	**27.**	48	114			
7.	37	207	**14.**	63	53	**21.**	71	88	**28.**	49	98			

Mean: θ = 58.13, L/W = 122.22

Table F-4 Data for $M_2(HT)_2$-5 sample

No.	θ	L/W	No.	θ	L/W	No.	θ	L/W	No.	θ	L/W	No.	θ	L/W
1.	57	77	**8.**	28	140	**15.**	38	140	**22.**	34	105	**29.**	38	80
2.	48	90	**9.**	32	152	**16.**	43	98	**23.**	29	85	**30.**	35	88
3.	41	109	**10.**	40	102	**17.**	52	140	**24.**	29	74	**31.**	34	104
4.	47	87	**11.**	30	132	**18.**	55	165	**25.**	32	84	**32.**	35	95
5.	45	124	**12.**	33	130	**19.**	54	87	**26.**	51	88	**33.**	36	70
6.	65	80	**13.**	33	90	**20.**	36	74	**27.**	47	101	**34.**	37	80
7.	48	130	**14.**	30	107	**21.**	39	103	**28.**	40	93	**35.**	39	75

Mean: θ = 40.29, L/W = 102.26

Table F-5 Data for $M_2(HT)_2$-7 sample

No.	θ	L/W	No.	θ	L/W	No.	θ	L/W	No.	θ	L/W	No.	θ	L/W
1.	5	71	**12.**	33	51	**23.**	22	132	**34.**	18	85	**45.**	15	47
2.	19	61	**13.**	25	75	**24.**	28	30	**35.**	2	89	**46.**	39	35
3.	11	54	**14.**	6	95	**25.**	8	30	**36.**	21	112	**47.**	48	24
4.	32	94	**15.**	0	87	**26.**	30	45	**37.**	17	104	**48.**	4	36
5.	31	108	**16.**	5	103	**27.**	21	22	**38.**	2	102	**49.**	52	47
6.	44	122	**17.**	19	164	**28.**	30	48	**39.**	30	68	**50.**	52	42
7.	2	145	**18.**	5	102	**29.**	16	35	**40.**	13	62	**51.**	5	49
8.	54	166	**19.**	7	102	**30.**	5	112	**41.**	42	44	**52.**	9	32
9.	11	114	**20.**	33	32	**31.**	45	40	**42.**	36	52			
10.	2	145	**21.**	16	106	**32.**	31	102	**43.**	34	41			
11.	40	84	**22.**	10	147	**33.**	5	85	**44.**	1	42			

Mean: θ = 26.33, L/W = 77.35

Table F-6 Curve Fitting of Oxygen Permeability data of $M_2(HT)_2$ sample with Modified Nielsen Equation

ϕ_f	$P/P_{0\ Exp.}$	$L/W_{Exp.}$	$L/W_{avg\ Exp.}$	$\theta_{Exp.}$	$\theta_{avg\ Exp.}$	L/W_{Guess}	θ_{Guess}	$P/P_{0\ Cal.}$	EXP. $(P/P_{0\ Exp} - P/P_{0\ Avg})^2$	CAL. $(P/P_{0\ Exp} - P/P_{0\ Cal})^2$
0	1	0	109	0	45	114	44	1	0.046	0
0.0026	0.859066	135		55.96				0.926	0.005	0.004416025
0.0083	0.812896	122		58.13				0.796	0.001	0.000277481
0.0155	0.658064	102		40.29				0.675	0.016	0.000289456
0.0237	0.597383	77		26.33				0.575	0.035	0.000512944
average	0.785482									
SUM									0.104	0.005
R^2									0.9471	

 # 1 Fixed L/W , Cal S (θ)

L/W	θ	R^2
109	45	0.940
109	44	0.945
109	43	0.947
109	43	0.9469

 # 2 Fixed S (θ) , Cal L/W

L/W	θ	R^2
109	**45**	0.940
111	**45**	0.943
113	**45**	0.945
115	**45**	0.946
118	**45**	0.9471

L/W_{avg} =	114
θ_{avg} =	44

Table F-7 Curve Fitting of Nitrogen Permeability data of $M_2(HT)_2$ sample with Modified Nielsen Equation

ϕ_f	$P/P_{0\ Exp.}$	$L/W_{Exp.}$	$L/W_{avg\ Exp.}$	$\theta_{Exp.}$	$\theta_{avg\ Exp.}$	L/W_{Guess}	θ_{Guess}	$P/P_{0\ Cal.}$	EXP. $(P/P_{0\ Exp} - P/P_{0\ Avg})^2$	CAL. $(P/P_{0\ Exp} - P/P_{0\ Cal})^2$
0	1	0	109	0	45	119	43	1	0.046	0
0.0026	0.867735	135		55.96				0.920	0.007	0.002761075
0.0083	0.775909	122		58.13				0.784	0.000	0.000065926
0.0155	0.694837	102		40.29				0.659	0.008	0.001304454
0.0237	0.539411	77		26.33				0.557	0.061	0.000296921
average	0.775578									
SUM									0.122	0.004
R^2									0.9637	

 # 1 Fixed L/W , Cal S (θ)

L/W	θ	R^2
109	45	0.935
109	43	0.953
109	42	0.959
109	41	0.962
109	40	0.9637

 # 2 Fixed S (θ) , Cal L/W

L/W	θ	R^2
109	**45**	0.935
117	**45**	0.954
122	**45**	0.961
127	**45**	0.964
129	**45**	0.9637

L/W_{avg} =	119
θ_{avg} =	43

Table F-8 Curve Fitting of Carbondioxide Permeability data of $M_2(HT)_2$ sample with Modified Nielsen Equation

ϕ_f	$P/P_{0\ Exp.}$	$L/W_{Exp.}$	$L/W_{avg\ Exp.}$	$\theta_{Exp.}$	$\theta_{avg\ Exp.}$	L/W_{Guess}	θ_{Guess}	$P/P_{0\ Cal.}$	**EXP.** $(P/P_{0Exp} - P/P_{0\ Avg})^2$	**CAL.** $(P/P_{0\ Exp} - P/P_{0\ Cal})^2$
0	1	0	109	0	45	114	44	1	0.046	0
0.0026	0.884487	135		55.96				0.926	0.010	0.001683658
0.0083	0.810198	122		58.13				0.796	0.001	0.000259652
0.0155	0.658964	102		40.29				0.675	0.016	0.000334283
0.0237	0.593018	77		26.33				0.575	0.037	0.000335857
average	0.789333									
SUM									0.109	0.002
R^2									0.9774	

 # 1 Fixed L/W , Cal S (θ)

L/W	θ	R^2
109	45	0.971
109	44	0.975
109	43	0.977
109	43	0.9773

 # 2 Fixed S (θ) , Cal L/W

L/W	θ	R^2
109	**45**	0.971
111	**45**	0.974
113	**45**	0.976
115	**45**	0.977
118	**45**	0.9774

L/W_{avg} =	114
θ_{avg} =	44

Appendix G

Relation between P_c and wt% and vol% of PE-g-MA

$\rho_{PE\text{-}g\text{-}MA}$ = 0.930 g/cm^3

ρ_{LDPE} = 0.919 g/cm^3

Table G-1 Permeability Data of LDPE/PE-g-MA/Org-MMT at Various wt% Compatibilizer

Code	%wt PE-g-MA	%vol PE-g-MA	P_1	P_2	P_3	P_4	$P_{c\ Mean}$	%error
100/0/0	0.00	0.00	254533	291822	295687	274096	279035	6.75
97/3/0	3.00	2.97	265026	283447	290720	273709	278226	4.03
95/5/0	5.00	4.94	300411	307549	298968	280600	296882	3.87
93/7/0	7.00	6.92	324625	312508	287878	286160	302793	6.24
91/9/0	9.00	8.90	312738	312972	295133	322362	310801	3.66
88/12/0	12.00	11.87	293672	302787	304316	285548	296581	2.94
50/50/0	50.00	49.70	276160	276338	293825	269256	278895	3.76
30/70/0	70.00	69.75	337163	313877	283586	303384	309502	7.21
0/100/0	100.00	100.00	307159	297591	278024	303246	296505	4.36

Code : x/y/z is wt% LDPE / wt% PE-g-MA / wt% clay.

P_c is oxygen permeability of composites in cm^3.μm/m^2.atm.day.

$$vol\%compatibilizer = \left(\frac{\frac{wt\%compatibilizer}{\rho_{compatibilizer}}}{\frac{wt\%compatibilizer}{\rho_{compatibilizer}} + \frac{wt\%polymer}{\rho_{polymer}}} \right) \times 100$$

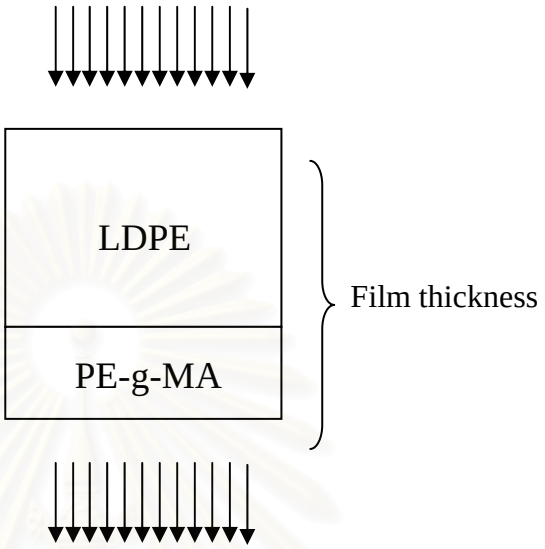

Assumption 1. Materials are separated into two layers along the diffusion path.

2. Each layer has the same surface area.

Permeability of film are following as:

$$\frac{X_T}{P_T} = \frac{X_1}{P_1} + \frac{X_2}{P_2} = \frac{(X_T - X_2)}{P_1} + \frac{X_2}{P_2}$$

P_T = Permeability of Composites

P_1 = Permeability of Polymer

P_2 = Permeability of Compatibilizer

X_T = Thickness of Composites

X_1 = Thickness of Polymer

X_2 = Thickness of Compatibilizer

$$\frac{1}{P_T} = \frac{1-\left(\frac{X_2}{X_T}\right)}{P_1} + \frac{\left(\frac{X_2}{X_T}\right)}{P_2} \quad , \quad \frac{X_2}{X_T} = \text{Thickness fraction of Compatibilizer}$$

wt% compatibilizer ⟶ vol% compatibilizer ⟶ thickness% compatibilizer

$$vol\ \ fraction\ \ compatibilizer = \frac{\dfrac{wt\%compatibilizer}{\rho_{compatibilizer}}}{\dfrac{wt\%compatibilizer}{\rho_{compatibilizer}} + \dfrac{(100 - wt\%compatibilizer)}{\rho_{polymer}}}$$

vol fraction polymer = 1 - vol fraction compatibilizer

From Assumption 2, it can be shown that

thickness fraction compatibilizer = vol fraction compatibilizer

$$\frac{1}{P_T} = \frac{1}{P_1} - \frac{\left(\frac{X_2}{X_T}\right)}{P_1} + \frac{\left(\frac{X_2}{X_T}\right)}{P_2}$$

$$\frac{1}{P_T} = \frac{1}{P_1} + \left(\frac{X_2}{X_T}\right)\left(\frac{1}{P_2} - \frac{1}{P_1}\right)$$

$y = mx + c$ *Linear Equation*

$$y = \frac{1}{P_T}$$

$$m = \left(\frac{1}{P_2} - \frac{1}{P_1}\right)$$

$$x = \frac{X_2}{X_T}$$

$$c = \frac{1}{P_1}$$

VITA

Mr. Pinyo Hovilailux was born in Bangkok, Thailand on March 1, 1983. He completed high school at Watsuthiwararam School, Bangkok, Thailand in 2001 and received a Bachelor of Science degree from the Department of Chemical Technology, Faculty of Science, Chulalongkorn University, Bangkok, Thailand in 2005. He began his study for Master of Engineering degree at the Department of Chemical Engineering, Faculty of Engineering, Chulalongkorn University, Bangkok, Thailand in 2005.